

Towards topological fixed-point models beyond gappable boundaries

A. Bauer¹, J. Eisert^{1,2}, C. Wille³

1 Dahlem Center for Complex Quantum Systems, Freie Universität Berlin, Arnimallee 14, 14195 Berlin

2 Helmholtz-Zentrum Berlin für Materialien und Energie, 14109 Berlin, Germany

3 Institut für Theoretische Physik, University of Cologne, 50937 Cologne, Germany

We consider fixed-point models for topological phases of matter formulated as discrete path integrals in the language of tensor networks. Such zero-correlation length models with an exact notion of topological invariance are known in the mathematical community as state-sum constructions or lattice topological quantum field theories. All of the established ansatzes for fixed-point models imply the existence of a gapped boundary as well as a commuting-projector Hamiltonian. Thus, they fail to capture topological phases without a gapped boundary or commuting-projector Hamiltonian, most notably chiral topological phases in $2 + 1$ dimensions. In this work, we present a more general fixed-point ansatz not affected by the aforementioned restrictions. Thus, our formalism opens up a possible way forward towards a microscopic fixed-point description of chiral phases and we present several strategies that may lead to concrete examples. Furthermore, we argue that our more general ansatz constitutes a universal form of topological fixed-point models, whereas established ansatzes are universal only for fixed-points of phases which admit topological boundaries.

I. INTRODUCTION

Topological phases of matter have received a lot of attention in the past decades. They are interesting for fundamental physical reasons, but are also seen as being instrumental for devising schemes for topological quantum computing. The classification of phases of matter is a challenging task due to a very rich underlying mathematical structure, requiring tools from higher algebra and category theory.

There are two different approaches to classification. The first consists in describing phases via their lower-dimensional defects. The most prominent example of this is the classification of $2 + 1$ -dimensional intrinsic bosonic topological phases via *unitary modular tensor categories (UMTCs)*, which describe the co-dimension 2 defects known as *anyons* as well as the co-dimension 3 defects corresponding to fusion events of the latter. Mathematically, those defect data correspond to so-called (non-fully extended axiomatic) *topological quantum field theories (TQFTs)*. The problem with axiomatic TQFTs is that the correspondence to actual microscopic phases is not necessarily one-to-one: On the one hand, it can happen that a given defect data cannot be realized by any microscopic model. For example, defect data of $2+1$ -dimensional symmetry-enriched topological phases are given by *G-crossed braided fusion categories*, which cannot always be realized microscopically due to anomalies [1]. On the other hand, for some defect data, there might be many different microscopic phases. E.g., all invertible phases do realize the same trivial defect data, including SPT phases, the Kitaev chain, or the bosonic E_8 bosonic quantum Hall state.

So, if we want a systematic and reliable classification, we should instead describe topological phases in terms of concrete microscopic realizations. For this second approach to classifying phases of matter, it is favourable to work with particularly simple representatives of phases, which are exactly soluble by algebraic means. A great success has been the study of so-called *fixed-point models*, which are representatives of the phase which exhibit a *zero correlation length*. The name stems from the idea that those models are fixed-points under so-called *renormalization-group transformations* where in each step large blocks of the original model are considered as indi-

vidual constituents of the resulting model. By repeated application of this ‘zooming out’ procedure the correlation length will decrease until we hopefully converge to a model with zero correlation length.

Fixed-point models for topological phases are usually formulated as *commuting-projector Hamiltonians*. All such known commuting-projector Hamiltonians are equivalent to the more mathematical *state-sum* constructions, or equivalently *lattice TQFTs*, which represent a discrete path integral on a triangulated Euclidean space-time manifold. A wealth of different families of commuting-projector Hamiltonians and the corresponding state-sum constructions can be found in the literature, with the probably most known example being the *Levin-Wen string-net models* [2] which are equivalent to the *Turaev-Viro-Barrett-Westbury state-sum* [3, 4].

Unfortunately, all fixed-point ansatzes we are aware of suffer from a severe restriction: They can only describe phases which possess gapped/topological boundaries. Accordingly, phases for which the boundary must necessarily be gapless do not have any fixed-point descriptions to date. Those include important examples, most notably *chiral* intrinsic topological phases in $2 + 1$ dimensions, including one of the few families of phases which have actually been realized experimentally, namely fractional quantum Hall systems. The restriction is easily explained by the fact that all established state-sum models possess a standard topological boundary via a ‘cone’-construction, as explained in the main text. Furthermore, it has been argued that chiral topological phases cannot be described by any commuting projector Hamiltonian [5], which again makes them incompatible with established ansatzes.

In this work, we make a significant step towards fixed-point descriptions of phases without gapped boundaries: We provide a fixed-point ansatz which is compatible with the absence of such boundaries, and which at the same time does not give rise to commuting-projector models. We do this by formalizing and generalizing state-sum constructions via the language of *tensor-network path integrals*, which are tensor networks describing the imaginary-time evolution in Euclidean spacetime. This is to be contrasted with the use of ground state tensor networks in the framework of *MPO-injective PEPS* [6], which do imply (and in fact are) gapped boundaries. Roughly, the dif-

ference between our ansatz and established state-sum constructions is that the latter associate tensors (such as the F -symbols of a fusion category) to the simplices in a triangulation. Our ansatz associates tensors to the vertices, which are allowed to depend on the *star* of that vertex, that is, the combinatorics of the surrounding triangulation.

To this date, we have not been able to find a concrete example for a model without gappable boundary which is captured by our fixed-point ansatz. However, there are some indications which leave hope that this is possible. Most notably, an exact quantum cellular automaton disentangling the three-fermion Walker-Wang model has been found recently [7]. If this quantum cellular automaton can be extended to a full topological invertible domain wall to vacuum, this would immediately yield a fixed-point model for the chiral three-fermion phase.

In addition to providing a more general fixed-point ansatz, we also show that this ansatz is in fact the *most* general ansatz: It is *universal*, in the sense that it captures any other fixed-point ansatz, no matter how complicated. We also explore the notion of universality under the assumption that a gapped boundary exists, and find that in this case ordinary triangulation-based state-sums are indeed universal. This provides us with a very clean explanation for the structure of known fixed-point models, and with a clear route for finding their most general form.

The structure of the remainder of this work is as follows. In Section II. we introduce generic tensor-network path integrals and their phases of matter. We then move on to discuss fixed-point tensor-network path integrals and their phases and motivate the study of the latter from the former. We argue that topological fixed-point path-integrals fulfil exact tensor-network equations corresponding to topological deformability. Different fixed-point ansatzes correspond to different sets of tensor-network equations for tensor variables, which we refer to as *liquids*. In Sections III., IV., and V., we describe all the relevant ideas for the case of $1+1$ space-time dimensions. Note that in this dimension, the classification of phases is considered mostly complete, and all phases appear to have gapped boundaries. We thus cannot expect our generalized fixed-point ansatz to yield any models for new phases. However, as most of our argumentation takes place on a purely diagrammatic level, the $1+1$ -dimensional case is perfectly suited to introduce the general principles.

Specifically, in Section III., we look at conventional lattice TQFT which corresponds to a liquid which we call the *triangle liquid*. In Section III.5, we show how models of this liquid yield commuting-projector Hamiltonians on a purely diagrammatic level. In Section IV., we show how liquids can also be used as fixed-point ansatzes for topological boundaries and all sorts of defects, and provide a diagrammatic construction for a standard boundary of any triangle-liquid model. We show that any topological liquid with a gapped boundary is equivalent to the triangle liquid and thus implies the existence of a commuting-projector Hamiltonian. In Section V.3, we define the more complicated *vertex liquid*, which provides a more general fixed-point ansatz for topological phases in $1+1$ dimensions. In particular, in Sections V.3, V.4, V.5 we demonstrate that any attempt to emulate the vertex liquid using the triangle liquid, to construct a standard boundary for the vertex liquid, and to construct a commuting-projector Hamiltonian for vertex liquid models, must fail, at least if the constructions are

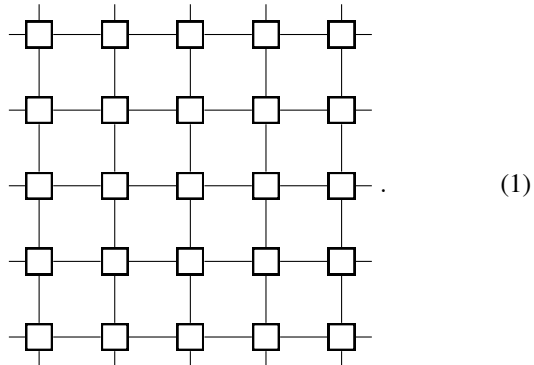
supposed to work on a diagrammatic level. In Section V.6, we show that the vertex liquid is universal, in the sense that it can emulate any other topological liquid in $1+1$ dimensions on a diagrammatic level.

In Section VI., we describe how all the previously presented concepts carry over to higher space-time dimensions, which happens in a rather straight-forward manner. In Section VII. we discuss where and how we would expect our more general liquids to yield fixed-point models beyond commuting-projector Hamiltonians and gapped boundaries. In particular, we describe how the phenomenology of chiral phases of matter fits into the picture.

II. PHASES IN TENSOR-NETWORK PATH INTEGRALS

II.1 Tensor-network path integrals

In the literature, ‘tensor networks’ usually refer to the efficient classical description of (ground) states of many-body quantum Hamiltonian models in terms of tensor networks that have the same geometry as the underlying space, known as *PEPS*, or *MPS* in one spatial dimension [8, 9, 10, 11]. The degrees of freedom correspond to open (uncontracted) *physical indices*, whereas *virtual indices* are contracted neighbouring tensors. This is *not* the way in which we use tensor networks. Instead, we describe physical models in terms of a *tensor-network path integral* which has the dimensionality of space-time, not space and there is no distinction between virtual and physical indices. Unless we explicitly describe an *open boundary* there are no open indices. As an example, a diagram of a tensor-network path integral that captures the real- or imaginary time-evolution of a one-dimensional lattice model could look like the following,

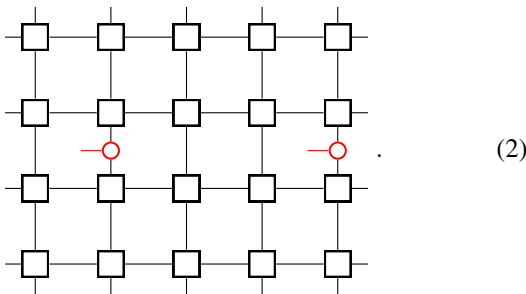


For the tensor-network path integrals we have in mind, all the tensors are the same, i.e., the model is translation invariant and given by a single tensor. This allows us to speak of a thermodynamic limit and of phases of matter.

Tensor-network path integrals provide a unified way to formalize basically any physical model with a notion of space. In Ref. [12], we describe how Trotterization can be used to approximate the real- or imaginary time evolution of a quantum spin system by a tensor-network path integral. For the imaginary time evolution, this path integral lives in a Euclidean space-time and captures the ground state properties of the model. If we want to describe thermal states, we have to compactify the imaginary time into a circle whose circumference is the inverse temperature, yielding a tensor-network path integral living in space only. It is easy to see that also thermal

classical statistical systems such as the classical Ising model are described by tensor-network path integrals living in space, without any need for approximation. Also very different types of models like fermionic or single-particle models [13, 14, 15] can be captured by tensor-network path integrals, if we do not use arrays of complex numbers for the individual tensors, but consider more general *tensor types* [16].

What does it mean for a model to be represented by a tensor-network path integral? Ultimately, the predictions we obtain from a quantum physics model are the statistics of the outcomes of local measurements. The measurements (e.g., in the quantum case, the *positive operator valued measures* (POVM) corresponding to the measured observables) are themselves tensors, and so are the probability distributions over the outcomes. The latter can be obtained from the former and the tensor-network path integral in a simple way: We insert the measurement tensors into the tensor-network path integral and evaluate it. E.g., a POVM acting on one degree of freedom is given by a vector of density matrices, hence a 3-index tensor. If we want to obtain the joint probability distribution over outcomes of a 2-point measurement of the thermal state of a local spin Hamiltonian in 1 spatial dimension, we have to evaluate a tensor-network like the following,



with periodic boundary conditions. The two red tensors are the POVMs, and their classical indices stay open. The resulting tensor describes the probabilities of pairs of measurement outcomes at both places. Every row of tensors corresponds to the imaginary time evolution with a fixed inverse temperature β , so the described thermal state has inverse temperature 4β . If we scale the network both in the horizontal spatial direction and the vertical time direction, we will obtain ground-state measurement outcomes in the thermodynamic limit.

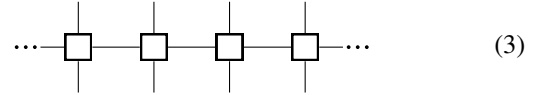
II.2 Spectral gaps and phases of matter

A very common definition of a (quantum) phase of matter is an equivalence class of gapped, translation-invariant, local lattice Hamiltonians under continuous deformations that do not close the gap. A Hamiltonian is gapped if its spectrum has a system-size independent separation of a constant number of low-energy values from the rest of the spectrum, whereas the separation between a possible constant number of low-energy eigenvalues vanishes with increasing system size.

Models with a spectral gap are ‘generic’ in the following sense. It is believed that for any perturbation, there is a finite perturbation strength such that the perturbed model remains gapped for all smaller perturbations. This has been proven so far only for perturbations around fixed-point models of topological order [17]. Consequently, the set of gapped models is an open subset of the space of all models, and in any few-parameter family of models (i.e., in any phase diagram), there

are either no gapped models at all or they have a non-zero volume.

The definition of phases of matter carries over to the tensor-network path integrals: A gapped Hamiltonian H yields a gapped imaginary-time evolution operator $e^{-\beta H}$, just that now the gap separates the *high-lying* values from the rest of the spectrum. In n space-time dimensions, consider an $n - 1$ -dimensional constant-time layer of a tensor-network path integral, such as



for a square lattice tensor network in $1 + 1$ dimensions. Suppose the tensor-network path integral comes from Trotterizing an imaginary-time evolution. Then this layer, as an operator from the bottom indices to the top indices, with N tensors and with periodic boundary conditions connecting left to right, approximates $e^{-\beta H}$ where β is the chosen discretization step in time direction. Tensor networks of this form are known as *projected entangled pair operators* (PEPO), or *matrix product operators* (MPO) [8] in $n - 1 = 1$ dimension, and are often called *transfer operator*.

From the tensor-network path integral point of view, this notion of gap seems a bit unnatural as it specifically involves the transfer operator in imaginary time direction. The path integral lives in Euclidean space-time, so space and imaginary time should be treated on equal footing. Instead of demanding a spectral gap of the imaginary-time transfer operator, it is natural to demand a spectral gap for the tensor network along any n -dimensional curve in space-time, interpreted as an operator from one to the other side. Unfortunately, this has the technical problem that the indices (and thus the Hilbert spaces) on the two sides of an arbitrarily curved transfer operator can be different, and hence we cannot talk about eigenvalues. In the following, we give a definition which we believe is the natural tensor-network path integral analogue to the spectral gap of Hamiltonians. It is based on the observation that for a gapped Hamiltonian for intrinsic robust topological order on a sphere, the normalized operator $e^{-\beta H}$ gets exponentially close to becoming a rank-1 operator in the ‘width’ β of the transfer operator.

For a more formal definition in n space-time dimensions, we consider how an *annulus network*, i.e., a patch tessellated with a regular network whose topology is $S_{n-1} \times [0, 1]$, behaves when its *width* d_A , given by the minimum number of bonds it takes to get from some open index at the inside- to some open index at the outside boundary, is increased. Let I_A and E_A denote the *inside boundary* and *outside boundary* of an annulus network A and let $X[A]$ denote a tensor-network path integral X evaluated on A . We can interpret $X[A]$ as a linear operator from the open indices on the inside boundary to those of the outside boundary.

Definition 1 (Robust gap of a tensor-network path integral). We say that a tensor-network path integral X has a *robust gap* with *correlation length* bounded by some $\xi > 0$, if the following holds.

- For any interior boundary I , there exists a pre-factor C_I and two tensors $\langle V_I |$ and $| W_I \rangle$ whose open indices match those of I .

- For every annulus network A , and every tensor $\langle T|$ with indices matching those of E_A , we have

$$\begin{aligned} & \|\langle T| X[A] - \langle T| X[A] |W_{I_A}\rangle \langle V_{I_A}|\| \\ & < \|\langle T| X[A]\| C_I e^{-\frac{d_A}{\xi}}. \end{aligned} \quad (4)$$

Note that the choice of norm in Eq. (4) does not matter as the corresponding vector space has a finite dimension only depending on I , so we can make up for possible changes of the norm by adapting C_I . Also note that the tensor $\langle V_I|$ in the definition is unique, whereas the choice of $|W_I\rangle$ is almost arbitrary. Moreover, *the* correlation length of X is the smallest ξ for which X has a robust gap. Furthermore, if $X[A]$ is a rank-1 operator, then we can find W_{A_I} and V_{A_I} such that the left hand side is always 0, and this is the case for fixed-point models like we introduce them later. If we have fermionic tensors or tensors with symmetries, then it suffices if $X[A]$ is rank-1 within the fermion-parity-even, or symmetric subspace. For tensor-network path integrals coming from a Trotterized Hamiltonian, a robust gap of the path integral implies a gap of the Hamiltonian. We neither know a proof nor counter-examples for whether the opposite implication is true.

We can now define phases on the level of tensor-network path integrals.

Definition 2 (Phase). Two tensor-network path integrals X_0 and X_1 with a robust gap are *in the same phase* if there is a continuous family of tensors $X(s)$, $s \in [0, 1]$, $X(0) = X_0$, $X(1) = X_1$, such that

- $X(s)$ has a robust gap for all s , and
- there is a choice of $s \mapsto \langle V_I| (s)$ which is continuous.

II.3 Fixed-point models and exact phases of matter

Generic tensor-network path integrals have non-zero correlations at arbitrary distances d , which gives them an approximate and messy nature and makes them hard to cope with using analytic and algebraic tools. In contrast, *fixed-point models* are models for which the correlation length ξ is zero, that is, both sides of Eq. (4) are exactly zero for all d_A larger than some constant. The tensors of such fixed-point models are often found to satisfy exact algebraic relations, which enable us to analytically calculate some the properties of those models. In the best case, we can even use those algebraic relations themselves to classify phases of matter via fixed-point models. In particular, if two fixed-point models are in the same phase, then we often find that they are related by an exact algebraic relation rather than a continuous path of non-fixed-point models. We can define *exact phases* which are equivalence classes under exact algebraic relations.

Definition 3 (Invertible domain wall). An *invertible domain wall* between two tensor-network path integrals A and B is defined by the following.

- There is a set of *domain wall tensors*.
- The tensors of A and B together with the domain wall tensors satisfy a set of tensor-network equations.
- Using the tensor-network equations we can transform the networks of A into the networks of B and vice versa.

If such an invertible domain wall exists, then A and B are said to be in the same *exact phase*.

The perhaps simplest invertible domain wall consists in A and B being related by an on-site unitary, as described in Ref. [12]. We will give a slightly more involved example, namely two square-lattice tensor networks being related via the conjugation by a *simple MPO*. This is, there are 2 additional tensors,

$$\begin{array}{c} \text{---} \square \text{---} \\ | \\ \text{---} \end{array}, \quad \text{---} \circ \text{---}, \quad (5)$$

which together with A and B fulfil the equations

$$\begin{array}{c} b \\ | \\ \text{---} \square \text{---} \\ | \\ d \end{array} \begin{array}{c} b \\ | \\ \text{---} \square \text{---} \\ | \\ d \end{array} = \begin{array}{c} b \\ | \\ \text{---} \square \text{---} \\ | \\ \text{---} \square \text{---} \\ | \\ d \end{array} \begin{array}{c} b \\ | \\ \text{---} \square \text{---} \\ | \\ d \end{array}, \quad (6)$$

$$\begin{array}{c} x \\ | \\ \text{---} \square \text{---} \\ | \\ w \end{array} \begin{array}{c} z \\ | \\ \text{---} \square \text{---} \\ | \\ y \end{array} = \begin{array}{c} x \text{---} \circ \text{---} z \\ a \text{---} \text{---} b \\ w \text{---} \circ \text{---} y \end{array}, \quad (7)$$

and

$$\begin{array}{c} \circ \\ | \\ \circ \text{---} \circ \text{---} \circ \\ | \\ \circ \end{array} = 1. \quad (8)$$

The empty right hand side of the last equation denotes the scalar 1.

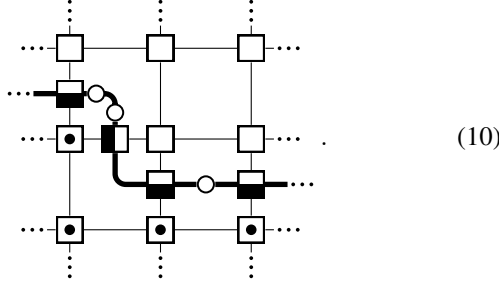
There are two different but equivalent pictures in which we can think about the definition of invertible domain walls given above. The first picture is that the square-lattice B -network can be transformed into the square-lattice A -network using the moves of the invertible domain wall in parallel. For the example of a simple MPO, this looks as follows,

$$\begin{array}{c} \dots \\ \vdots \\ \dots \square \dots \\ \vdots \\ \dots \square \dots \\ \vdots \\ \dots \end{array} \rightarrow \begin{array}{c} \dots \\ \vdots \\ \dots \square \dots \\ \vdots \\ \dots \square \dots \\ \vdots \\ \dots \end{array} \rightarrow \begin{array}{c} \dots \\ \vdots \\ \dots \square \dots \\ \vdots \\ \dots \square \dots \\ \vdots \\ \dots \end{array} \rightarrow \begin{array}{c} \dots \\ \vdots \\ \dots \square \dots \\ \vdots \\ \dots \square \dots \\ \vdots \\ \dots \end{array}. \quad (9)$$

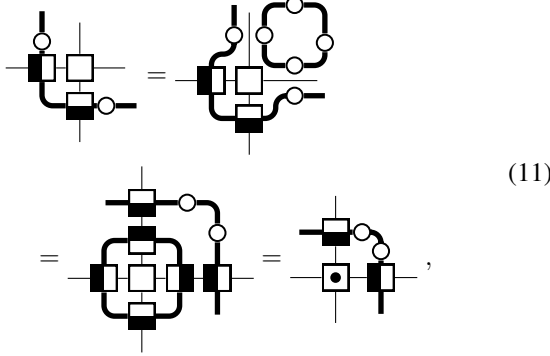
We first apply Eq. (6) to every tensor of the B -network, then Eq. (7) at every bond of the original B -network, and then Eq. (8) at every plaquette of the original B -network, yielding the A -network.

The second viewpoint on an invertible domain wall in n dimensions is as an $n - 1$ -dimensional membrane separating an

A -network on the one side and a B -network on the other side. For our example, this could look like



The membrane does not have to be a straight line or hyper-plane such as a physical domain wall in a condensed matter model, but can be arbitrarily curved. The internal bonds (thick lines) connecting the domain wall tensors can be straight or bent. Straight bonds include one normalization matrix, and bonds bending around a B -tensor include twice the normalization matrix. The moves in Eq. (6), Eq. (7), and Eq. (8) can be used to move the location of the domain wall. E.g., in our example, the invertible domain wall can be ‘pulled through’ by an A -tensor yielding a B -tensor,



where we used first Eq. (8), then twice Eq. (7), and then Eq. (6). Moves of this type make the line in the tensor-network path integral a *topological* domain wall. The domain wall is also *invertible*, which corresponds to the additional moves of creating or erasing small loops via Eq. (6), and fusing two lines via Eq. (7).

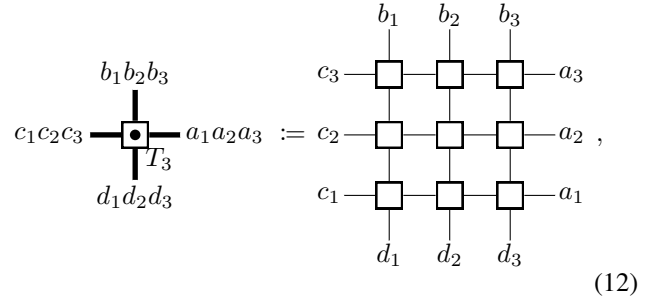
Note that the definition of phases from the previous section is similar to but different from the notion of exact phases here. First, invertible domain walls of tensor-network path integrals cannot change the correlation length. So, generically, two tensor-network path integrals will not be in the same exact phase, even if they are in the same phase. Vice versa, it is not a priori clear whether an invertible domain wall between two path integrals A and B can be turned into a continuous gapped path. In some cases we can find a model for an invertible domain wall between A and A of the same form, and a continuous family of domain wall models connecting it to the desired invertible domain wall between A and B . E.g., consider domain walls relating A and B by conjugation with an on-site unitary U . Taking $\mathbb{1}$ for U defines an invertible domain wall between A and A , and for every U we can find a Hermitian H such that $U = e^{iH}$. $\hat{U}(s) = e^{isH}$ then defines a continuous family of invertible domain walls interpolating between $\hat{U}(0) = \mathbb{1}$ and $\hat{U}(1) = U$. On the other hand, let us restrict to real tensors which is what we need to model spin systems with a time-reversal symmetry, and consider an invertible domain wall consisting of on-site orthogonal maps O . If O has determinant -1 , i.e., it involves a

reflection, we cannot interpolate between $\mathbb{1}$ and O by a continuous path as before. So in this case, it is unclear whether we can interpolate between the original model and the O -conjugated model with a gapped path, without breaking the time-reversal symmetry.

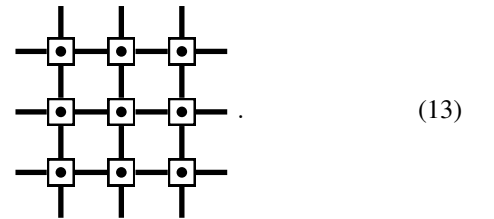
In practice, invertible domain walls are an accepted way for defining phases for fixed-point models, even though their relation to gapped paths has not been rigorously settled. E.g., the phase equivalence of certain Levin-Wen models via the Morita equivalence of the underlying fusion categories is an example of an invertible domain wall.

II.4 Fine-graining

A priori, it is unclear whether any phase possesses a fixed-point model. A vague argument of why this is the case is provided by the idea of *renormalization group (RG) flow*. As this term as such is rather uninformative and used for too many distinctly different concepts, we will use the simpler name *fine-graining mapping*. Given a tensor-network path integral T , we can construct a new path integral T_λ by taking blocks whose linear size λ is called the *fine-graining scale*, and grouping them together into a single tensor each. E.g., for $\lambda = 3$ and a square-lattice tensor network in $1 + 1$ dimensions, we define a new tensor by



forming a new tensor-network path integral,



This comes at the expense of the bond dimension of the new tensor network increasing exponentially in λ .

Two points in the new tensor-network path integral with a combinatorial distance d have a distance λd in the original network. Thus, if the correlation length of the old tensor-network path integral was ξ , then the new correlation length is ξ/λ . The idea is that by choosing larger and larger λ , we will eventually arrive at a fixed-point model with $\xi = 0$.

There are, however, two major difficulties with this idea. First, to arrive at a fixed-point model, we would need the sequence T_λ to converge. As such, this does not make any sense, as the different T_λ have different bond dimensions corresponding to different vector spaces. To fix this, we need to use invertible linear maps S_λ which embed the different vector spaces into one common vector space $V_\infty \subset \mathbb{C}^{\mathbb{N}}$. Now the question is

Or, we could still demand 4 faces meeting at a vertex, but in addition to 4-gon faces also allow triangle faces and 5-gon faces, represented by two further tensors,

$$(21)$$

Assume we have a tensor-network path integral in n space-time dimensions extended to arbitrary irregular networks. Consider two different networks representing an n -ball which look the same at the boundary, in particular they have the same open indices. Now, we enlarge both networks by adding the same annulus-shaped margin of width d to them. We say that the extended tensor-network path integral has *topological invariance* if for every such configuration it evaluates to the same tensor for both enlarged networks, up to an error exponentially small in d . For $n = 1 + 1$, we have schematically,

$$(22)$$

The two orange ellipses with grid represent the two different networks, and the blue annulus is the width- d annulus enlarging both of them. C_0 is a pre-factor only depending on the boundary of the red n -balls. α is a scalar pre-factor, which is necessary in the general case, but can be set to 1 for many phases (namely for phases without a chiral anomaly). For tensor-network path integrals with a robust gap, the tensor associated to the blue network as an operator from the inside to the outside is an approximate rank-1 operator, so the equation holds no matter what the red networks on both sides are. However, this is only true if the blue network is flat and regular. It is not a priori clear that we can find an extension to irregular networks such that also all irregular annuli are approximate rank-1 operators.

It is common for tensor-network path integrals with a robust gap to be extendable to ones with topological invariance. However, there are many counterexamples, such as the anti-ferromagnetic Ising model from the previous section. In fact, the only counter-examples that the authors are aware of are of that kind, namely they consist of a topological path integral with topological defects, which are arranged on a fixed space-time grid. Note that many of these defect networks do become topological after fine-graining at certain scales λ , but fracton phases are examples in $3 + 1$ dimensions which are not topological at any fine-graining scale [18].

Now consider a fixed-point model, where the annulus operator is exactly a rank-1 operator, and assume that it is extended to irregular lattices such that any (irregular) annulus operator is rank-1, too. Then, topological invariance corresponds to exact

tensor-network equations, such as

$$(23)$$

corresponding to a re-cellulation

$$(24)$$

Different networks of the extended path integral represent different space-time geometries. For an equation like Eq. (23), imagine the left-hand side occurs as a subnetwork of a larger network. The equation can be applied by cutting out the left-hand side and replacing it by the right-hand side, or vice versa. The networks together with the equation are a combinatorial version of topological manifolds with homeomorphism, in the following sense. Each network represents some topological manifold, and two networks correspond to homeomorphic manifolds, if and only if they are related by applying the moves.

By reverse engineering we can pick a set of tensor variables and equations which are a continuum version of topological manifolds, and use it as an ansatz for fixed-point path integrals of topological order. Using and building upon a language introduced in Ref. [12], we refer to the diagrammatic combinatorial structure of tensors and equations such as in the example above as a *liquid*. The tensor-network diagrams are called *networks*, the diagram pairs of the tensor-network equations *moves*. The actual choice of tensors fulfilling the equation is referred to as *model* of the liquid. Such models also have a physical interpretation as fixed-point models for topological phases.

One of the key ideas of this work is that we cannot only find different models of a given liquid corresponding to different fixed-point models of different topological phases. We can also try to use different liquids as ansatz. In general, it is conceivable that some liquids contain models for phases which are missed by other liquids.

The most straight-forward way of representing a (piece-wise linear) topological manifold combinatorially is via a triangulation. For any liquid describing topological n -manifolds, we can construct triangulations from the networks of that liquid and vice versa. So another way to think about a liquid is as a local prescription to associate a tensor-network to triangulations. Local means that the structure of the network and the tensors at a place in the triangulation are allowed to depend on the combinatorics of the triangulation inside a constant-size neighbourhood. For established fixed-point ansatzes, this dependence is particularly trivial, namely, we place one copy of the same tensor on each n -simplex. For more general ansatzes, the tensor network could depend on the triangulation in an environment of combinatorial size b measured in the combinatorial distance. By ‘fine-graining’ and ‘blocking’, we can make b smaller and smaller. This is the basic idea of the *universality mapping*, which will play a crucial role in later sections. However, using fine-graining, we do *not* necessarily arrive at an established fixed-point ansatz. Instead, it is possible to arrive at

a more complicated liquid, namely the vertex liquid which will be introduced later.

III. SIMPLE LIQUIDS IN 1 + 1 DIMENSIONS

In this section we introduce two simple liquids (i.e., two different fixed-point ansatzes) whose models are fixed-point models for topological phases in 1 + 1 dimensions. Even though there are no intrinsic robust phases, the simple liquids in 1 + 1 dimensions are suitable to demonstrate all the principles of our formalism on a diagrammatic level. Furthermore, imposing symmetries on the tensors would lead to a classification of symmetry-breaking and symmetry protected topological phases. At hand of the two liquids we explain how to show the equivalence of different liquids, and how to construct commuting-projector Hamiltonians from liquids, on a purely diagrammatic level. We also discuss an attempt to show that one of the liquids includes any other fixed-point ansatz, and point out the problems and potential failure of the latter. The specific way how this attempt fails is of conceptual importance and leads us to consider more general fixed-point ansatzes in Section V.

III.1 The triangle liquid

As the name indicates, the networks of the *triangle liquid* represent triangulations of 2-manifolds. More precisely, each triangle is represented by a copy of the same 3-index tensor, and the tensors at neighbouring triangles share a *bond*, i.e., a contracted index pair. Also, the triangulation is equipped with a *branching structure* (or simply *branching*), that is, every edge has a direction, such that the directions are non-cyclic around every triangle. Furthermore, the triangulation has an orientation and the tensors at triangles with two clockwise-directed edges differ from those at triangles with two counter-clockwise-directed edges,

$$(25)$$

For Hermitian models of the liquid, those two tensors are complex conjugates of each other.

There are a number of moves, the main one is given by

$$(26)$$

The move corresponds to a local change of the triangulation which itself is known as a 2-2 *Pachner move*,

$$(27)$$

It is known that the 2-2 *Pachner move* together with an additional 1-3 *Pachner move* form a discrete analogue of continuum homeomorphisms [20]. So, if we add versions of the move above with different edge orientations as well as the 1-3 *Pachner move*, we have a topological liquid. For a more detailed description of the liquid, we refer the reader to Ref. [12].

Models of the liquid can be constructed from finite-dimensional $*$ -algebras. The discrete path-integrals are equivalent to what is known as *lattice TQFT* [21].

III.2 The edge liquid

In this section, we consider a new topological liquid in 1 + 1 dimensions that corresponds to a different way of combinatorially representing 2-manifolds. Instead of representing each triangle by a tensor, we associate a copy of a 4-index tensor to every edge. More precisely, an orientation of the manifold is implemented by equipping each edge with a clockwise- or counter-clockwise ‘helicity’ which we indicate by little arrows at both the edge and the symbol for the associated tensor,

$$(28)$$

An edge with different helicity is represented by the same tensor, just flipped,

$$(29)$$

Two edge tensors share a common bond if they are adjacent to a common vertex and a common triangle. This description also works for cell complexes with arbitrary n -gons as faces instead of just triangles, e.g.,

$$(30)$$

There are 3 moves. The first move has a geometric representation as taking the endpoint of one edge and moving it along another edge,

$$(31)$$

In terms of networks, we have

$$(32)$$

The second move corresponds to removing a ‘dangling’ edge with a vertex that is only adjacent to this edge,

$$(33)$$

In terms of networks, this is

$$(34)$$

The third move removes a ‘loop’ edge which has the same end-point twice,

$$(35)$$

In terms of networks,

$$(36)$$

III.3 Equivalence of the liquids

For the triangle liquid, we could make use of a theorem by Pachner to argue that it has a ‘topological’ character. For the edge liquid, such a formal argument is missing, though it seems conceivable that the presented deformations of cellulations are as powerful as Pachner moves. Instead of trying to directly prove a second Pachner theorem for the edge liquid, we take a simpler route and show its local combinatorial equivalence to the triangle liquid.

We do this by introducing two so-called *liquid mappings* – one mapping from the triangle liquid to the edge liquid and the other mapping vice versa. Intuitively, such a liquid mapping is a way to locally express one combinatorial representation of 2-manifolds in terms of the other. Formally, a liquid mapping from a liquid \mathcal{A} to a liquid \mathcal{B} associates to each tensor of \mathcal{A} a network of \mathcal{B} . Using the map on a network of \mathcal{A} , we obtain a network of \mathcal{B} . Usually, the \mathcal{B} -network will be ‘larger’ or ‘more fine-grained’ than the \mathcal{A} -network.

We can map a cellulation underlying an edge-liquid network to a triangulation underlying a triangle-liquid network by replacing every edge by two triangles,

$$(37)$$

In other words, the triangulation is obtained by subdividing each face into triangles in a ‘pizza-like’ manner, with a new vertex in the middle. Formally, this liquid mapping from the edge liquid to the triangle liquid is given by

$$(38)$$

Liquid mappings must be consistent with the moves. I.e., applying the mapping to a move of \mathcal{A} we obtain an equation between two \mathcal{B} -networks, and this equation must be *derivable* from the moves of \mathcal{B} , that is, the two sides are connected by applying the moves. E.g., applying the mapping above to the move in Eq. 36, we obtain the equation

$$(39)$$

which follows from the complete set of triangle-liquid moves in Ref. [12]. Under the mapping defined in Eq. (38) a model of the triangle liquid is mapped to a model of the edge liquid. The compatibility with the moves ensures that the obtained 4-index tensor is indeed a model in the sense that it fulfils all the equations corresponding to the moves.

Let us now give the opposite mapping from the edge liquid to the triangle liquid. A branching structure triangulation can be turned into a cellulation by replacing every triangle by two of its edges,

$$(40)$$

Note that an edge of the triangulation might yield two edges of the cellulation, one coming from both adjacent triangles, separated by a 2-gon. It might also yield one or no edges, depending on the branching structure of the two adjacent triangles. Formally, the mapping is given by

$$(41)$$

As indicated by the two-letter labels on the left-hand side, each index of the triangle liquid corresponds to two indices of the edge liquid. If we want to use this formula to get a triangle-liquid model from an edge-liquid model, we have to evaluate the right-hand side, and then block pairs of indices into single indices.

To establish the equivalence of two structures using maps between them, the two maps should be inverses of each other. For the presented liquid mappings above, this is not true in a literal sense. If we start with a triangle-liquid network, map it to an edge-liquid network and back to the triangle liquid, we do not obtain the original network but a more fine-grained one. However, the resulting network describes the same topological manifold, and is therefore connected to the original network by applying the triangle-liquid moves. In general, two liquid mappings showing the equivalence between two liquids \mathcal{A} and \mathcal{B} need to be only *weak inverses*. That is, the mapping $\mathcal{A} \rightarrow \mathcal{B} \rightarrow \mathcal{A}$ applied to a \mathcal{A} -network without open indices is equal to a sequence of \mathcal{A} -moves, and vice versa.

The two mappings being not literal inverses of another implies that applying both mappings in the reverse direction to a model of \mathcal{A} , we will in general not end up with the same model again. Indeed, as one of the mappings involves a blocking of indices, the bond dimension of the resulting model will be the square of the original bond dimension. However, the two mappings being weak inverses of another implies that the model

and the twice-mapped model will be related by an invertible domain wall. So even if the original and the resulting models are different, they are in the same exact phase. Thus, the phases of equivalent liquids, such as the edge liquid and the triangle liquids, are in one-to-one correspondence. They are therefore equally powerful for classifying or representing phases of matter. However, the representation of a phase as model of \mathcal{A} might be more convenient than its representation as a model of \mathcal{B} , or vice versa.

III.4 Universality mapping and the corner problem

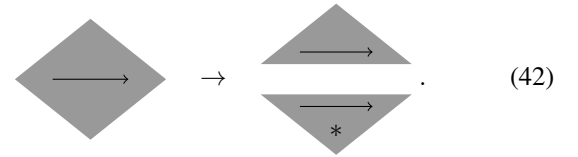
In the previous sections, we defined two liquids describing topological 2-manifolds, and found that they are equivalent on a diagrammatic level. One might be tempted to think that not only the edge liquid, but *every* liquid whose networks describe topological 2-manifolds is equivalent to the triangle liquid, and therefore describes the same phases. To further investigate this thought we will attempt to show that any two-dimensional topological liquid \mathcal{B} is equivalent to the triangle liquid via weakly invertible liquid mappings and in fact fail to do so. Instead, we will encounter fundamental difficulties which strongly indicate that not every topological liquid is equivalent to the triangle liquid and hint at the possibility of non-equivalent liquids. Based on the insights gained in this discussion, we will be able to construct an explicit example of a non-equivalent liquid which is discussed in Section V.

We consider an arbitrary two-dimensional topological liquid \mathcal{B} . As \mathcal{B} describes topological 2-manifolds, the \mathcal{B} -networks can be expressed in terms of triangulations and hence, we assume that there exists a mapping from \mathcal{B} to the triangle liquid. In the other direction, a weakly invertible mapping from the triangle liquid to an arbitrary liquid \mathcal{B} , will be called a *universality mapping* since it shows that the triangle liquid is universal as a fixed-point ansatz. However, our attempt to construct such a universality mapping fails due to a reason we call the *corner problem*.

There are two main ways in which an invertible mapping between two liquids \mathcal{A} and \mathcal{B} can fail to be a liquid mapping. First, the mapping might produce *invalid* \mathcal{B} -networks when applied to an \mathcal{A} -network, which do not represent a patch of a 2-manifold. For the triangle and edge liquid introduced above, any network is valid. However, for some more general liquids \mathcal{B} , in particular for the extended triangle and vertex liquid we will introduce in Section V., \mathcal{B} -networks representing a patch of 2-manifold are subject to some constraints. E.g., the vertex-liquid networks representing 2-manifolds are required to only have triangle plaquettes, whereas, e.g., tensor-network diagrams with 4-gon plaquettes are considered invalid. Second, the mapped moves of \mathcal{A} must be derivable from the moves of \mathcal{B} . If the networks on both sides of the \mathcal{B} -moves are very large compared to those of \mathcal{A} , it might not be possible to apply them to the mapped moves of \mathcal{A} . This problem can be tackled by using large \mathcal{B} -networks in the mapping itself. That is, the mapping will be similar to a mapping with fine-graining scale λ such as in Eq. (12).

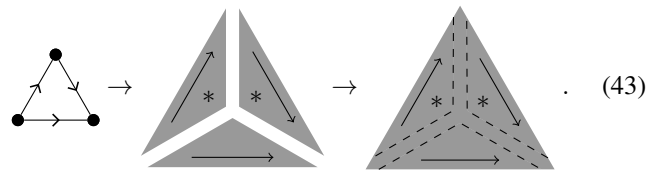
Let us now attempt to construct a weakly invertible mapping from the triangle liquid to \mathcal{B} , i.e., to associate a \mathcal{B} -network to each triangle tensor. To construct a suitable \mathcal{B} -network, we use the following construction. We fill a rhombus with some \mathcal{B} -network, such that the corners have a combinatorial distance

(i.e., minimum number of bonds in a connecting path) of at least λ . Then, we split the rhombus and the \mathcal{B} -network on it vertically into two triangles,

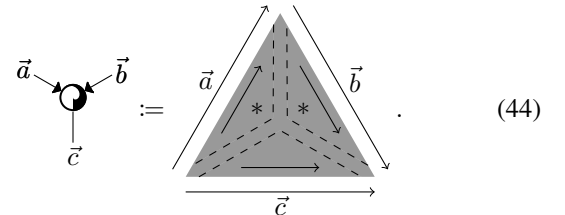


Note that the arrow directions together with the underlying orientation are necessary to make an unambiguous choice of the cut.

Next, we combine three of the triangle-shaped network patches into a single triangle-shaped network by bringing placing them next to each other and filling the gaps between them with some \mathcal{B} -network as follows,

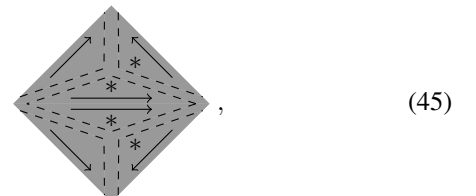


The branching structure of the reference triangle on the left is important to make an unambiguous choice of such a filling. The resulting \mathcal{B} -network is associated to the triangle tensor for the attempted mapping,

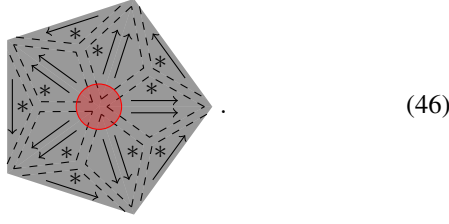


The \mathcal{B} -network on the right has many open indices along its open boundary, their number scaling linearly with λ . The open indices along each of the three edges are ordered according to the branching and blocked together to yield one of the indices \vec{a} , \vec{b} and \vec{c} , respectively. The bond dimension of the triangle-liquid model is the product of all the bond dimensions of the indices along one edge, and therefore grows exponentially in λ . Note, that in the bottom left corner (as well as in the other corners), the filling between the triangles can give rise to additional open indices. For each such index, we have to make a choice of whether to assign it to \vec{a} or \vec{c} , and analogously for the other corners. The construction for the mapping of the counter-clockwise triangle is analogous, gluing together three triangles with the opposite orientations.

In order to test whether this mapping works, we need to first check whether every valid triangle-liquid network patch is mapped to a valid \mathcal{B} -network patch. If we apply the mapping to two neighbouring triangles,

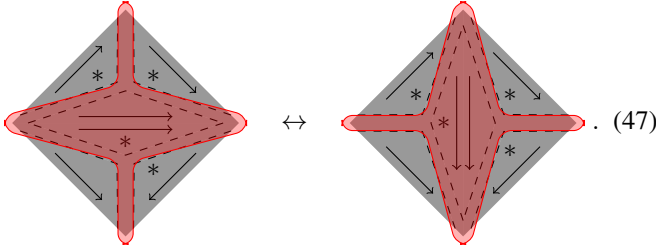


this is the case per construction as we just re-glue the cutting in Eq. (42). However, the situation is different when we consider a patch of triangles around a vertex, e.g.,

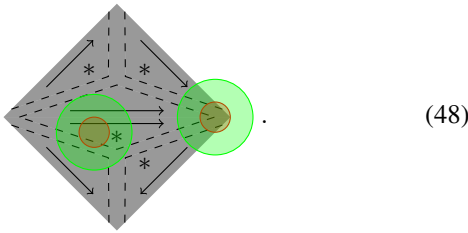


The network in the red marked region around the central vertex does not originate from a cut which is re-glued. We thus have no guarantee that the network in the red marked region is valid and represents a disk-like patch of 2-manifold. Note that this network also depends on the arbitrary choice of whether the open indices in the corners of Eq. (44) are associated to \vec{a} , \vec{b} or \vec{c} .

We also need to test whether the mapped Pachner moves can be derived from the \mathcal{B} -moves. E.g., the mapping of the 2-2 Pachner move in Eq. (26) yields



We notice that the \mathcal{B} -network only changes within the red shaded area. If we want to change the \mathcal{B} -network within some region by \mathcal{B} -moves, the latter need to act within this region enlarged by a margin of constant size measured in the combinatorial distance. E.g., in order to perform changes within one of the red circles in the following picture, we need to apply moves within the respective larger green regions,



For any red region far from the boundary, the green region is fully contained inside the overall \mathcal{B} -network, if we choose the fine-graining scale λ large enough. Consequentially, changes in these regions can be performed using the \mathcal{B} -moves, no matter how complicated the latter are. However, this does not hold for changes right at the boundary. Thus, a mapping based on fine-graining only provides a valid mapping for an arbitrary liquid \mathcal{B} to the triangle liquid, if the two \mathcal{B} -networks of every mapped move differ only in regions distant from the boundary. As we can see in Eq. (47), the present construction almost succeeds in doing so. Most of the regions on which the two networks differ are located in the bulk of the network. The problem only arises at the corners of Eq. (47), hence we refer to the encountered obstruction as the ‘corner problem’.

In addition to the corner problem, the attempted universality mapping is also incompatible with Hermiticity. We will describe in more detail how this problem arises and how to resolve it towards the end of Section IV.4, where we circumvent the corner problem using the existence of a topological boundary.

III.5 Commuting-projector mapping

As mentioned in the introduction, tensor-network path integrals are a discrete-time version of the (imaginary-)time evolution of quantum spin systems with local Hamiltonians. An approximate tensor-network path integral can be obtained from a Hamiltonian by Trotterization. However, when the Hamiltonian terms commute, Trotterization is not necessary, and an exact tensor-network path integral can be obtained by simply taking the product of time evolutions under the individual Hamiltonian terms.

A translation-invariant, local *commuting-projector model* is given by a *local ground-state projector* P acting on the degrees of freedom on a lattice inside a block of some fixed size. The Hamiltonian of the model is given by

$$H = \sum_i (1 - P_i), \quad (49)$$

where i runs over all lattice sites, and P_i denotes P acting on a block centred at site i , tensored with the identity everywhere else. P needs to fulfil

$$P_i P_j = P_j P_i \quad (50)$$

for all sites i and j , which is automatic if the blocks centred at i and j do not overlap. So commuting-projector models are models of a liquid, as they are given by a finite set of tensors fulfilling a finite set of equations. In 1+1 dimensions, after sufficient fine-graining, P is an operator acting on two consecutive degrees of freedom in a spin chain, i.e., a 4-index tensor,

$$P_{cd}^{ab} = \begin{array}{c} a \quad b \\ \square \\ c \quad d \end{array}. \quad (51)$$

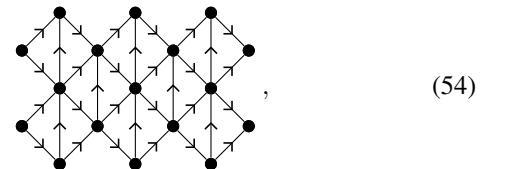
P being a projector corresponds to a move,

$$\begin{array}{c} a \quad b \\ \square \\ c \quad d \end{array} = \begin{array}{c} a \quad b \\ \square \\ c \quad d \end{array}, \quad (52)$$

and the commutativity is a move,

$$\begin{array}{c} a \quad b \\ \square \\ c \quad d \end{array} \begin{array}{c} e \\ \square \\ f \end{array} = \begin{array}{c} e \quad a \\ \square \\ c \quad d \end{array} \begin{array}{c} b \\ \square \\ f \end{array}. \quad (53)$$

Consider a regular triangulation of the plane like the following,



and the associated triangle liquid tensor network. We notice that this network has the form of a circuit, i.e., a product of local operators P , associated to patches

$$P \rightarrow \begin{array}{c} \bullet \\ \swarrow \quad \searrow \\ \bullet \quad \bullet \\ \swarrow \quad \searrow \\ \bullet \end{array} \quad (55)$$

This suggests that we have a liquid mapping

$$\begin{array}{c} a \quad b \\ \swarrow \quad \searrow \\ \bullet \\ \swarrow \quad \searrow \\ c \quad d \end{array} := \begin{array}{c} a \\ \downarrow \\ \bullet \\ \downarrow \\ c \end{array} \rightarrow \begin{array}{c} b \\ \downarrow \\ \bullet \\ \downarrow \\ d \end{array} \quad (56)$$

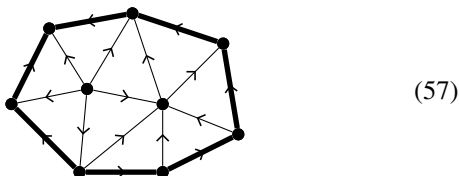
from the commuting-projector liquid to the triangle liquid. Indeed, if we plug Eq. (56) into Eq. (52) or Eq. (53), we see that those can be derived from the moves of the triangle liquid. So every model of the triangle liquid yields a commuting-projector model.

IV. LIQUIDS IN 1 + 1 DIMENSIONS WITH BOUNDARY

In this section we describe how liquids do not only yield ansatzes for fixed-point models of topological phases, but also models for the boundaries thereof as well as other sorts of defects. The boundaries themselves have a topological deformability, which implies that the model has a gap as an open chain. We show that every triangle-liquid model has a standard topological boundary, using the so-called boundary cone mapping. Conversely, we find that the existence of a boundary can be used to circumvent the corner problem in the universality mapping. This implies that all liquids with a topological boundary can be mapped (in a weakly invertible fashion) to the triangle liquid. We also show how to reduce any other sort of defect to a topological boundary using the so-called compactification mapping. Any boundary-liquid model gives rise to a matrix product state (MPS) ground state for the commuting-projector Hamiltonian derived in Section III.5. Furthermore, we introduce invertible domain walls as a kind of topological defect, which provide a way to assert whether two triangle-liquid models are in the same phase.

IV.1 The boundary triangle liquid

In this section we extend the triangle liquid to a liquid on topological 2-manifolds with boundary, which we call *boundary triangle liquid*. It is based on triangulations of 2-manifolds with boundary, such as



for a triangulation of a disk. For better visibility, we draw the boundary edges as thicker lines. A triangle-liquid tensor is associated to each triangle in the interior. Additionally, there is one tensor associated to each boundary edge. More precisely,

the tensor depends on whether the edge is oriented clockwise or counter-clockwise,

$$\begin{array}{c} \vdots \\ \vdots \\ \bullet \quad \bullet \\ \vdots \\ \vdots \end{array} \rightarrow \begin{array}{c} \vdots \\ \vdots \\ \bullet \\ \vdots \\ \vdots \end{array}, \quad (58)$$

and

$$\begin{array}{c} \vdots \\ \vdots \\ \bullet \quad \bullet \\ \vdots \\ \vdots \end{array} \rightarrow \begin{array}{c} \vdots \\ \vdots \\ \bullet \\ \vdots \\ \vdots \end{array}, \quad (59)$$

which for Hermitian models are complex conjugates. The two indices which run along the boundary are drawn with thick lines and potentially have a different bond dimension than the bulk indices, and we must not contract the two different types of indices. Note, that here the boundary is a *physical boundary* where the network terminates without any open indices, in contrast to the open boundary which corresponds to cutting off a network such that open indices emerge.

In order to model homeomorphisms, we also need to be able to change the triangulation of the boundary itself. This is achieved by adding *boundary Pachner moves* which attach (remove) triangles to (from) the boundary. The 2-2 boundary Pachner move,

$$\begin{array}{c} \vdots \\ \vdots \\ \bullet \quad \bullet \\ \vdots \\ \vdots \end{array} \leftrightarrow \begin{array}{c} \vdots \\ \vdots \\ \bullet \quad \bullet \\ \vdots \\ \vdots \end{array}, \quad (60)$$

$$\begin{array}{c} x \quad y \\ \swarrow \quad \searrow \\ \bullet \\ \downarrow \\ a \quad b \end{array} = \begin{array}{c} x \quad y \\ \downarrow \quad \downarrow \\ a \quad b \end{array} \quad (61)$$

is the most important move of the liquid. For full topological invariance, we also need a 1-3 move and different versions of the moves for different choices of branching structure. One move which is useful to consider is

$$\begin{array}{c} \bullet \\ \downarrow \\ \bullet \\ \downarrow \\ a \quad b \end{array} = a \text{ --- } b, \quad (62)$$

which can be interpreted as removing a triangle only attached to a single vertex,

$$\begin{array}{c} \vdots \\ \vdots \\ \bullet \\ \downarrow \\ \bullet \end{array} \leftrightarrow \begin{array}{c} \vdots \\ \vdots \\ \bullet \end{array} \quad (63)$$

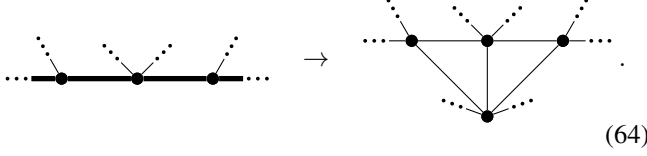
It is possible to find a small set of generating moves, using the principles from Ref. [12], but this is not the focus of this work.

Similar to how the models of the triangle liquid are $*$ -algebras, the models of the boundary triangle liquid are *unitary representations* of those $*$ -algebras. Up to technical details, the boundary triangle liquid is equivalent to the state-sum construction for topological manifolds with boundary in Ref. [22].

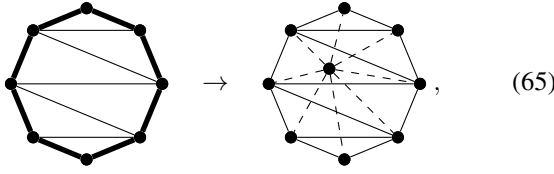
IV.2 The boundary cone mapping

In this section we show that any triangle-liquid model can be extended to a boundary-triangle-liquid model on a purely diagrammatic level. In more physical terms, any fixed-point model of triangle type automatically admits a standard topological boundary.

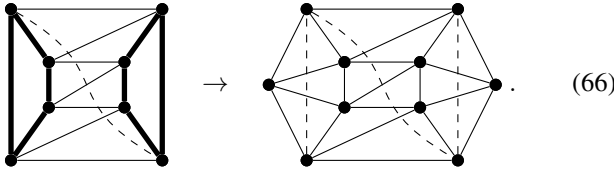
The statement can be formalized as a liquid mapping, which we call *boundary cone mapping*. The mapping maps a triangulation of a manifold with boundary to a triangulation of a closed manifold by filling each boundary circle with a ‘cone’. That is, for every boundary circle, we add one single new central vertex, and for each boundary edge we add a new triangle spanned by that edge and the central vertex,



On the level of manifolds, this amounts to removing the boundary by gluing a disk to every boundary circle. This way, a disk becomes a sphere,



where the drawing on the right consists of a front, and a back layer. Likewise, when the mapping is applied to an annulus, we again obtain a sphere,



Formally, the mapping is given by

$$x \text{---} \square \text{---} y \quad \equiv \quad x \text{---} \bigcirc \text{---} y, \quad (67)$$

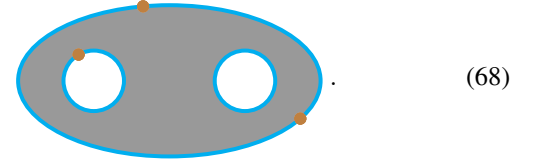
and analogously for the opposite orientation. It is easy to see that the mapped boundary Pachner moves can be derived from the bulk Pachner moves, e.g., the mapping of Eq. (61) directly yields a 2-2 Pachner move. As mentioned earlier, models of the triangle liquid are \ast -algebras, and models of the boundary triangle liquid are unitary representations of the latter. The cone mapping in Eq. (67) simply uses the \ast -algebra as a representation of itself, which is known as the *regular representation*.

IV.3 Other defects and the compactification mapping

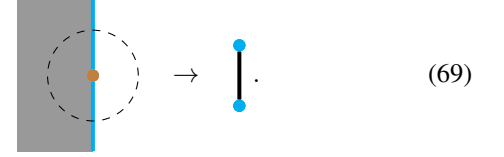
Just like for manifolds with boundary, we can construct liquids for any type of *higher order manifold* (cf. Ref. [23]), i.e., composites of manifolds of different dimensions, meeting, terminating at, and embedded into each other. For example, one can construct liquids describing $2 + 1$ -dimensional manifolds with an embedded $0 + 1$ -dimensional manifold. Models of this liquid are fixed-point models for an anyon worldline/ribbon operator inside a $2 + 1$ -dimensional topological model.

Let us give a very simple example for a type of higher order manifold, which is used in the following section – a 2 -manifold terminating at a 1 -manifold corresponding to a boundary which itself has an embedded 0 -manifold corresponding to *boundary*

defects, e.g.,



In general, the type of a topological defect in a higher order manifold is specified by its dimension d , and its *link*. The link (not to be confused with the link of a simplex in a triangulation, which is similar but different) is another higher order manifold which is obtained by considering the normal space of the defect at an arbitrary point, and then taking the set of points of a fixed distance ϵ from the origin within that normal space. Intuitively, we take the intersection of the higher order manifold with a perpendicular $n - d$ -sphere around a point of the defect, when (locally) embedded in n -dimensional Euclidean space for a large enough n . E.g., for a $d = 0 + 1$ -dimensional anyon worldline in a $n = 2 + 1$ -dimensional space time, the normal space is a plane perpendicular to the anyon world line, and the distance- ϵ set, and hence the link, is simply a circle. For a boundary (in any dimension), the normal space is a half-line and the distance- ϵ set is a single point. For the brown $0 + 0$ -dimensional boundary defect above, the normal space is a half-plane, hence the link is a half-circle, or equivalently, an interval,



Let us give an example of a liquid describing higher order manifolds of the type above. It consists of tensors describing the bulk, the boundary and the boundary defects and a collection of moves which allow topological deformations. As a concrete example we consider the boundary triangle liquid, and add one 2 -index tensor describing the boundary defects and one move which allows to move the defects along the boundary. The defects are represented by special vertices in the boundary to which we associate the 2 -index tensor, i.e.,



To guarantee topological invariance, we need a move that changes the position of the boundary defects,

$$a \text{---} \square \text{---} \bullet \text{---} b \quad = \quad a \text{---} \bullet \text{---} \square \text{---} b. \quad (71)$$

Note that the equation is linear in the defect tensor, so its models (solutions) for array tensors consist of a whole sub-vector space. It is in fact a feature of any kind of $0 + 0$ -dimensional defect that their models form a vector space.

It is useful to note, that models of a d -dimensional defect with link C within some higher-order-manifold liquid are in one-to-one correspondence with models of ordinary $d + 1$ -dimensional boundary liquids via the following *compactification mapping*. Loosely speaking, this is a mapping which maps an ordinary $d + 1$ -manifold M to the higher-order manifold $M \times C$. More precisely, it is a mapping from some network of

an ordinary $d + 1$ -dimensional liquid to a network of the original higher-order-manifold liquid which only extends in the C -direction by some constant combinatorial distance. As an example consider the $d = 0$ -dimensional defect in Eq. (69) and its link. We map a network representing a $0 + 1$ -dimensional manifold M , e.g., a line, to a network representing the 2-dimensional manifold $M \times C$, i.e., a line times a strip of small, constant width,

$$\text{---} \rightarrow \text{---} . \quad (72)$$

A concrete example for a compactification mapping is the mapping from the one-dimensional liquid in Section VI.1 to the boundary triangle liquid,

$$a_0 a_1 \text{---} \blacklozenge \text{---} b_0 b_1 := \begin{array}{c} a_1 \text{---} \blacksquare \text{---} b_1 \\ \downarrow \\ a_0 \text{---} \blacksquare \text{---} b_0 \end{array} . \quad (73)$$

We can extend the compactification mapping to $d + 1$ -dimensional manifold with boundary, by closing off $M \times C$ with $\partial M \times \text{Cone}(C)$. Here, $\text{Cone}(C)$ is $C \times [0, 1]$ with $C \times 1$ contracted to a single point identified with the defect itself. For the defect link in Eq. (69), we close off the thin strip with a point defect,

$$\text{---} \bullet \rightarrow \text{---} \bullet . \quad (74)$$

Further, we can consider coupling the higher-order-manifold liquid to the $d + 1$ -dimensional ordinary liquid by letting the latter terminate at the defect. There is a mapping from this coupled liquid to the higher-order-manifold liquid without the defect, in our case,

$$\text{---} \rightarrow \text{---} . \quad (75)$$

Furthermore, there is a mapping from the higher-order-manifold liquid to the coupled liquid where the $d + 1$ -dimensional liquid additionally has a boundary, by attaching to the defect a thin layer of $d + 1$ -manifold terminated by the boundary, in our case,

$$\text{---} \bullet \rightarrow \text{---} \bullet . \quad (76)$$

Now, using the mapping in Eq. (72), we get an ordinary $d+1$ -dimensional liquid model coupled to the original liquid model via Eq. (75). We can use Eq. (74) to get a model for a boundary of the $d + 1$ -dimensional liquid from the model of the defect. Vice versa, we can use Eq. (76) to obtain a model of the defect from a model of the boundary. We notice that applying first Eq. (76) and then Eq. (74) together with Eq. (75) yields the trivial mapping, so defect models and boundary models of the $d + 1$ -dimensional model are in one-to-one correspondence.

In addition to decorating manifolds with lower-dimensional defects, we can also consider adding moves which change the topology. The implications of this on the possible models are discussed in the next section, where we consider the the following topology-changing move,

$$\text{---} \bullet = \text{---} . \quad (77)$$

Both sides represent a manifold with an open boundary on the outside, but the left-hand side has a puncture with physical boundary on the inside. The brown dot on the blue line represents the $0 + 0$ -dimensional defect on the boundary. The equation symbolizes a move between two concrete networks representing the two corresponding topologies. It suffices to impose one such move, and all equations between other concrete representatives can be derived using the topology-preserving moves.

As a concrete example, consider the boundary-triangle liquid with boundary defects described above. A simple version of a move as above is given by

$$\text{---} \bullet = \text{---} . \quad (78)$$

where the left-hand side represents a ‘1-gon hole’ inside a two-dimensional triangulation, while a self-glued triangle fills the hole on the right-hand side. In terms of networks this move reads

$$\text{---} \bullet = \text{---} . \quad (79)$$

We can use compactification mappings to better understand the structure of the equations that correspond to topology changing moves such as the move in Eq. (77). For the right-hand side of Eq. (77) we consider the compactification mapping,

$$\text{---} \rightarrow \text{---} , \quad (80)$$

needed to calculate models for point defects in the bulk, whose link is a circle,

$$\text{---} \bullet = \text{---} . \quad (81)$$

At endpoints of the line, we can close the tube by a little cup, this time without a point defect at the end,

$$\text{---} \bullet \rightarrow \text{---} . \quad (82)$$

Using this mapping, we can obtain a model on 1-manifolds with boundary from a model on 2-manifolds. For the left-hand side of Eq. (77) we consider the domain wall between the interval-compactification mapping and the circle-compactification mapping,

$$\text{---} \bullet = \text{---} , \quad (83)$$

where the right-hand side corresponds to a tube where we cut out a half-disk with physical boundary on one side. The compactified version of the move in Eq. (77) yields

$$\text{---} \bullet = \text{---} . \quad (84)$$

To interpret the algebraic structure of this move, we note that as we will see in Section VI.1, every model of a one-dimensional liquid is equivalent to a projector. For quantum systems these are (super-)linear maps which can be restricted to their support,

such that a model is simply given by a (super-)vector space. The $0+1$ -dimensional boundaries are vectors x and w , and the domain wall is a matrix M . The above equation is then of the form $Mx = w$, so a boundary defect fulfilling Eq. (77) exists if w is in the image of M .

IV.4 Universality mapping with boundary

In the previous section, we have seen that any model of the triangle liquid admits a standard topological boundary. Thus, this fixed-point ansatz is only suitable for topological phases which admit a gapped/topological boundary. In this section, we will conversely argue that *any* liquid \mathcal{B} for topological 2-manifolds with boundary is equivalent to the triangle liquid. That is, the universality mapping attempted in Section III.4 can be made to work, if we have a topological boundary available.

In order to precisely define the universality mapping we require that the generic topological boundary liquid \mathcal{B} also includes a boundary defect as in Eq. (68) such that the move in Eq. (77) holds. While the topology changing effect of the move is essential for the mapping, the inclusion of the boundary defect on the left hand side of the move is needed to make it work generic models. When we map the triangle liquid to \mathcal{B} , we need to include a tensor corresponding to the boundary defect for the triangle liquid, i.e., we consider a slight generalization of the triangle liquid which includes further 2-index tensors called *vertex weights*.

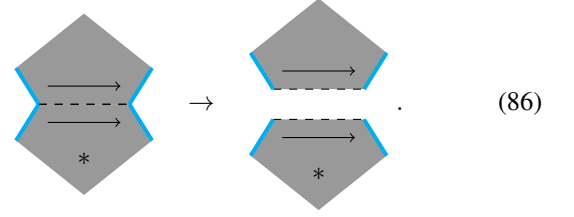
A liquid with vertex weights is defined by the additional condition that we need to insert exactly one vertex weight at one of the bonds of each plaquette that correspond to the network around a vertex of the triangulation. E.g., a valid network representing a triangulation around a 3-valent vertex could look like



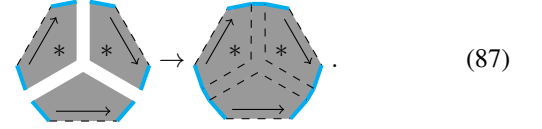
Note, that the generalizations to triangle liquids with vertex weights or boundary liquids with boundary defects are very mild. I.e., any model of a plain boundary liquid can be extended to a model of the full \mathcal{B} under mild conditions, namely that ω is in the image of M in Eq. (84) written as $Mx = \omega$. For robust bosonic intrinsic, SPT or SET topological order, per definition, the model evaluated on a tube is a rank-1 operator. Thus, the one-dimensional model arising from the circle-compactification in Eq. (80) is trivial and corresponds to a 1-dimensional vector space. For symmetry-breaking or fermionic topological order, the corresponding graded- or super-vector-space is still one-dimensional when we restrict to the symmetric or even-fermion-parity sector. So in those cases, we can still trivially find a solution for x . The only examples where we cannot find a solution for x are *non-robust* symmetry-breaking models where we do *not* impose the symmetry with a non-symmetric boundary projecting on one of the symmetry-broken sectors. But even with such a symmetry-breaking bulk, we can find x if we take the symmetric boundary instead of a symmetry-breaking boundary.

Equipped with these prerequisites we are now able to explicitly construct the mapping. To this end we take the rhombus in Eq. (42) and cut off the left and right corner. At the cut we

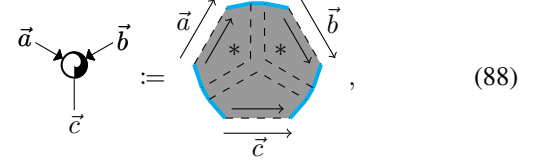
terminate the \mathcal{B} -network using the physical boundary. We then cut it into two corner-truncated triangles,



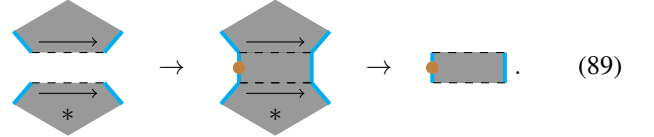
The turquoise line denotes the physical boundary, which does not have any open indices in contrast to the open boundary. Next, we take three corner-truncated triangles and fill the gaps between them,



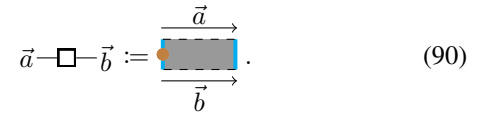
The network obtained in this way is what we associate to the triangle tensor,



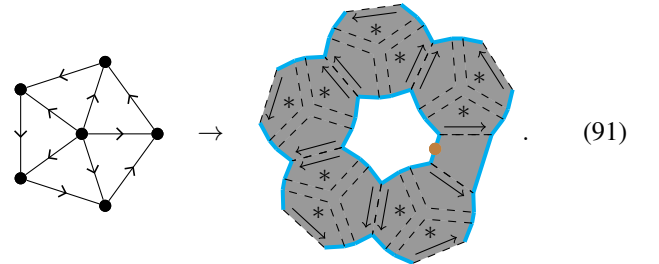
and analogous for the opposite orientation. Now, consider filling the space between two corner-truncated triangles such that there is a boundary defect on one side,



The piece in the middle is what we associate to the vertex weight,

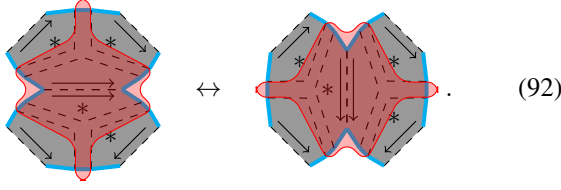


With this choice, the network around any vertex is always valid, irrespective of the configuration of surrounding triangles, e.g.,



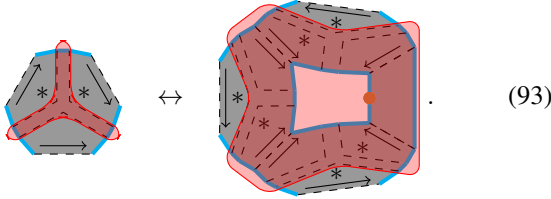
This is because we are just re-gluing patches of \mathcal{B} -networks in the same way they have been cut before. If we apply the mapping to a triangulation, we obtain a manifold with a puncture at each vertex of the triangulation. Every such puncture carries exactly one boundary defect and can thus be removed using the move in Eq. (77). Thus, the mapping is topology-preserving.

The next thing that we have to check is whether the mapped Pachner moves can be derived from the \mathcal{B} -moves. For the 2-2 Pachner move we have



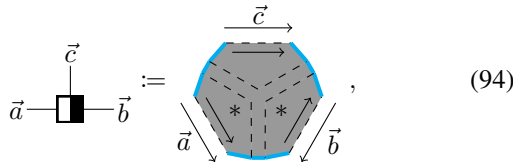
The \mathcal{B} -networks on both sides differ only within the red shaded area. Even though this area involves parts of the physical boundary, it is well isolated from the open boundary. More precisely, the combinatorial distance to the open boundary can be made arbitrarily large by choosing a larger and larger fine-graining scale λ . Thus, no matter how complicated the moves of \mathcal{B} are, we can use them to transform the two sides into each other.

For the 1-3 Pachner move we have

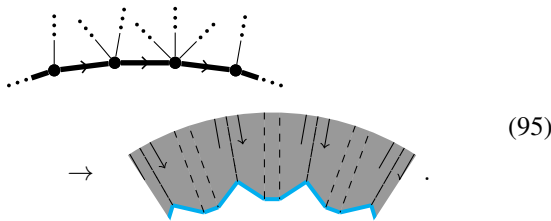


Again, the \mathcal{B} -network only changes in the red shaded region which is separated from the open indices. To transform both sides into each other we also need the move in Eq. (77), in order to remove the puncture on the right-hand side.

We have seen that the triangle liquid is a universal fixed-point form for two-dimensional topological liquid models for which a boundary exists. We will now argue that in addition to that, the boundary triangle liquid is also a universal fixed-point form for the boundary itself. The corresponding universality mapping,



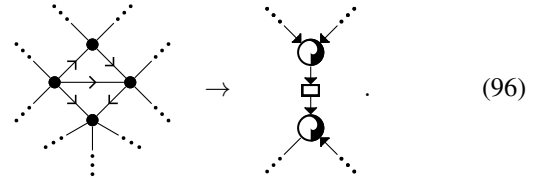
is nothing but the universality mapping in Eq. (88) combined with the cone mapping in Eq. (67). As a consequence, all moves of the boundary triangle liquid are derivable from the moves of the triangle liquid which in turn are derivable from the moves of \mathcal{B} . Furthermore, it is easy to see that the universality mapping applied to a triangulation of a manifold with boundary yields the same manifold with boundary again,



There is one problem with the universality mapping described above though, namely that it is not compatible with

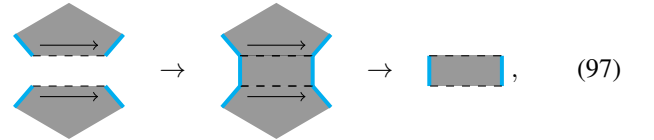
Hermiticity. The latter is a property in liquids with an orientation, i.e., liquids where 1) each index of each tensor is either input or output, 2) in the networks inputs can only be connected to outputs and vice versa, and 3) for each tensor, there is an orientation-reversed dual with inputs and outputs exchanged. A Hermitian model is one where each tensor and its dual are complex conjugates of another. For the triangle liquid, the clockwise and counter-clockwise triangles are duals, and the input indices are were marked with ingoing arrows.

For the Hermiticity of the triangle liquid to follow from Hermiticity of \mathcal{B} , we would need the two truncated triangles in Eq. (86) to be the same apart from orientation reversal. However, there is no guarantee that it is possible to cut the truncated rhombus such that this is the case. Instead, if we want to derive Hermiticity, we have to consider a slight generalization of the triangle liquid. Namely, we have to insert an additional 2-index *edge weight* at each bond (i.e., at each edge of the triangulation), e.g.,



Obviously, we have to also modify the moves by inserting edge weights, e.g., one on each side of the 2-2 Pachner move. For Hermitian models, the clockwise and counter-clockwise triangle tensors are complex conjugates of another as before, and additionally the edge weight is a Hermitian matrix.

In Eq. (86), we cut a truncated rhombus into two halves which couldn't be guaranteed to be equal up to orientation reversal. With the modified liquid, we can instead start with two equal halves (up to orientation reversal), fill the gap between them,



and then use this gap as the edge weight,



Since the two halves in Eq. (97) are equal up to orientation reversal, the \mathcal{B} -networks constructed for the clockwise and counter-clockwise triangle tensor in Eq. (88) will also be equal up to orientation reversal. Furthermore, even if the \mathcal{B} -network in Eq. (98) is not reflection symmetric, it can be chosen so within an arbitrarily large neighbourhood of the open boundary, and thus the original and reflected network are related by \mathcal{B} -moves for a sufficient fine-graining scale. Thus, the Hermiticity of the resulting edge-weight-triangle-liquid model can be derived from the Hermiticity of the \mathcal{B} -model.

If an edge weight X is not only Hermitian but also positive semi-definite, then we can find a square root $X = AA^\dagger$, and include A and A^\dagger to the adjacent triangle tensors. This way, we obtain a Hermitian model of the ordinary triangle liquid without edge weight. However, if X has negative eigenvalues, then

we cannot do so. There are, in fact, models where this is the case. E.g., let the triangle tensor be the \mathbb{Z}_2 group algebra where the output is multiplied with a Pauli Z matrix, let the vertex weight be the scalar $\frac{1}{2}$, and the edge weight be the Pauli Z matrix. In the network representing a triangulation, we get \mathbb{Z}_2 algebra tensors on all triangles and Pauli Z matrices on all edges between a clockwise and a counter-clockwise triangle. So this is a discrete gauge theory summing over a 1-cocycle A with action $(-1)^{(A, \omega_1)}$. ω_1 is a 1-cycle representing the first Stiefel-Whitney class as defined in Section VII.4, and in this case consists of the edges between a clockwise and a counter-clockwise triangle.

IV.5 Ground state tensor networks

Consider a model of the boundary triangle liquid, and a network consisting only of the tensors associated to the boundary edges,

$$\dots \rightarrow \dots \square \square \square \dots \quad (99)$$

of some arbitrarily large boundary circle. The following move,

$$\begin{array}{c} a \\ \diagdown \quad \diagup \\ \square \\ \diagup \quad \diagdown \\ b \\ x \quad y \end{array} = \begin{array}{c} a \\ \circ \quad \circ \\ b \\ x \quad y \end{array} = \begin{array}{c} a \\ \square \quad \square \\ b \\ x \quad y \end{array}, \quad (100)$$

defined via the commuting-projector mapping from Eq. (56), can be derived from the moves in Eq. (61) and a 3-1 Pachner move of the triangle liquid. That is, the tensor in Eq. (99) is invariant under applying the local ground state projectors of the corresponding commuting-projector model. Thus, the tensor is a ground state of the model on a triangulated circle. Tensor networks of the form in Eq. (99) are known as *matrix product states (MPS)* and are commonly used to represent groundstates of gapped local one-dimensional Hamiltonians. Note, that different boundaries for the triangle liquid yield different MPS representations for different families of ground states.

IV.6 Invertible domain walls

In the previous sections, we have found a fixed-point form, and an explicit mapping showing that this form is universal for any model with topological deformability and topological boundary. For a full classification, we still need to answer the question of which fixed-point models are in the same exact phases. In this section we address this problem for models which allow topological boundaries, and obtain algebraic relations which determine whether two models are in the same exact phase. We should keep in mind that as discussed in Section II.3, there might be technical differences between exact phases of fixed-point models and phases defined via continuous gapped paths of path integrals or Hamiltonians.

For n -dimensional topological fixed-point models such as the triangle-liquid models in $n = 2$, a domain wall can be interpreted as a $n - 1$ -dimensional topological defect separating two models. Along the lines of Section IV.3, the link of the defect consists of two points, each corresponding to one of the two models. The corresponding compactification mapping on the models acts as stacking the two models and identifying them with a single model. Models for domain walls are then in one-

to-one correspondence with boundaries of the stacked model, which is well-known as the ‘folding trick’.

As we have seen in Section IV.4, every model with topological boundary can be reshaped into a (boundary) triangle-liquid model, and so can the stack of the two given models. Models of a domain wall then become boundary-triangle-liquid models with respect to the stacked model in the bulk. Such a boundary triangle liquid is determined by a boundary tensor,

$$\begin{array}{c} \text{red} \\ \square \\ \text{blue} \end{array}, \quad (101)$$

whose bulk index is divided into a red and a blue part, corresponding to the two different stacked models. It has to obey the equations coming from the boundary Pachner move with the triangle tensor being a tensor product of a red and blue triangle tensor. Via weakly invertible liquid mappings, this liquid is equivalent to a slightly refined liquid consisting of one separate boundary for the blue and red liquid. The boundaries form a domain wall by ‘interacting’ in the following way. The boundary bond dimensions are equal and the two different boundary tensors (here red and blue) commute,

$$\begin{array}{c} \text{red} \\ \square \\ \text{blue} \end{array} \begin{array}{c} \text{blue} \\ \square \\ \text{red} \end{array} = \begin{array}{c} \text{blue} \\ \square \\ \text{red} \end{array} \begin{array}{c} \text{red} \\ \square \\ \text{blue} \end{array}. \quad (102)$$

The equivalence of this *domain-wall triangle liquid* with the less elegant liquid determined by Eq. (101) is shown in Appendix D.

We want the domain wall to be invertible, which corresponds to further, topology-changing moves as described in Section II.3. These moves allow to generate isolated islands (bubbles) of either model inside of the other, and joining or splitting those bubbles,

$$\begin{array}{c} \text{red} \\ \text{blue} \end{array} \begin{array}{c} \text{red} \\ \text{blue} \end{array} = \begin{array}{c} \text{red} \\ \text{blue} \end{array}, \quad (103)$$

$$\begin{array}{c} \text{red} \\ \text{blue} \end{array} \begin{array}{c} \text{red} \\ \text{blue} \end{array} = \begin{array}{c} \text{red} \\ \text{blue} \end{array}, \quad (104)$$

and

$$\begin{array}{c} \text{blue} \\ \text{red} \end{array} \begin{array}{c} \text{blue} \\ \text{red} \end{array} = \begin{array}{c} \text{blue} \\ \text{red} \end{array}. \quad (105)$$

In general dimensions, invertibility corresponds to moves

$$B_x^{br} \times B_{n-x} = B_x \times B_{n-x}^{rb} \quad (106)$$

for all $0 \leq x \leq n$. Here, B_x is the x -ball, B_x^{br} is a red x -ball with a smaller blue x -ball in the center separated by a domain wall, and B_x^{rb} is the same x -ball but with blue and red exchanged. Note, that the open boundaries on both sides are topologically equal, even though geometrically they are not.

If we apply the universality mapping in Section IV.4 at a sufficiently large fine-graining scale, moves of the above form become moves for the domain-wall triangle liquid,

$$(107)$$

$$(108)$$

and

$$(109)$$

We have thus given a classification of (fixed-point models of) topological order in $1 + 1$ dimensions with topological boundary, in the sense that we have identified those phases with a fixed set of equations (the triangle liquid) for tensor-valued variables modulo another fixed set of tensor variables fulfilling equations (the domain-wall triangle liquid).

V. MORE COMPLEX LIQUIDS IN $1 + 1$ DIMENSIONS

In the previous sections, we have discussed simple liquids with topological boundaries and found a universal ansatz to describe the latter. In this section, we will consider two examples of more complex liquids and show that due to the corner problem discussed previously, one cannot map the triangle liquid to the latter by means of a universality mapping. We also show that in accordance with this, the boundary cone mapping and the commuting projector mapping fail. At last, we show that one of the more complex liquids is a universal for two-dimensional topological liquids, irrespective of the existence of topological boundaries. To do so, we construct a universality mapping to an arbitrary topological liquid which does not suffer from a corner problem. As the more complex liquid has more complicated moves which makes it difficult to find concrete non-trivial models, we provide a strategy called the *operator ansatz* to simplify the description of a liquid at the end of this section.

V.1 The extended triangle liquid

In Section III.4, we tried to argue via a universality mapping that every liquid \mathcal{B} representing two-dimensional topological manifolds is equivalent to the triangle liquid. We found that the corner problem poses an obstruction to this argument. Here we give a first explicit example of a liquid, namely the *extended triangle liquid* for which such a universality mapping indeed fails.

For the extended triangle liquid, a triangulation is again represented by a network with one tensor at every triangle, just as it is the case for the triangle liquid. However, the tensors are not all the same, but depend on the valencies, i.e., the number of adjacent edges, of their corner vertices. Diagrammatically, the tensors are drawn in the same way as for the triangle liquid,

just that we add labels indicating the valencies, e.g.,

$$(110)$$

A model of this liquid consists of one tensor for every triple of numbers, such as $\{4, 5, 7\}$ in the example above. General triangulations can have vertices with arbitrarily high valencies, so in order to represent any triangulation we would need an infinite number of different tensors. However, we can without loss of generality restrict to a finite set of different adjacencies, as we show in Appendix A.

The moves of the liquid are again based on the Pachner moves. However, the 2-2 Pachner move changes the valency of the four vertices at the corners. If we apply a 2-2 Pachner move to a triangulation, this changes not only the tensors at the two triangles directly involved in the move, but also those at the triangles adjacent to the four vertices at the corners. E.g., for the Pachner move below, the tensors at the triangles marked in red *and* blue change

$$(111)$$

Here, the labels at the boundary vertices indicate their valencies. The tensor network equation corresponding to the move above is given by

$$(112)$$

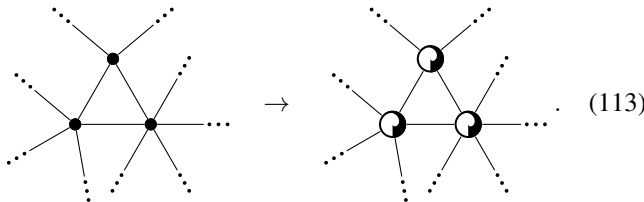
As there are many different 'embeddings' of a Pachner move into a neighbourhood with different adjacencies at the corner vertices, there is a large number of different moves, namely one for each combination of valencies in Eq. (111). This is no conceptual problem since the set of moves is still finite when

we restrict the vertex valencies as hinted at above, but it makes finding concrete models very difficult.

V.2 The vertex liquid

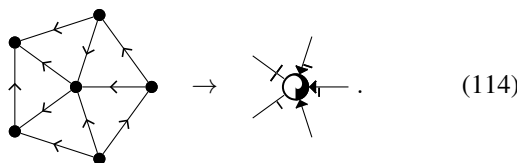
The extended triangle liquid from the previous section has a very large number of complicated moves and is a bit ad hoc. In this section, we will define a more refined liquid called the *vertex liquid*, which is also inequivalent to the triangle liquid, i.e., there is no weakly invertible mapping from the triangle to the vertex liquid due to the corner problem. More interestingly though, we will show in Section V.6 that we can construct a universality mapping to map the vertex liquid to any two-dimensional topological liquid without encountering a corner problem. As a consequence, the vertex liquid is a universal ansatz to describe two-dimensional topological fixed-point tensor network path integrals in the sense that it can emulate any other ansatz.

As the name indicates, the vertex liquid associates one tensor to each vertex of a triangulation. The edges of the triangulation correspond to bonds of the tensor network, such that the diagram of the network looks like the drawing of the triangulation itself, e.g.,



As the vertices in a triangulation have different numbers of adjacent edges, they are represented by different tensors with different numbers of indices. As the number of indices is apparent from the diagrammatic calculus, we use the same shape for these different tensors. E.g., in the network above, all 3 tensors are different, as they have 4-, 5-, and 6 indices, respectively. As for the extended triangle liquid, we would need an infinite amount of tensors to represent triangulations with arbitrary valencies, but we can again restrict to a finite set of adjacencies as shown in Appendix A.

We again consider a triangulation equipped with a branching structure. The tensor associated to a vertex depends on its *star*, that is, the configuration of triangles containing the vertex, including their edge directions. This dependency is indicated by marking the bonds of the tensor with an ingoing arrow, if the corresponding triangle edge is pointing inwards. Also, for triangles with two inward-pointing or two outward-pointing edges, the direction of the third edge opposite to the vertex will be signified by adding a tick to one of the two bonds. The following example illustrates the marking,



For Hermitian models, tensors whose stars are related by a reflection are complex conjugates of each other. The bond dimension of an index at an edge is allowed to depend on the *star* of that edge, i.e., the configuration of the two adjacent triangles including the edge directions. As a consequence, we

are only allowed to contract index pairs corresponding to the opposite corners of the same star. More generally, vertex-liquid networks which do not represent branching-structure triangulations, since they contain non-triangular plaquettes non-matching decorations/markings, are considered *invalid*.

We now describe the moves of the liquid. Instead of giving a finite set of generating moves, it is more convenient to describe a larger infinite set moves which can be derived. The arguments in Appendix A then make it clear that it is always possible to find a finite generating subset. While for the triangle liquid, any equation between two planar, disk-topology networks defines a derived move, this is not possible for the vertex liquid, since valid vertex liquid networks are restricted to triangular plaquettes. E.g., consider the following equation

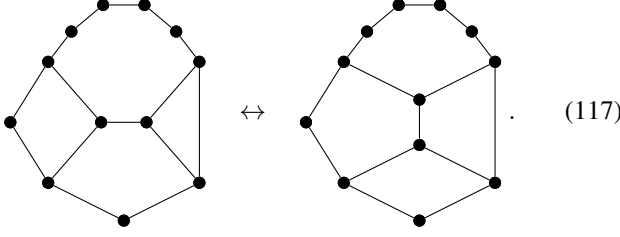
as a move that replaces the network on the left, embedded in some larger vertex-liquid network, with the network on the right. On the left-hand side of the equation, the right-most tensor corresponds to the corner of a triangle which has edges d and e . Applying the move inserts an additional edge between d and e , so the triangle becomes a 4-gon which yields an invalid network. Thus, the equation above cannot define a vertex-liquid move.

Instead, all moves of the vertex liquid must satisfy the following condition: For each pair of consecutive open indices, the numbers of bonds separating them along the boundary on the left and on the right side have to be equal. In Eq. (115), d and e are separated by zero bonds on the left, but by one bond on the right. A straight-forward way to obtain moves which do obey the condition is to take Pachner moves and represent each involved vertex by a tensor. E.g., a 2-2 Pachner move yields

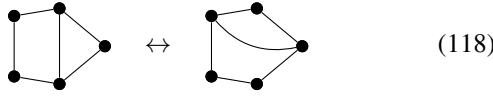
There is one such move for each quadruple of stars for the vertices at the corners. Note that these Pachner moves would already be sufficient to obtain a topological liquid, but it is more convenient to allow further moves.

To get a better feeling for the moves of the vertex liquid, it is instructive to go to the dual lattice, where n -valent vertices become n -gon faces, and triangles become 3-valent vertices. Ignoring all the decorations for a moment, the Pachner move in

Eq. (116) becomes

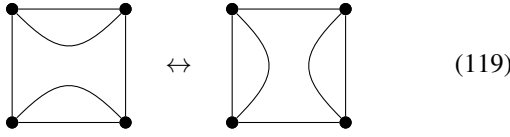


As we can see, it is a 3-valent re-cellulation where the number of internal edges adjacent to each individual boundary vertex (which is either 0 or 1) does not change, such that all vertices remain 3-valent. Intuitively speaking, the move does not change the vicinity of the boundary. This is the key property which will allow us to map to *any* topological liquid from the vertex liquid in Section V.6. When we reconsider Eq. (115) in this picture, it becomes

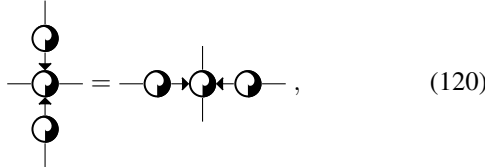


and we immediately see that this re-cellulation does *not* define a move, since there are vertices which have no adjacent internal edge on the left side but one adjacent internal edge on the right side, and vice versa.

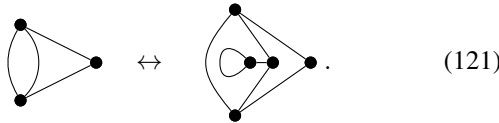
For future reference and to illustrate the set of moves some more, we consider two more examples. The re-cellulation



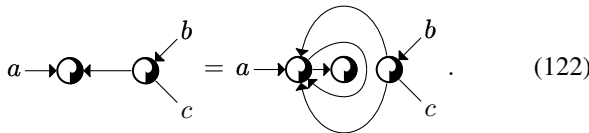
defines the following valid move of the vertex liquid,



and the re-cellulation



corresponds to the following move



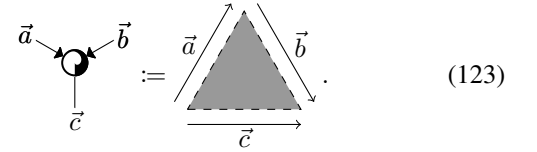
As we can see it is allowed that the non-dual networks do not contain any triangles. The fact that on the left-hand side the boundary bonds separating a and b as well as a and c are the ‘two sides of the same bond’ is not a problem.

V.3 Failure of mapping to the triangle liquid

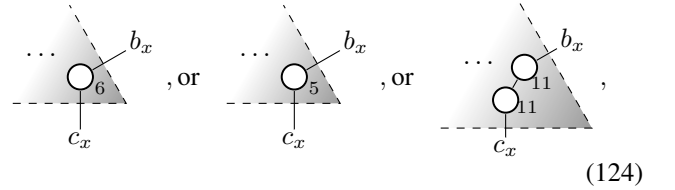
In Section III.4, we have seen that when we attempt to apply a universality mapping to map to an arbitrary liquid \mathcal{B} from the

triangle liquid, we potentially encounter the so-called corner problem and can neither guarantee that the networks obtained via the mapping are valid nor derive the moves via the mapping. In this section we provide two explicit examples where the potential failure actually occurs and show that there cannot be any invertible mapping from the triangle liquid to the extended triangle liquid or the vertex liquid. More precisely, we show that any attempted mapping does neither yield valid networks, nor is compatible with the moves of the extended-triangle-, or vertex liquid.

We start with the extended triangle liquid. The attempted mapping associates to the triangle a connected, planar extended-triangle-liquid network with disk topology, represented by a triangular area

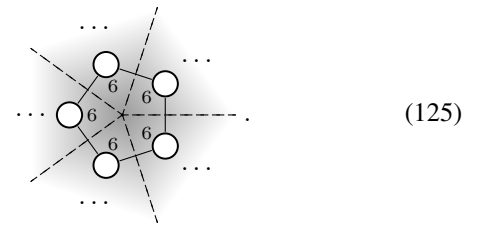


Here, \vec{a} corresponds to a sequence a_0, \dots, a_x of open indices on the boundary of the extended-triangle-liquid network, ordered according to the arrow direction, and \vec{b} and \vec{c} are given analogously. We consider the bottom right corner and the extended-triangle-liquid network connecting the index components b_x and c_x . For different possible choices of the mapping, this corner could look like



or b_x and c_x could be separated by more bonds and the valency labels in the corner could take other values. The point is, that regardless of the specific choice we make for the mapping, no choice can result in a valid extended triangle liquid networks for all initial networks of the triangle liquid. This is due to the fact that the triangle liquid allows for l -valent vertices for *any* l whereas the tensors at the corner of the mapping have fixed adjacency labels. As a result, for every choice of the mapping, there exists a small patch of the triangle liquid with a vertex of adjacency l , such that the adjacency l does not match the adjacency labels of the network obtained from the mapping.

E.g., for the first case in Eq. (124) and an $l = 5$ vertex, we obtain a 5-gon plaquette with tensors valency-6 tensors



The valencies do not match and hence the resulting network is invalid.

Another problem with the attempted mapping is that the mapped moves of the triangle liquid cannot be derived from the extended-triangle-liquid moves. This problem again originates from the fact that the tensors of the triangle liquid do not

carry any information about the adjacency of vertices, whereas this is the case for the extended triangle liquid. E.g., applying the mapping to the 2-2 Pachner move yields

If the mapping is given, e.g., by the first case in Eq. (124), the upper corner of this move looks like

However, this move cannot be derived from the moves of the extended triangle liquid, as it changes the number of edges in the plaquette containing a_x and b_0 by one. So in order to be derivable from the moves of the extended triangle liquid, either the 6 on the right would have to be a 5, or the 6s on the left would have to be 7s. Similar arguments apply for any other choice of the mapping.

For the vertex liquid the situation is similar. Again, an attempted mapping associates to the triangle a vertex-liquid network as in Eq. (123). In the bottom right corner, this network could look like

There could also be more bonds separating b_x and c_x or different ingoing/outgoing arrows. Again, no matter what specific network we choose for the mapping, the resulting networks will be invalid at l -valent networks for some l . E.g., for a 6-valent vertex and the first of the mappings in Eq. (128), we obtain

This network is invalid as it contains a plaquette which is a 6-gon rather than a triangle.

Also, again the Pachner move can not be derived. If we consider the top corner of the move in Eq. (126) for the first mapping candidate in Eq. (128) we obtain

This move cannot be derived from vertex-liquid moves, as a_x and b_0 are two consecutive open indices which are separated by one bond on the left-hand side, but by no bond on the right-hand side.

V.4 Failure of boundary cone mapping

In this section we discuss why there is no analogue to the boundary cone mapping from Section IV.2 for the vertex liquid. In order to be able to talk about a hypothetical boundary cone mapping, we need to extend the vertex liquid with a boundary first, and the simplest way to do so is the following *boundary vertex liquid*. This liquid associates tensors to the boundary vertices of a triangulation of a 2-manifold with boundary, e.g.,

The boundary Pachner moves are implemented by moves such as

Note that under the mild assumption of an extra boundary point defect fulfilling Eq. (77), we can apply the universality mapping in Section IV.4 to obtain a weakly invertible mapping from the simpler boundary triangle liquid. Such a point defect exists in all physically relevant models, so any vertex-liquid model with boundary-vertex-liquid boundary can also be written as a triangle-liquid model with boundary-triangle-liquid boundary. So the boundary vertex liquid is useless for the task of capturing new phases.

Assume there was a boundary cone mapping from the boundary vertex liquid (with boundary point defect) to the vertex liquid. Then we could combine it with the universality mapping in Section IV.4 to obtain a weakly invertible mapping from the triangle liquid to the vertex liquid. As such a mapping does not exist according to Section V.3, also the boundary cone mapping cannot exist. We will nonetheless give a direct argument for why there is no boundary cone mapping, as it is instructive and does not depend on the existence of a boundary point defect.

Assume there was a mapping from the boundary vertex liquid to the vertex liquid. Consider the network that this mapping associates to a boundary vertex tensor. This is a connected planar network with the topology of a disk whose boundary is half-open, half-physical,

Here, \vec{a} and \vec{b} correspond to the sequences of open indices a_0, \dots, a_x and b_0, \dots, b_x , respectively, of the network on the right which are ordered according to the arrow directions. We again consider different possible realizations of the mapping. E.g., along the physical boundary, from the index components a_0 to b_0 , the vertex-liquid network on the right could look like

or like a network with more bonds separating a_0 and b_0 and with another choice of arrow directions.

We again show, that for every possible choice of the mapping, there exist boundary vertex liquid networks which result in invalid vertex liquid networks under the mapping. To this end, we consider a network with a boundary circle consisting of, e.g., four boundary vertices. For, e.g., the first case in Eq. (134) we obtain

$$\text{Diagram (135)} \quad (135)$$

The resulting network has a non-triangular 4-gon plaquette and is hence invalid. For the second case in Eq. (134) we would even obtain an 8-gon.

Moreover, there is a problem when we apply the mapping to boundary vertex liquid moves such as Eq. (132). E.g., for the first case in Eq. (134), we obtain

$$\text{Diagram (136)} \quad (136)$$

This equation cannot be derived from the moves of the vertex liquid as x_0 and y_0 are consecutive open indices which are separated by two bonds on the left-hand side but by only one bond on the right-hand side.

Let us provide some more intuition for why the boundary cone mapping works for the triangle liquid, but does not for the vertex liquid. The networks of both the triangle and the vertex liquid represent triangulations, however, for the triangle liquid we can have x -valent vertices for arbitrarily high x , whereas for the vertex liquid we have $x < l$ for some constant l . In terms of triangulations, the boundary cone mapping fills a boundary circle consisting of b edges by adding the corresponding b -gon and then dividing it into triangles in a pizza-like manner, e.g. for $b = 21$, we have

$$\text{Diagram (137)} \quad (137)$$

On the left is a circle of boundary edges surrounded by 2-manifold on the outside, and a hole in the middle. The right side denotes filling that hole with a triangulation of a disk. The essence of why the boundary cone mapping works is that the network associated to the right side has a one-dimensional structure, in particular, the distance between any of the triangles to the boundary is a constant independent of b . This construction does not work for the vertex liquid, as there is a b -valent vertex on the right, so the corresponding vertex-liquid network is invalid for $b > l$.

If we want to close the hole generated by the boundary by a vertex liquid network, we need to fill the interior of the b -edge circle by a triangulation with some maximum adjacency l , such

as for $l = 7$,

$$\text{Diagram (138)} \quad (138)$$

Closing off the boundary with such a triangulation cannot be formalized as a liquid mapping though, as the combinatorial distance between some vertex in the middle and the boundary becomes arbitrarily large for large b .

To see the last point, define *removing a layer* of a triangulation of a disk as removing all the triangles which contain a boundary edge or a boundary vertex. Removing a layer cannot decrease the size b of the boundary more than by a constant factor, depending on the maximum allowed adjacency l . Thus, we need to remove at least $\sim \log(b)$ layers until nothing is left. On the other hand, the number of layers we have to remove is proportional to the combinatorial distance of some vertices in the middle to the boundary. So this distance grows unboundedly with increasing b .

Note that the tensor network in Eq. (138) has a hyperbolic geometry with a constant negative curvature, similar to a *MERA* state which is usually used for states with conformal instead of topological symmetry.

V.5 Failure of the commuting-projector mapping

In this section, we argue that there also is no analogue of the commuting-projector mapping from Section III.5 for the vertex liquid. We assume that such a mapping exists and then show that it does neither yield valid vertex-liquid networks, nor is it compatible with the vertex-liquid moves. The hypothetical mapping associates to the projector a connected planar vertex-liquid network with disk topology,

$$\text{Diagram (139)} \quad (139)$$

Here, \vec{a} corresponds to a sequence a_0, \dots, a_x of open indices ordered according to the direction of the arrow on the right, and the same holds for \vec{b} , \vec{c} , and \vec{d} . For some choices of the hypothetical mapping, the left corner of the network connecting the index components a_0 and c_0 looks like

$$\text{Diagram (140)} \quad (140)$$

while other choices of mapping can have more bonds separating a_0 and c_0 . The same holds for the other corners with the index pairs (a_x, b_0) , (c_x, d_0) , and (b_x, d_x) .

The plaquettes in commuting-projector-liquid networks can be arbitrary large l -gons, whereas in the vertex-liquid networks only triangle plaquettes are allowed. However, applying

any hypothetical mapping to l -gon plaquettes of a commuting-projector-liquid network, yields vertex-liquid networks with m -gon plaquettes, such that m gets arbitrarily large when l does. E.g., a 4-gon plaquette of the commuting-projector liquid,

$$\dots \begin{array}{c} \square \\ \square \\ \square \\ \square \end{array} \dots, \quad (141)$$

yields a 4-gon plaquette of the vertex liquid for the mapping given by the first diagram in Eq. (140), and to a plaquette with more than four edges in the other cases. Thus, no matter what vertex-liquid network we take on the right hand side in Eq. (139), the mapping does not yield valid networks.

Moreover, the moves of the commuting-projector liquid can map between l -gon plaquettes for different l , whereas the moves of the vertex liquid map triangle plaquettes to triangle plaquettes. Therefore, the mapped commuting-projector-liquid moves cannot be derived from the vertex-liquid moves. E.g., the move in Eq. (52) for the first case in Eq. (140) in the left corner yields

$$\begin{array}{c} a_0 \\ \triangle \\ c_0 \end{array} \dots = \begin{array}{c} a_0 \\ \triangle \\ c_0 \end{array} \dots \quad (142)$$

The resulting move cannot be derived by the vertex-liquid moves, as the consecutive open indices a_0 and c_0 are separated by 0 bonds on the left, but by 1 bond on the right.

V.6 Universality mapping for the vertex liquid

In Section V.3, we have seen that the corner problem described in Section III.4 actually appears when trying to map the vertex liquid from the triangle liquid. In this section, we look at the converse direction and argue that *any* liquid \mathcal{B} describing topological 2-manifolds can be mapped from the vertex liquid using a universality mapping. That is, we show that the vertex liquid is a universal fixed-point ansatz for 2-dimensional topological order, which can emulate any other ansatz. This can be done without running into a corner problem and without any extra conditions on \mathcal{B} .

In order to construct the mapping we again resort to a cutting and gluing procedure. We start with a \mathcal{B} -network on a triangle, such that the corners have combinatorial distance λ and divide this network into 3 kite-shaped parts,

$$\begin{array}{c} \triangle \\ \mathcal{B}\text{-network} \end{array} \rightarrow \begin{array}{c} \text{cut triangle} \\ \text{into 3 kite-shaped parts} \end{array}, \quad (143)$$

which form the building blocks of our construction. Note, that all three kite-networks are different as the arrows indicate. The cuts of the triangle which define the detailed structure of the building blocks can be chosen unambiguously using the branching structure of the reference triangle on the left. We can associate the orientation-reversed network and decomposition to the counter-clockwise triangle.

To construct the \mathcal{B} -network associated to the l -index vertex tensor, we eventually want to glue together l kite-networks around a vertex. Before that, we need to choose a consistent way to glue the kite-networks along the edges. We do this for each star of the edges, i.e., every configuration of two triangles adjacent to the edge. We decompose both triangles into kite-networks, pick the two pairs of kites adjacent to the edge, and place them next to the edge such that they are separated by a gap along the edge. We then fill this gap with some \mathcal{B} -network, and then cut the network along a line perpendicular to the edge, e.g.,

$$\begin{array}{c} \text{Two adjacent triangles} \\ \rightarrow \text{Decomposition into kite-networks} \\ \rightarrow \text{Removal of gap} \\ \rightarrow \text{Filling of gap with B-network} \end{array} \quad (144)$$

Now, for each star of a vertex, we decompose the surrounding triangles into kite-networks, and keep only the kite-networks adjacent to the vertex. We fill the gaps between the kite networks according to Eq. (144), such that only a small gap around the central vertex remains. At last, we fill this remaining gap with \mathcal{B} -network, e.g.,

$$\begin{array}{c} \text{Star of triangles} \\ \rightarrow \text{Decomposition into kite-networks} \\ \rightarrow \text{Filling with B-network} \end{array} \quad (145)$$

The \mathcal{B} -network constructed in this way is used for the mapping, i.e.,

$$\begin{array}{c} \text{Vertex liquid network} \\ \rightarrow \text{B-network patch} \end{array} \quad (146)$$

We now verify our claim, that this prescription defines a valid mapping. To this end, we consider any patch of vertex-liquid network and the associated \mathcal{B} -network, e.g.,

$$\begin{array}{c} \text{Patch of vertex-liquid network} \\ \rightarrow \text{B-network patch} \end{array} \quad (147)$$

At all the points and lines where the different \mathcal{B} -network patches meet, we just re-glue parts which have been cut before. Thus, the resulting \mathcal{B} -network is valid everywhere.

Next we check that the mapped moves of the vertex liquid can be derived from the \mathcal{B} -moves. We consider a move of the vertex liquid, such as

$$\text{Diagram (148)} \quad (148)$$

which, after applying the mapping, corresponds to the following equation between \mathcal{B} -networks,

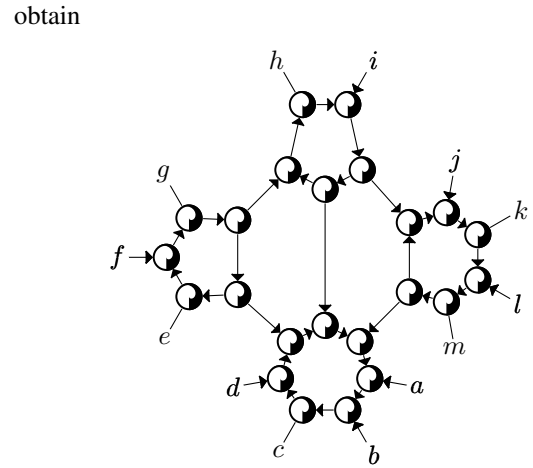
$$\text{Diagram (149)} \quad (149)$$

We observe that the two \mathcal{B} -networks only differ inside the red shaded region. This region is separated from the open boundary by a combinatorial distance which scales linearly with the fine-graining scale λ . Thus, no matter how complicated the moves of \mathcal{B} are, we can use them to transform the networks on the left-hand side to the network on the right-hand side (or vice versa), if we choose a sufficiently large fine-graining scale λ .

Having provided an argument that *any* liquid representing topological 2-manifolds is equivalent to the vertex liquid via a universality mapping, let us now consider two concrete examples. First, we consider the case of \mathcal{B} being the triangle liquid. We can choose a mapping where we replace the n -index vertex tensor with a cycle of n triangle tensors, such as

$$\text{Diagram (150)} \quad (150)$$

Be aware that the tensor on the left-hand side is a vertex liquid tensor, whereas the tensors on the right-hand side are triangle liquid tensors, even though we use the same symbols. If we use the mapping on, e.g., the vertex-liquid move in Eq. (148), we



$$\text{Diagram (151)} \quad (151)$$

This equation corresponds to a retriangularization of a disk, which can be performed by a sequence of Pachner moves. As a consequence the mapped vertex liquid move can be derived from the triangle liquid moves. The same holds true for all other vertex liquid moves.

As a second example, we consider the extended triangle liquid for \mathcal{B} . In this case, we need a slightly larger network,

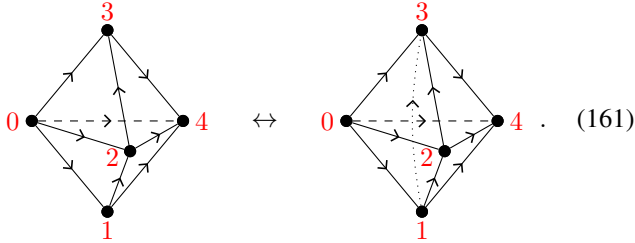
$$\text{Diagram (152)} \quad (152)$$

We cannot take a mapping of the same form as Eq. (150), because for this mapping, the retriangularization resulting from, e.g., Eq. (148) requires Pachner moves involving triangles which contain boundary vertices or edges. If we use the mapping in Eq. (152) instead, the corresponding retriangularization can be performed with Pachner moves acting only on triangles which are distant from the boundary.

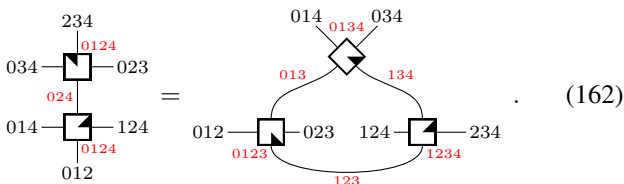
V.7 Operator ansatz

The vertex liquid is quite complicated, as its models consist of a large set of tensors fulfilling a large set of tensor-network equations. More precisely, there is one tensor for every vertex star, and one move for every combination of vertex star for

The Pachner moves in n dimensions can be obtained by considering the boundary of the $n + 1$ -simplex, and dividing it into two parts consisting of x and y n -simplices, respectively, such that $x + y = n + 2$. E.g., for $n = 3$, one Pachner move is given by dividing the boundary of a 4-simplex into two parts containing three and two simplices each,



Here, the left-hand side represents two tetrahedra glued at the 024 face and the right-hand side represents three tetrahedra sharing the 123 edge. As an equation between networks the move corresponds to



For a more detailed description of the simplex liquid in 2+1 dimensions, including a simplified version and the connection to established descriptions of non-chiral topological order via state sums or commuting projector Hamiltonians we refer the reader to Ref. [12].

VI.3 The vertex liquid in higher dimensions

The vertex liquid has a generalization to n dimensions as well. The generalization is straight-forward apart from one subtlety, namely that the vertex-liquid networks in higher dimensions describe triangulations with not only a branching structure, but also a *dual branching*, as defined below. The latter is trivial in the case of triangulations of $1 + 1$ -dimensional oriented manifolds.

To describe the dual branching, we first need to introduce some definitions. The *link* of an x -simplex X in an n -dimensional triangulation is defined as the triangulation of an $n - x - 1$ -sphere formed by the $n - x - 1$ -simplices which together with X span an n -simplex. The *star* $\text{Star}(X)$ is the configuration of all n -simplices containing X . We also consider all sub-simplices of those n -simplices as part of the star, which is sometimes called “closed star” in the literature. The sub-simplices containing X are called the *internal* simplices. We will usually think of the link and star as simplicial complexes on their own rather than as sub-complexes of the triangulation. Note that X can be contained in an n -simplex multiple times, in which case the star contains multiple copies of this n -simplex, and analogous reasoning applies to the link. As such, the link and star contain the same combinatorial information, as the latter is simply spanned by the former together with an x -simplex. However, if the triangulation has a branching structure, then we will also equip the edges of the star with directions, including the edges which are not part of the link.

We conjecture that it suffices to restrict ourselves to triangulations with a finite but large enough set of allowed stars (including branching structure), with canonical representatives. This can be seen using an argument analogous to Appendix A, via a higher-dimensional analogue of a zig-zag triangulation of the n -cells in the cellulation dual to the triangulation. A *dual branching* of an x -simplex X is an identification of the star of X with its canonical representative. If this star does not have any symmetries, then there is only one possible dual branching, otherwise there are as many as there are elements of the symmetry group of the star. Hence, there is a unique dual branching for the edges in a 2-dimensional triangulation, as the two adjacent triangles cannot have any symmetries. Note, that reflection symmetries are not allowed if the triangulation is equipped with an orientation.

An *x -dual-branched triangulation* is one where all the y -simplices with $y \geq x$ carry a dual branching. More precisely, we equip the star of an z -simplex for $z < x$ in a x -dual-branched triangulation with the dual branchings of its internal z -simplices with $z \geq x$. Consequently, also the standard representatives of stars should be equipped with such dual branchings. Thus, in order to define the dual branching we should proceed inductively, starting defining standard representatives for the $n - 1$ -simplex stars, then defining standard representatives for the $n - 2$ -simplex stars containing dual branchings of the internal $n - 1$ -simplices therein, and so on.

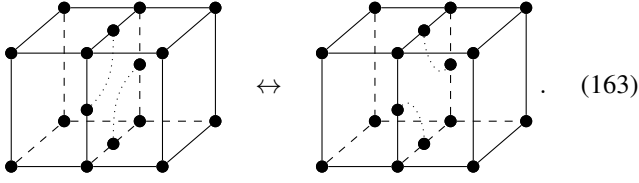
The vertex liquid in n dimensions represents 1-dual-branched, branched triangulations as a network with one tensor at every vertex, depending on the star of that vertex, including the 1-dual-branching of the internal simplices of the star. At every edge, there is a bond, whose dimension is allowed to depend on the star of that edge.

The moves correspond to Pachner moves of the triangulations, and consist of the tensors at all the vertices involved in the Pachner move. This is a sufficient set of generating moves, however, we can write down a larger family of moves which can be consistently added. To this end we go from the triangulation to its dual cellulation, where vertices become n -cells whose boundary is dual to a $n - 1$ -dimensional triangulation. Then, every pair of n -sphere cellulations, which do not differ in the vicinity of the boundary, defines a move. Not differing in the vicinity of the boundary means that the star of all boundary vertices (restricted to the interior) stays the same.

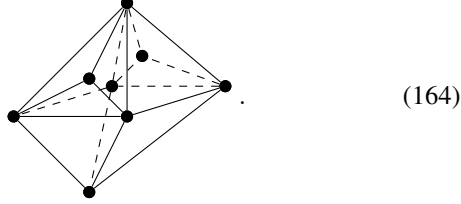
Let us consider the case of $n = 2 + 1$ to be more specific. Possible vertex links are two-dimensional triangulations such as the tetrahedron, the octahedron, or a cube with diagonal edges over all 6 faces. The corresponding stars can be obtained by adding a central vertex spanning simplices with all existing simplices. These stars carry a branching, i.e., non-cyclic edge directions. They also carry a 1-dual-branching, meaning that the configuration of tetrahedra surrounding every internal edge is identified with a canonical configuration. E.g., if there are l surrounding tetrahedra with edge directions allowing for full rotation invariance, then there are l possible choices for the dual branching of that edge. The dual branching of internal triangles is trivial since the two adjacent tetrahedra cannot have any symmetries due to the orientation of the 3-manifold.

The moves are Pachner moves, such as the 2 - 3 Pachner move in Eq. (161) which has five tensors on both the left and right. There is one such move for each choice of stars of the involved vertices. More generally, consistent moves are dual to

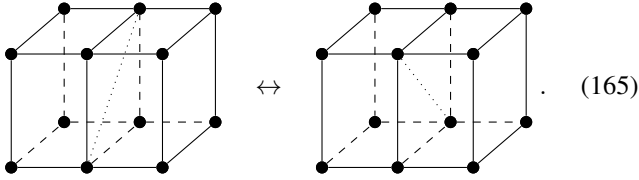
recellulations which do not change the vicinity of the boundary. An example of such a move (not drawing branching and dual branching) is



It consists of two vertex tensors on each side, with three indices contracted between them. The dual 3-cells correspond to vertices of the original triangulation whose link is given by



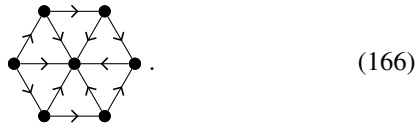
An example for a recellulation which does *not* give rise to a move of the 3-dimensional vertex liquid is



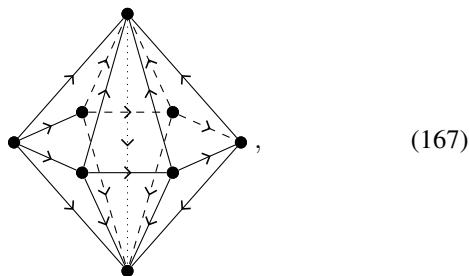
Even though both cellulations have the same boundary, some of the vertices are adjacent to an interior edge on the left but not on the right (or vice versa).

VI.4 Commuting-projector mapping

The commuting-projector mapping from Section III.5 generalizes straight-forwardly to the simplex liquids in n dimensions. The commuting-projector model has degrees of freedom associated to the $n - 1$ -simplices of a $n - 1$ -dimensional triangulation. Consider a star L of a vertex in this $n - 1$ -dimensional triangulation, i.e., a configuration of $n - 1$ -simplices around a vertex. E.g., for $n = 3$, one such configuration is given by



For each such L , there is a projector acting on the degrees of freedom around the vertex, and the Hamiltonian is given by (minus) the sum over the projectors for all vertices. The projector for a given L is obtained from the n -simplex liquid model by evaluating the latter on the n -dimensional triangulation spanned by the exterior simplices of L and an edge. E.g., for the example above in dimension $n = 3$, we obtain a triangulation with 6 tetrahedra,

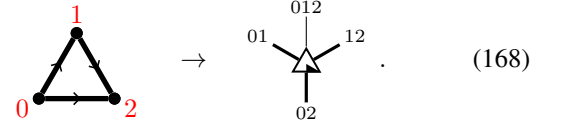


sharing a central edge. The simplex-liquid model for this cellulation evaluates to a 12-index tensor, which is a projector from the 6 bottom indices to the 6 top indices.

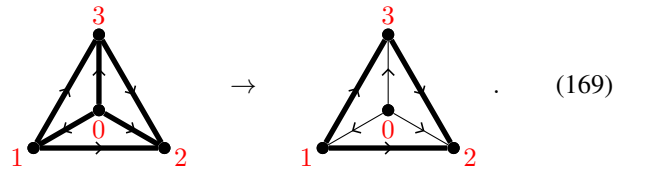
On the other hand, an attempted commuting-projector mapping for the vertex liquid must necessarily fail for reasons analogous to those given in Section V.5. E.g., we could look at a pair of open indices right at the bottom and top of one of the edges on the equator of Eq. (167) which correspond to a plaquette of the network surrounding that edge. Since in a product of projectors, an edge can be adjacent to arbitrarily many projectors, this plaquette cannot always be triangular. Moreover, the projector move equating Eq. (167) with two stacked copies mapped to the vertex liquid would change the plaquette from the triangular to something else, and thus cannot be derived from vertex-liquid moves.

VI.5 Boundary liquid and cone mapping

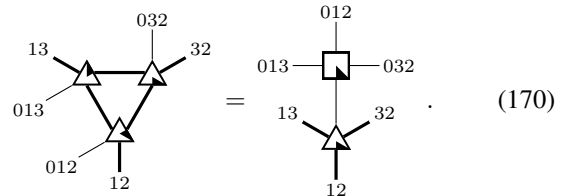
The boundary triangle liquid can be straight-forwardly generalized to a *boundary simplex liquid* in n dimensions. The liquid is based on triangulations of manifolds with boundary. In addition to associating one tensor to each bulk n -simplex, another tensor is associated to the boundary $n - 1$ -simplices. The boundary tensor has one additional index which is connected to a bulk-tensor index. E.g., for $n = 3$, we have an additional triangle tensor,



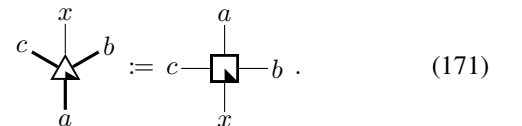
The index labelled 012 is contracted with the indices of the tetrahedron tensors in the bulk, whereas the indices labelled by 01, 02 and 12 are contracted with indices of other boundary tensors and have a potentially different bond dimension than the 012 index. In addition to the bulk Pachner moves, there are boundary Pachner moves that correspond to attaching (removing) a bulk n -simplex to (from) the boundary. E.g., in $n = 3$ dimensions a boundary Pachner move is



As a tensor-network equation this corresponds to



In the same way, the boundary cone mapping from Section IV.2 can be generalized, mapping the boundary $n - 1$ -simplex to the bulk n -simplex. E.g., for $n = 3$, we have



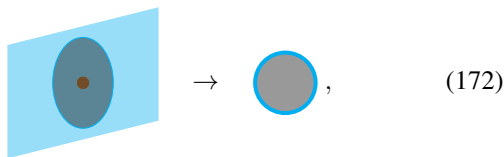
When using this assignment for the boundary Pachner move in Eq. (170), the move reduces to the bulk Pachner move in Eq. (161). As a consequence, every simplex-liquid model has a standard topological boundary obtained from the cone mapping.

Meanwhile, a boundary cone mapping is not possible for the vertex liquid, for reasons analogous to the ones given in Section V.4. We cannot fill boundary triangulations of arbitrary size with a bulk triangulation of constant thickness, due to the restricted finite set of allowed links. The best we can get is again a hyperbolic geometry with a triangulation of logarithmic depth. In higher dimensions, we have the additional problem that closing the boundary with a cone is not a topological operation, as we get a singularity at the center of the cone if the boundary is not a $n-1$ -sphere (which is always the case at least for the connected components in $1+1$ dimensions). This is not a problem for the simplex liquid, as the latter can in fact be defined on n -manifolds with singularities, but the vertex liquid cannot since all vertex links are supposed to be triangulations of spheres.

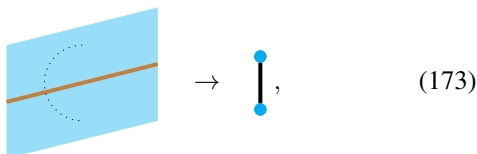
VI.6 Universality mapping with boundary in $2+1$ dimensions

Let us now consider the generalization of the converse direction, namely the universality mapping for topological liquids with boundary \mathcal{B} from Section IV.4. For simplicity, let us first consider the simplex liquid with $n=3$. Similar to the construction in $1+1$ dimensions given in Section IV.4, we need to generalize the boundary liquid \mathcal{B} slightly and require the existence of defects and topology-changing moves similar to the move in Eq. 77. Concomitantly, we also need to generalize the simplex liquid and consider a variant which includes *vertex weights* as well as *edge weights*. I.e., around each edge of the triangulation we need to include one edge weight associated to one of the contracted index pairs 'encircling' the edge, and around each vertex we need to include one vertex weight associated to one of the surrounding index pairs (cf. Ref. [12]).

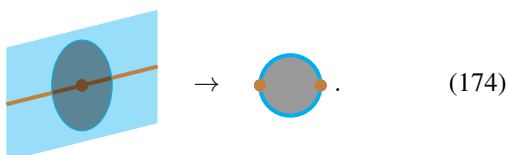
For the boundary liquid \mathcal{B} we require the following additional properties. We need to introduce a $0+0$ -dimensional defect within the $1+1$ -dimensional boundary, whose link (cf. Section IV.3) is a disk,



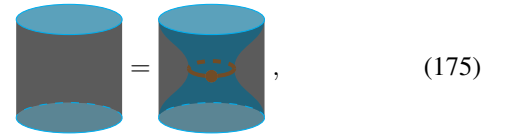
a $0+1$ -dimensional defect within the boundary, whose link is an interval,



and a $0+0$ -dimensional defect within the aforementioned $0+1$ -dimensional defect, whose link is a disk with two defect points,

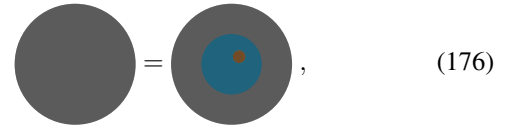


We then require the following two topology-changing moves. The first move



equates a cylinder of \mathcal{B} -network with physical boundaries on the top and the bottom and an open boundary on the side, with a solid torus whose boundary is split into a physical boundary on the inside and an open boundary on the outside. The physical boundary on the inside is decorated with a loop of the defect line that hosts one point defect.

The second move



equates an open-boundary 3-ball with a 3-annulus ($S^2 \times [0, 1]$), that has an open-boundary sphere on the outside and a physical-boundary sphere containing a single point defect on the inside.

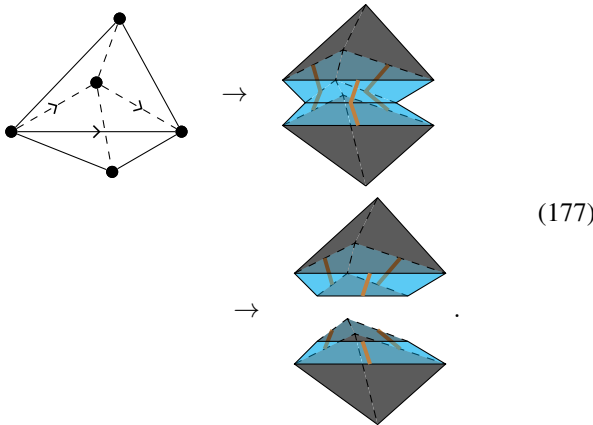
From a practical point of view, it is important to know when a given \mathcal{B} -model with boundary can be extended to a model with additional defects such that the equations above hold. We will answer this question by relating the defects and moves to their lower dimensional counterparts obtained via compactification.

We first consider the move in Eq. (175) which involves a boundary line defect containing a point defect. To find the latter two, we apply the idea compactification mappings from Section IV.3. The line defect in Eq. (173) corresponds to the boundary of the $1+1$ -dimensional model given by compactifying the $2+1$ -dimensional model with the link in Eq. (173). Using that same compactification, the point defect on the line defect becomes a point defect on the boundary of the $1+1$ -dimensional model. If we apply the compactification mapping to Eq. (77), we precisely obtain the move in Eq. (175), which in the reverse direction can be imagined by squeezing the latter in the vertical direction. So the existence of line and point defects fulfilling Eq. (175) is equivalent to the existence of a boundary with point defect of the compactified $1+1$ -dimensional model fulfilling Eq. (77). The latter are exactly the conditions for the $1+1$ -dimensional universality mapping with boundary in Section IV.4. As we argued in that section, those conditions can be seen to be satisfied for any physically relevant phase using another compactification.

We now consider the second move of the generalized liquid stated in Eq. (176) and the point defect needed to define it. Using the compactification mapping for the link of the point defect in Eq. (172), we establish an equivalence between point defects and boundaries of the resulting $0+1$ -dimensional model. Those $0+0$ -dimensional boundaries form a vector space, which from a physical point of view, corresponds to a ground state space of the non-compactified model on a disk. Applying the compactification mapping to Eq. (84) yields Eq. (176), so the latter condition reduces to the former. Analogously to our argumentation in Section IV.4, the former equation holds automatically for any type of robust topological order (including symmetry-breaking order if we do impose the symmetry) with non-degenerate boundary, as the ground space on a disk is one-dimensional.

Let us be more concrete and take a look at the situation for $2 + 1$ -dimensional intrinsic bosonic topologically ordered phases whose anyons form a UMTC \mathcal{M} . In this case different boundaries are in one-to-one correspondence with different fusion categories \mathcal{F} whose Drinfel'd center is \mathcal{M} . The compactification with Eq. (173) yields a non-robust symmetry-breaking-without-symmetry $1 + 1$ -dimensional model, i.e., a GHZ-like superposition of trivial sectors, with one sector for each simple object of \mathcal{F} . More precisely, each sector consists of an α^λ Euler-characteristic classical invariant (cf. Section VII.4) with α being the *quantum dimension* of the simple object. Thus, the irreducible $0 + 1$ -dimensional boundaries of the compactified model and the boundary line defects of the $2 + 1$ -dimensional model are in one-to-one correspondence with the simple objects of \mathcal{F} . In order to guarantee the existence of a boundary defect fulfilling Eq. (175), we need to take as boundary a direct sum in which every simple object occurs at least once. The canonical choice is a boundary which contains each simple object exactly once, such that the vector space of point defects on that line defect is spanned by the simple objects. Then there is a unique choice of the point defect fulfilling Eq. (175), namely the vector formed by the quantum dimensions d_i .

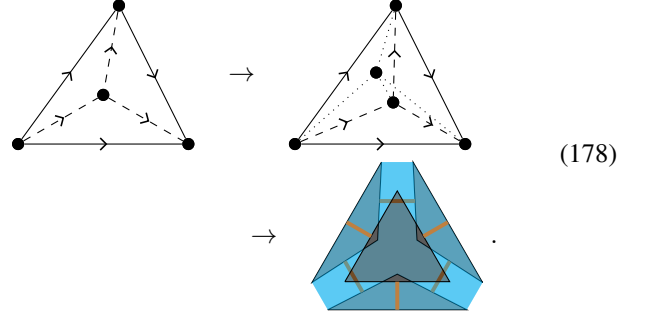
Having analysed the requirements that allow for additional boundary defects and topology-changing moves, we are now in the position to formulate the invertible mapping from the simplex liquid to \mathcal{B} . We start by considering two tetrahedra glued together at one of their faces, and consider them as a patch of 3-manifold with open boundary. Then we remove a neighbourhood of all edges and vertices which are shared by both tetrahedra. The boundary created by the removal is a physical boundary. Next, we place a defect line running across the physical boundary near the center of every edge shared by both tetrahedra. We then fill this manifold including all the defects with \mathcal{B} -network such that all corners have a combinatorial distance of at least λ . Finally, we cut the network into two halves corresponding to the original tetrahedra,



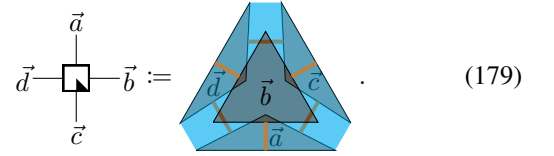
Note, that the triangle shared by both tetrahedra carries a branching structure, which is used to make an unambiguous choice of the cut.

Next, we take four of the tetrahedra whose bottom edges are truncated, bring their top vertices near each other, and glue them by filling all the spaces between them. We obtain a tetra-

hedron where all edges are truncated,

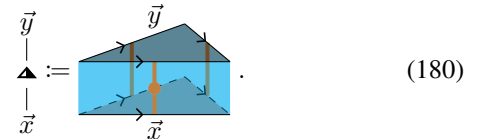


In order to make an unambiguous choice of filling, we can use the branching structure of the reference tetrahedron on the left. The resulting \mathcal{B} -network is what we associate to the tetrahedron tensor,

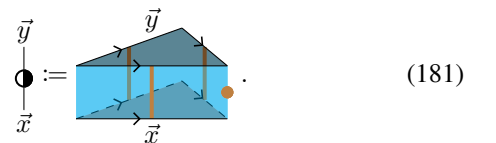


\vec{a} stands for the composite of the open indices located on the corresponding open-boundary triangle, whose ordering can be chosen unambiguously using the branching structure of the corresponding face of the tetrahedron. The same holds for \vec{b} , \vec{c} , and \vec{d} .

The edge weight, which is inserted at some of the bonds corresponding to the triangles of the triangulation, is mapped to a triangle prism which fills the gap between two tetrahedra after performing the cut in Eq. (177). This triangle prism has an open boundary on the bottom and top, and a physical boundary on the sides. Across each side there is a boundary defect line, and a boundary line point defect is placed on the side which corresponds to the edge of the simplex triangulation to which the edge weight is associated. I.e., there are three types of triangle prism, corresponding to the 01, 12 and 02 edge weights as defined in Ref. [12]. As an example, the 02 edge weight mapping is depicted as follows,



The vertex weight is mapped to the same prism, just that instead of the point defect on the line defect, we add a point defect on the boundary



Similar to the edge weights, we can define vertex weights corresponding to the other two corners of the triangle by placing the point defect there.

If we apply the mapping to a triangulation of a 3-manifold, we have to replace every tetrahedron by the truncated-tetrahedron 3-manifold in Eq. (178). This results in a valid

\mathcal{B} -network since we just re-glue parts in the same way we cut them in Eq. (177). However, this \mathcal{B} -network does not represent the original 3-manifold, but one where the neighbourhood of all the vertices and edges of the triangulation has been removed, with the 3-manifold terminating at a physical boundary. Along each edge of the triangulation, there is a tube of vacuum surrounded by a physical boundary, and around this tube wraps a line like defect with one point defect on it. We can use the move in Eq. (175) to fill the tube of vacuum with a cylinder of 3-manifold. Then we are left with a 3-ball of vacuum at every vertex, with one boundary point-defect on the physical boundary. We can use the move in Eq. (176) to fill this ball of vacuum with a ball of 3-manifold. We thus see that the mapping yields a valid \mathcal{B} -network representing the same 3-manifold.

Also, it is easy to see that the mapped Pachner moves yield equations between \mathcal{B} -networks which differ only at places with a certain distance from the open boundary. By choosing a larger and larger fine-graining scale λ for the mapping, we are eventually guaranteed that the two networks are related by \mathcal{B} -moves. In addition, we need the move in Eq. (175) in the derivation of the mapped 2-3 Pachner move, and 4 times Eq. (175) plus one time Eq. (176) in the derivation of a mapped 1-4 Pachner move.

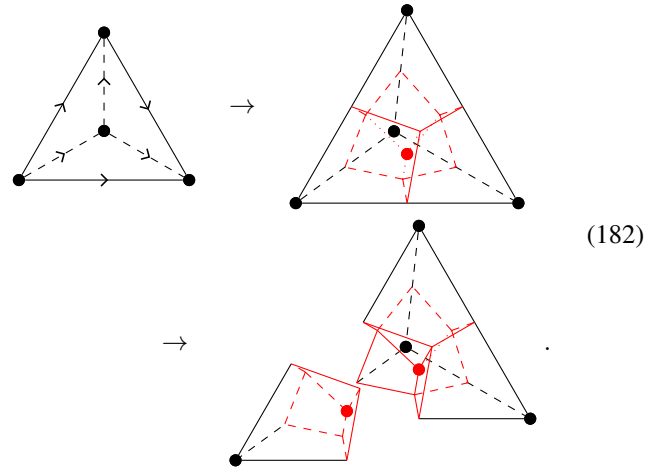
Note that for any robust topological order (including intrinsic, symmetry-breaking, SPT/SET, fermionic models), the space of point-like defects on the boundary is equal to the (symmetry-preserving, even-parity) ground state space on a disk and its dimension is equal to 1. Hence, the vertex weight is just a number. For intrinsic topological order given by a UMTC \mathcal{M} , this number is the inverse square root of the total quantum dimension of \mathcal{M} (which is the inverse total quantum dimension of the fusion category \mathcal{F} describing the boundary). Furthermore, for intrinsic topological order, consider the right hand side of Eq. (180) or Eq. (181) without the point defect as an operator from the bottom to the top. This operator is a projector, and its support can be identified with the fusion space of the three boundary line defects in \mathcal{F} . This way we directly obtain the Turaev-Viro-Barrett-Westbury state sum, which is a slightly refined formulation of simplex liquid models.

VI.7 Universality mapping for vertex liquid

The universality mapping for the n -dimensional vertex liquid generalizes even more straight-forwardly than the one for the simplex liquid with boundary, without the need to add any weight tensors or assuming any extra conditions with defects for \mathcal{B} . For clarity, let us stick to the case $n = 3$. The mapping proceeds in four steps.

In step one, we fill the branching-structure tetrahedron with a \mathcal{B} -network with fine-graining scale λ . We then cut the tetrahedron into 4 ‘kite’ volumes, each of which is the convex hull of one of the corner vertices and the centers of each adjacent edge, triangle, and of the tetrahedron itself. Geometrically, a kite is the same as a deformed cube, where one cube vertex is a corner of the tetrahedron and the cube vertex on the opposite side is the center of the tetrahedron. The cut can be chosen unambiguously using the branching structure or the original tetrahedron. The following picture shows the edges of the cut in red, as well

as what it looks like removing one of the kites,

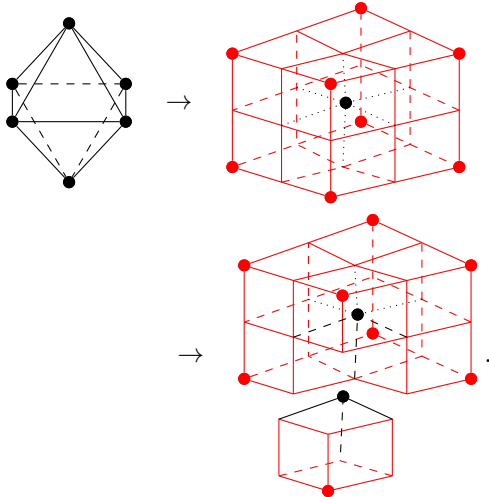


In step two, for each star of a triangle, consider the three adjacent kites of each of the two adjacent tetrahedra, separated by a gap where the triangle is. We then fill the gap and choose a way to cut the result into three pieces, in the same way as we cut the triangle into 2-dimensional kites. The filling can be chosen unambiguously using the orientation of the 3-manifold, and the cut can be chosen using the branching structure on the triangle.

In step three, for each star of an edge, consider the two adjacent kites of each adjacent tetrahedron, with gaps between all of the tetrahedra. Fill the gaps along the triangles between the kites of different tetrahedra using the choices from step two, such that a gap along the edge itself remains. Then, fill this gap with \mathcal{B} -network, and cut it into two pieces along the perpendicular plane going through the center of the edge. Note that in order to fill the gap unambiguously we need the dual branching of the edge which removes any symmetries of its star, and the branching structure of the edge is needed to unambiguously define the cut.

Finally, in step four, for each star of a vertex, consider the adjacent kite of each adjacent tetrahedron, with gaps between the different tetrahedra. Fill the gaps between the tetrahedra along the triangles and the edges using the choices from step two and step three, such that only a gap at the vertex itself remains. Then, fill the remaining gap with \mathcal{B} -network. Note that the choice of filling does not matter since it is distant from the boundary of the surrounding kites, so we do not need a dual branching of the vertices. The so-obtained volume can be identified with the volume dual to the vertex in the dual cellulation. E.g., if the link is an octahedron, then the surrounding kites

yield a volume which looks like a cube,



(183)

The obtained volume is what we associate to the vertex tensor with the same star. Each index of the vertex tensor corresponds to an internal edge of the star. Each such index is mapped to the composite of all the indices on the face of the volume which is dual to this internal edge. In the above example, the open indices at each face of the cube form a composite index. Due to the dual branching of the internal edge dual to that face, we can choose an unambiguous ordering of indices when forming their composite.

We need to show that the \mathcal{B} -network obtained by applying the mapping to a triangulation is valid. To construct this \mathcal{B} -network we replace each vertex by the \mathcal{B} -network filling its dual 3-cell, and then glue all these 3-cells together. In doing so, we simply re-glue patches of \mathcal{B} -network in the same way they have been cut before in the construction. More precisely, at each face of the dual cellulation we re-glue the cut made in step three of the construction. At every edge of the dual cellulation we re-glue the cut from step two, and at every vertex of the dual cellulation we re-glue the cut from step one. We thus see that the resulting \mathcal{B} -network is valid everywhere.

Next we need to check whether the mapped moves of the vertex liquid can be derived from the \mathcal{B} -moves. Recall that the moves of the vertex liquid are dual to re-cellulations, where both sides agree at the boundary as well as at the immediate vicinity of the boundary, as shown in Eq. (163). Now decompose all the volumes of the re-cellulation into kites. We will find that all the kites which have contact with the boundary of the re-cellulation remain the same. The two cellulations only differ at kites in the interior, which are separated from the open boundary by a certain distance. This distance can be made arbitrarily large by increasing the fine-graining scale λ . Thus, no matter what the \mathcal{B} -moves are, they can be used eventually for deriving the mapped vertex liquid moves if we pick a large enough λ .

At this point, the generalization to $n > 3$ is straight-forward: First consider the intersection of an n -dimensional triangulation with its dual cellulation, yielding a decomposition of all x -simplices and all dual x -cells into kites, which are deformed cubes. Then, the construction proceeds in $n + 1$ steps $0, \dots, n$. In the i th step, for every star of an $n - i$ -simplex, we consider the $n - i + 1$ adjacent kites of each adjacent n -simplex (for $i = 0$ there are none), with gaps in between the kites at different tetrahedra. We fill the gaps at the y -simplices ($n - i < y < n$) be-

tween the kites at different n -simplices using the result of step $n - y$, such that only a gap along the $n - i$ -simplex remains. We fill this gap with valid \mathcal{B} -network, and choose a way to cut the resulting network into $n - i$ parts such that the $n - i$ -simplex itself is cut into $n - i$ -dimensional kites. When filling, we take the combinatorial distance between different corners to be at least λ .

VII. FIXED-POINT MODELS FOR NEW PHASES?

In the previous sections we have demonstrated that the potential of fixed-point models has not yet been fully exhausted by known state sum constructions, at least on a purely diagrammatic level. In this sense, we have developed a framework to potentially capture new phases of matter. However, from a practical point of view, the central question is still open: Are there phases which are captured by our new fixed-point ansatz, but not by any of the conventional ones? Unfortunately, at this point, we cannot give a definitive affirmative answer to that question yet. Though, in this section, we will list several indications for why we think this might indeed be the case. As we will see, an important candidate are so-called *chiral* phases of matter.

Before we continue to discuss this point in more detail, let us mention that the question of whether one liquid allows for more general phases than another depends on the tensor type, that is, on the interpretation of the Penrose diagrams in terms of data and computations. In fact, one can write down a tensor type for which the vertex liquid has more general models, however, this tensor type has no apparent physical significance. In this construction the tensors themselves are networks of the vertex liquid, modulo the moves of the latter. The tensor product is given by the disjoint union of networks and contraction is given by connecting open indices in the diagrams. Then, an obvious model of the vertex liquid is given by associating to each tensor the network consisting of that tensor itself. A model of the triangle liquid is the same as a mapping from the triangle liquid to the vertex liquid. One such model is given, e.g., by associating the empty vertex-liquid network to all triangle-liquid tensors. This model is obviously not in the same phase as the vertex-liquid model mentioned above. Models in the same phase would correspond to topology-preserving, hence invertible, mappings from the triangle to the vertex liquid which cannot exist as we argued in Section V.3.

Despite the fact that the example above shows, that we can construct tensor types for which the vertex liquid is more powerful than the triangle liquid, this does not seem to be the case in $1 + 1$ dimensions for array- and similar tensor types with physical significance. Indeed, SPT/intrinsic/fermionic topological phases of matter in $1 + 1$ dimensions have been classified in general to a relatively satisfactory level of rigour. All those phases have gapped/topological boundaries and are therefore captured by triangle-liquid models. The situation is different in $2 + 1$ dimensions as we will discuss in the next section.

VII.1 Chiral phases, commuting-projector models, and topological boundaries

In this section, we consider intrinsic topological phases of matter in $2 + 1$ dimensions which are *chiral*. It has been conjectured that intrinsic topological phases in $2 + 1$ dimensions are

specified by the UMTC \mathcal{M} describing their anyon content together with a number $c \in \mathbb{Q}$ known as the *chiral central charge* [24]. \mathcal{M} determines $c \pmod{8}$, and phases for the same \mathcal{M} but different c are related by stacking with the so-called E_8 phase, which is an invertible intrinsic topological phase with trivial anyon content and $c = 8$. Chiral phases are the ones with $c \neq 0$. They have a few properties which make them incompatible with established fixed-point ansatzes, as we will describe in the following.

Most importantly, chiral phases do not have gapped/topological boundaries. A non-microscopic description of such boundaries is given by the *module category* describing the boundary anyons, their fusion, and their condensation from bulk anyons. Such module categories are in one-to-one correspondence with fusion categories whose Drinfeld center is \mathcal{M} . The Drinfeld center of any fusion category always has a vanishing chiral central charge, thus there are no topological boundaries for chiral phases. Also in the study of non-fixed-point microscopic models for chiral phases, it turns out that no matter what boundary we use, it will always be gapless. In contrast, established fixed-point ansatzes always have topological boundaries via the boundary cone mapping, as we have seen in Section IV.2 and VI.5.

Furthermore, the non-zero chiral central charge of chiral phases is closely related to a non-zero *thermal Hall conductance*. It has been argued in Ref. [5] that chiral topological phases with non-zero thermal Hall conductance do not admit commuting-projector Hamiltonians. This parallels, but is different from the no-go theorem of Ref. [25] proving the vanishing of the *electric Hall conductance* for commuting-projector models. In contrast, established fixed-point ansatzes always allow for commuting-projector Hamiltonians via a commuting-projector mapping, as we have seen in Section III.5 and VI.4.

Moreover, there seem to be some obstructions to represent ground states of chiral Hamiltonians with tensor-networks [26], and certainly the classification of phases via *MPO-injective PEPS* is restricted to non-chiral phases [6]. In contrast, established fixed-point ansatzes always have tensor-network representations for their ground states. As argued in Section IV.5, topological boundaries and tensor-network representations of ground states are one and the same thing in our framework. A standard tensor-network representation can therefore be obtained using the boundary cone mapping, but there are also other representations corresponding to other boundaries.

All of the above restrictions can be circumvented using our more general fixed-point ansatz. As argued in Sections V.4, VI.5, V.5, and VI.4, the constructions for topological boundaries as well as commuting-projector models fail for vertex-liquid models. Furthermore, we have seen in Sections V.6, and VI.7 that the vertex liquid is a universal fixed-point ansatz. That is, if there are any fixed-point models for chiral phases, then there must also be vertex-liquid models of those phases.

We would like to stress once more that the failure of the commuting-projector and the boundary cone mapping is on a purely diagrammatic level, and does *not* concretely imply that there are models of the vertex liquid which do not possess commuting-projector Hamiltonians or topological boundaries. However, given how well the properties of chiral phases fit to the vertex liquid, it is tempting to believe that such models exist.

VII.2 Chiral anomaly and projective tensors

There are plenty of reasons why we would expect chiral topological path integrals to have the same topological deformability as non-chiral ones. An indication for this is that they can be described by a $3-2-1$ -*extended axiomatic TQFT*, namely the *Reshetikin-Turaev construction* [27] based on a UMTC. Also, many of them have microscopic field-theory models with topological invariance, namely *Chern-Simons theories* [28].

However, there is one important detail in which chiral phases differ from non-chiral ones. The topological invariance of the former holds only up to phase pre-factors. Chern-Simons theories with a non-zero chiral central charge have a so-called *chiral anomaly*, also known as *framing anomaly*. This means that the partition function associated to a manifold does not only depend on its topology, but changes by a phase factor when the metric is changed. As different triangulations for combinatorial manifolds play a similar role to different metrics for continuum manifolds, this suggests that a hypothetical discrete version of a chiral Chern-Simons theory should obey re-triangulization invariance only up to phase factors.

The metric dependence in Chern-Simons theory can be removed by introducing an additional structure known as *Atiyah 2-framing*. This structure is of the same type as an orientation or spin structure, with a discrete set of equivalence classes for a given topology. Changes of the Atiyah 2-framing are accompanied by a phase factor depending on the change and the chiral central charge.

Atiyah 2-framings are known to be equivalent to P_1 -structures via *obstruction theory*, similar to how orientations are equivalent to ω_1 -structures and spin structures are equivalent to ω_2 -structures, where P_1 , ω_1 , or ω_2 are *characteristic classes*, namely the first *Pontryagin class* and the first and second Stiefel-Whitney class. For an introduction to (simplicial) cohomology and characteristic classes, we refer the reader to Appendix C. Usually, an X -structure for a degree- i characteristic class X is a choice of $i-1$ -cocycle which trivializes X on a given manifold. However, a P_1 -structure on 3-manifolds cannot be exactly defined this way since P_1 is of degree 4 and does not exist on 3-manifolds, but is represented by a 4-cocycle on 4-manifolds. Thus, a P_1 -structure is represented by an arbitrary 3-cocycle F , and the idea that F trivializes P_1 is implemented only by how F changes when we change the metric. A continuous change of metric of a 3-manifold can be viewed as a 4-manifold Y bounding the initial and final 3-manifolds X_1 and X_2 . Now, the change ΔF corresponding to the change of metric is given by the value of P_1 on this changing 4-manifold.

The phase factor we get from a model with chiral anomaly by changing the metric between two 3-manifolds X_1 and X_2 via a 4-manifold Y is given by

$$e^{2\pi i \frac{c}{24} \int_Y P_1}, \quad (184)$$

where c is the chiral central charge. One way to make the model independent of the metric is to include a bounding 4-manifold Y and the above phase factor into its definition. This agrees with a common definition of an anomalous model – a model which is defined on the boundary of a model in one higher dimension which is somewhat trivial, in this case, the integration over a characteristic class.

Another option is to redefine the model on 3-manifolds X

with a P_1 -structure F by including a phase

$$e^{2\pi i \frac{c}{24} \int_X F}. \quad (185)$$

Again, the obtained model will not depend on the metric, but only on F .

The above viewpoint on chiral anomaly can be made more formal when working combinatorially with triangulations. As discussed, a hypothetical liquid model with chiral anomaly will have invariance under a Pachner move M only up to a phase factor

$$e^{2\pi i \frac{c}{24} \Delta F(M)}, \quad (186)$$

where $\Delta F(M)$ is an integer (or at least a rational number) depending only on what M looks like in a constant-size environment. Pachner moves in $2 + 1$ dimensions can be viewed as gluing 4-simplices to the $3 + 1$ -dimensional triangulation in a 4th dimension. A sequence of Pachner moves then yields a 4-dimensional triangulation bounding the initial and final $2 + 1$ -dimensional triangulations. As explained in Appendix C, P_1 comes with a local formula for a \mathbb{Z} -valued (or at least \mathbb{Q} -valued) 0-cycle with its value on a vertex depending on the star of the latter, and the anomaly in Eq. (184) gives rise to an all-scalar vertex liquid model on $3 + 1$ -dimensional triangulations. For a $3 + 1$ -dimensional triangulation coming from a sequence of $2 + 1$ -dimensional moves, we can redistribute the value of P_1 associated to the vertices such that there is one value for each move M . While it is not obvious that this is possible, the form of the local formula in Ref. [29] ensures this. $\Delta F(M)$ is then exactly given by this value, and accordingly the phase factor in Eq. (186) is given by redistributing the anomaly all-scalar liquid model in Eq. (184). The topological invariance of the $3 + 1$ -dimensional all-scalar liquid model is in accordance with the fact that the phase factors for sequences of moves connecting the same two triangulations have to be equal.

If we want to model chiral phases by a vertex liquid model, there are three kinds of constructions one could aim for. The first possibility is to consider models which fulfil the vertex-liquid equations only up to phase pre-factors. The second possibility is to modify the vertex liquid such that it does not only describe topological 3-manifolds, but also includes a discrete P_1 -structure. Such a P_1 -structure is represented by a 0-cycle F which changes at a Pachner move by ΔF which is given by redistributing the P_1 from vertices of a 4-triangulation to moves on a 3-triangulation. The third possibility is to define the model at the boundary of a 4-dimensional all-scalar (and therefore physically trivial) anomaly liquid model from Eq. (184). The moves of the combined liquid are boundary Pachner moves, attaching or removing a 4-simplex from the boundary. The phase factor in Eq. (186) we get from the corresponding $2 + 1$ -dimensional Pachner move on the boundary is canceled by the contribution of the 4-simplex to the all-scalar bulk liquid model in Eq. (184).

The evaluation of the model with a fixed 3-manifold is undefined for the first possibility above, depends on the P_1 -structure F for the second possibility, and on the bounding 4-manifold for the third possibility. In fact, P_1 is a cobordism invariant (such as all hermitian all-scalar liquid models), and so the evaluation only depends on the cobordism class of the bounding 4-manifold. A popular viewpoint is that different P_1 -structures encode different cobordism classes of bounding 4-manifolds.

According to Eq. (275) in the appendix following from the *Hirzebruch signature theorem*, $\int_Y P_1$ is divisible by 3 on any closed 4-manifold Y . In fact, the value of $\int_Y P_1/3$ precisely labels the different 4-dimensional cobordism classes. Thus, for phases with $c = 0 \pmod{8}$, the evaluation of the model does not depend on the bounding 4-manifold, so in a way one could say the anomaly vanishes *globally*. Those phases are precisely the invertible phases consisting of copies of the E_8 phase with trivial anyon content. It is important to note that this does not imply that the E_8 phase has no anomaly in the sense that we could define the model without P_1 -structure or bounding 4-manifold, since $P_1 \pmod{3}$ does not have a locally computable trivialization as explained in Section III.5. However, the phase obtained by stacking three copies of E_8 does not have an anomaly, and can be defined as a Chern-Simons theory without dependence on a 2-framing [30].

Note that a large part of the mathematical literature on state-sum constructions is motivated by distinguishing manifolds via invariants. Potential chiral state-sums are only moderately suited for this since without additional P_1 -structure or bounding 4-manifold the corresponding invariants are only defined up to a phase. However, this is not at all a problem from a physics perspective. Quantum mechanics or classical statistics ultimately predict probability distributions with a fixed normalization and are therefore agnostic to scalar pre-factors. On the level of tensor-network path integrals this means that it suffices to specify every tensor only up to multiplication with a scalar. If we conversely choose to work with a fixed representative for every tensor, then the tensor-network equations determining a liquid model only need to hold up to scalar pre-factors. We will call equivalence classes of tensors modulo scalar pre-factors *projective tensors*. Projective tensors define a consistent interpretation of the diagrammatic calculus of tensor networks which is formalized by the fact that they form a *compact closed category*, or more generally, a *tensor type* (cf. Ref. [16]).

VII.3 Renormalization and infinite tensors

In Section II.4 we described a fine-graining procedure which might converge to a zero-correlation-length fixed point path integral. If we apply this procedure to a path integral with approximate topological deformability as defined in Section II.5, this fixed-point model is a model of a liquid describing topological n -manifolds. By further fine-graining we can reshape this liquid model into a vertex-liquid model as described in Section V.6 and Section VI.7. If we apply this procedure to a $2 + 1$ -dimensional non-fixed-point tensor-network path integral in a chiral phase and the fine-graining sequence converges, we obtain a vertex-liquid fixed-point model for this phase.

It seems hard to imagine that this fine-graining procedure has no notion of convergence at all, given the variety of different invertible domain walls S_b we are allowed to apply at each fine-graining scale λ . However, it is well conceivable that the limit of the sequence does not converge to a tensor with *finite* bond dimension. So one might consider fixed-point models consisting of tensors with infinite bond dimension. The latter are represented by arrays for which some indices take arbitrary natural numbers as values instead of numbers in a finite range $\{0, \dots, d - 1\}$. The contraction of two indices with infinite bond dimension involves an infinite sum which does not necessarily need to converge. If we want to ensure that the eval-

uation of arbitrary tensor networks is well-defined, we have to impose some *decay condition* for the entries of the tensor, such as imposing that the tensor is normalizable with the norms in Eq. (16) or Eq. (17). For more details we refer to Ref. [16].

In contrast to projective tensors, we are not aware of any precise argument of why infinite tensors would be necessary for vertex liquid models of chiral topological phases. However, such a vertex liquid model would certainly yield a zero-correlation length quantum-spin-system state for a chiral phase, which has not been found to date. We would like to remark that taking finite versus infinite tensors is in principle independent of taking vertex versus simplex liquid models. In principle, there can be non-chiral liquid models with infinite tensor as well as chiral liquid models with finite tensors. The statement that simplex liquid models allow for a standard gapped boundary is independent of the tensor type, and thus holds also for infinite tensors. Conversely this means that even if we allow infinite tensors, we cannot avoid more complex liquids if we want to represent chiral phases.

An interesting example for an infinite-tensor liquid model is the standard state-sum construction [31] for the $2 + 1$ -dimensional group cohomology SPT phases for non-continuous $U(1)$ 3-cocycles, which has been studied in Ref. [32]. The state sum looks like a simplex liquid model, and thus possesses a commuting-projector Hamiltonian and a topological boundary (even though the latter would be symmetry-breaking with a continuous degeneracy). Accordingly, the phase is non-chiral without thermal Hall conductance. However, it has a non-zero electric Hall conductance, and evades the no-go theorem in Ref. [25] as the latter only contradicts *finite-dimensional* commuting-projector models. If we want to formally write the state-sum as a liquid model with infinite tensors we need to a Fourier basis, in which the homogeneous $U(1)$ 3-cocycle becomes a tensor with 4 \mathbb{Z} -valued indices satisfying a decay condition. However, at each vertex there will be a \mathbb{Z} -multiplication tensor which does not obey any decay condition. Potentially, this can be resolved by transferring some of the decay from the cocycle tensors to the \mathbb{Z} -multiplication tensors. If we do so, however, the state-sum has the form of a vertex liquid, and the modified \mathbb{Z} -multiplication tensor at a vertex does not define a commutative algebra any more and cannot be reshaped into a triangle liquid.

VII.4 All-scalar vertex liquid models

In this section we will try to support our conjecture that vertex-liquid models are more general than triangle-liquid models by restricting to models where all tensors are scalars. We will find all-scalar vertex-liquid models in exact phases which cannot be described by all-scalar triangle-liquid models and do not have all-scalar topological boundaries. Interestingly, all exact phases we consider do have non-scalar triangle-liquid models and boundaries though.

The tensor networks of all-scalar models are just products of scalars, so they are trivial as physical models without degrees of freedom and with a 1-dimensional Hilbert space. Furthermore, they are immediately trivial if we resort to projective tensors. Even though the models given in this section do not have any immediate physical relevance, they still demonstrate that there is no general scheme which tells us that triangle-liquid models are always sufficient.

All-scalar liquid models are equivalent to what is often referred to as *classical invariants* in the study of continuum manifolds. Roughly speaking, classical invariants are computed by integrating a quantity over the space-time manifold which only depends on the local presentation of that manifold (e.g., on the metric when expressed in a specific coordinate system). If we discretize the integral to a sum on a triangulation, which we then exponentiate, we obtain an all-scalar liquid model. In contrast, for *quantum invariants*, the local quantity also depends on a field configuration, and we sum an exponentiated action over all field configurations. In this section we look at two particularly simple examples of classical invariants in $1 + 1$ dimensions, and argue that one of them needs to be formulated as a vertex-liquid model. A more systematic approach to obtain all-scalar vertex-liquid models from so-called *characteristic classes* can be found in Appendix C.

The most basic example of a classical invariant is the *Euler characteristic* χ of a 2-manifold computed from a triangulation T by

$$\begin{aligned} \chi(T) &= |S_0(T)| - |S_1(T)| + |S_2(T)| \\ &= \sum_{s_0 \in S_0(T)} 1 + \sum_{s_1 \in S_1(T)} (-1) + \sum_{s_2 \in S_2(T)} 1, \end{aligned} \quad (187)$$

where $S_0(T)$, $S_1(T)$ and $S_2(T)$ are the sets of vertices, edges, and faces of T , respectively. Instead of χ , we can equivalently compute α^χ for some $\alpha \neq 0$, given by

$$\begin{aligned} \alpha^{\chi(T)} &= \alpha^{\sum_{s_0 \in S_0} 1 + \sum_{s_1 \in S_1} (-1) + \sum_{s_2 \in S_2} 1} \\ &= \prod_{s_0 \in S_0} \alpha \prod_{s_1 \in S_1} \alpha^{-1} \prod_{s_2 \in S_2} \alpha. \end{aligned} \quad (188)$$

This can be interpreted as the evaluation of a model of a liquid which associates tensors to the vertices, edges, and faces of a cellulation, where all tensors are scalars. The corresponding topological moves are easily seen to hold. E.g., the 1-3 Pachner move



$$\quad \quad \quad (189)$$

holds due to

$$\alpha(\alpha^{-1})^3 \alpha^3 = \alpha. \quad (190)$$

The two sides of the equation are given by the product of all scalars at the vertices, edges and faces shown in the two pictures above, except for the boundary edges and vertices which are the same for both sides. The model is in a non-trivial exact phase since its evaluation is not equal to 1 on some 2-manifolds, such as α^{-2} on a sphere. The model can be phrased as a triangle liquid model though, at least if we extend the liquid by vertex weights and edge weights as described in Section IV.4. The latter two are simply given by α and α^{-1} , whereas the triangle tensor itself is given by α .

So the α^χ model fails to provide the example we are looking for in this section, for a liquid model which requires the usage of a vertex liquid. In the following, we give another liquid model defined on triangulations of unoriented 2-manifolds, which in contrast is not in the same exact phase as any all-scalar triangle-liquid model, and does not appear to have a topological all-scalar boundary. We will refer to the model as the $(-1)^{\omega^2}$ -model, as it is based on a discretized version of the square of the

first Stiefel-Whitney characteristic class ω_1 , as defined in Appendix C. The model is defined on two-dimensional unoriented branching-structure triangulations with additional dual directions for all edges. It associates to each vertex a number ± 1 depending on its star as follows. We temporarily choose an orientation of the star and mark all internal edges which are between a clock-wise and a counter-clockwise triangle. Then we consider the number $\#r$ of marked edges whose dual direction points clockwise, and the number $\#l$ of marked edges pointing counter-clockwise. The number associated to the vertex is then given by

$$(-1)^{(\#l - \#r)/2} . \quad (191)$$

The result is always ± 1 since the total number of marked edges $\#l + \#r$ is always even and thus $\#l - \#r$ is divisible by 2. Furthermore, it is easy to see that the result is independent of the temporary choice of orientation.

The topological invariance can also be seen as follows. When applying the Pachner move consisting of only clockwise (or only counter-clockwise) triangles shown in Eq. (27), the edge in the interior of the move is not marked, and the markings of the boundary edges do not change, so the numbers $\#l$ and $\#r$ at the involved vertices are not altered. When changing the direction of an edge (if allowed), this changes the orientation of the two adjacent triangles, and thus the marking of the four other edges of those two triangles. Every edge is a clockwise dually oriented edge in the star of one of its vertices, and a counter-clockwise edge of the other, so those contributions cancel. Finally, changing the dual direction of an edge yields a factor of -1 at both of its adjacent vertices if it is marked, and no change otherwise.

The evaluation of the $(-1)^{\omega_1^2}$ model on unoriented 2-manifolds is the same as the evaluation of $(-1)^X$, namely -1 on manifolds of odd non-orientable genus, and 1 on manifolds with even non-orientable genus. However, the two models are not in the same exact phase. This can be seen by considering the evaluation of the two models on an open disk. For $(-1)^{\omega_2}$, we get -1 since the Euler characteristic of the disk is 1 and thus odd, but for $(-1)^{\omega_1^2}$, we get 1 since the disk is orientable. Of course, this evaluation is ambiguous in general since there can be tensors (in our case scalars) right on the open boundary for which we have to specify whether they belong to the disk or not. We will make the argument more precise in Appendix C.

Knowing that $(-1)^{\omega_1^2}$ is in a different phase from $(-1)^X$, it is easy to argue that it cannot be captured by an all-scalar triangle-liquid model given by a triangle tensor a , vertex weight b and edge weight c . The 1-3 Pachner move yields the only non-trivial equation,

$$a^3 b c^3 = a , \quad (192)$$

so we can choose a and c freely with $b = a^{-2} c^{-3}$. We can insert two factors $1 = x x^{-1}$ for some non-zero scalar x at every pair of adjacent edge and triangle, and associate all factors x to the triangles and all factors x^{-1} to the edges. Since each triangle has 3 edges and each edge has 2 adjacent triangles, this defines an invertible domain wall between the model given by a and c , and the model given by $a x^3$ and $c x^{-2}$. Choosing $x = (ac)^{-1}$, we get a domain wall to the model given by $a^{-2} c^{-3}$ and $(a^{-2} c^{-3})^{-1}$, i.e., the α^X model with $\alpha = a^{-2} c^{-3}$. Thus, every real all-scalar unoriented triangle-liquid model is equivalent to the α^X model for some α . As the $(-1)^{\omega_1^2}$ model is inequivalent to the $(-1)^X$ model, it cannot be described by

an all-scalar triangle-liquid model. So we have found an exact phase which admits an all-scalar vertex-liquid model, but not an all-scalar triangle-liquid model.

VII.5 Disentangling Crane-Yetter-Walker-Wang models

State-sum constructions for chiral phases already exist, if we are willing to include an auxiliary dimension. Namely, there is a $3 + 1$ -dimensional topological state-sum construction known as the *Crane-Yetter state-sum* [33] and models of the latter for which the $2 + 1$ -dimensional standard boundary corresponds to a chiral phase. Its commuting-projector Hamiltonian formulation is known in the physics literature as the *Walker-Wang model* [34], and we thus refer to it as the *CYWW model*. The CYWW model is defined for any *unitary braided fusion category* as input. It is a special case of a 4-simplex liquid model, and therefore has a standard topological boundary via the boundary cone mapping.

For the case where the braided fusion category is *modular* (i.e., an UMTC), it is believed that the CYWW model is in a trivial phase. While there is no direct formal proof, there are several indications for this. First, the CYWW for modular input is *invertible*, meaning that stacking two copies, one of them complex conjugated, yields a trivial phase. Even though there are examples of invertible but non-trivial phases with fermions (such as the Kitaev chain) or with symmetries (such as SPTs), all invertible non-chiral intrinsic bosonic topological phases in $2 + 1$ and $1 + 1$ dimensions turn out to be trivial, and one might expect that the same is true in $3 + 1$ dimensions. Note that invertibility implies that the ground state is non-degenerate on any manifold.

Second, the CYWW models have no non-trivial irreducible line or membrane defects, that is, no anyons or loop excitations. Along the lines of Section IV.3, membrane defects are in one-to-one correspondence with the boundaries of the 3-dimensional model obtained by compactifying one of the 4 dimensions into a circle. Line defects are in one-to-one correspondence with the boundaries of the 2-dimensional model obtained by compactifying two of the 4 dimensions into a sphere. Both the 3-dimensional and 2-dimensional model are trivial for the modular CYWW model.

Third, the partition function of the CYWW on a closed 4-manifold X is given by

$$Z(X) = e^{i c \pi \sigma(X)/4} , \quad (193)$$

and is an exponential of the *signature* σ [34], defined in Appendix III.5, whose basis is determined by the chiral central charge c of the input UMTC. Using the Hirzebruch signature theorem (cf. Appendix C), we can express this in terms of the first Pontryagin class P_1 ,

$$Z(X) = (e^{2\pi i \frac{c}{12}}) \int_X P_1 . \quad (194)$$

In Appendix C we discuss how to construct an all-scalar vertex-liquid model evaluating to exactly the same number, $\alpha \int_X P_1$ for $\alpha = e^{2\pi i \frac{c}{24}}$. This is precisely the physically trivial all-scalar model which we used to describe the chiral anomaly in Section VII.2. As we stressed in Section VII.4 and Appendix III.5, the fact that the modular CYWW evaluates to the same numbers as the all-scalar anomaly model does not necessarily imply that the two are in the same exact phase, but it can be seen as a

good indication. In any case, this provides a very neat interpretation of the modular CYWW as a physically non-trivial way of writing the chiral anomaly of the chiral model given by its standard boundary.

Last, and perhaps most importantly, in Ref. [7], the authors have found an explicit *quantum cellular automaton (QCA)* which disentangles the CYWW Hamiltonian model for the three-fermion UMTC on a regular spatial lattice. We will discuss this point more in Section VII.6.

Given the indications above, let us assume that the modular CYWW model is indeed in a trivial phase, and let us further assume that it is in a trivial exact phase (up to prefactors), i.e., it possesses an invertible domain wall to vacuum. An invertible domain wall to vacuum is nothing but a topological boundary with additional moves, and therefore we call it an *invertible boundary*. The latter assumption is supported by the fact that the quantum cellular automaton disentangling the three-fermion CYWW found in Ref. [7] is an overall Clifford map. It is therefore of a discrete, non-approximative nature, and does not involve any non-zero correlation length. One can thus hope that this QCA can be turned into a full fixed-point invertible domain wall. In the following, we first show how to construct a 2 + 1-dimensional model from the standard boundary of the CYWW model, and later motivate why this model indeed represents a chiral phase.

Consider the modular CYWW model together with its standard boundary. Then we can transform the CYWW model into vacuum everywhere inside the bulk using the invertible boundary, and are left with a stand-alone 2 + 1-dimensional model at its standard boundary. A more formal way to obtain the 2 + 1-dimensional model is via a compactification mapping with an interval with the standard boundary on the one side and the invertible boundary on the other side,

$$\begin{array}{c}
 \text{Standard} \\
 \text{boundary} \\
 \bullet \\
 | \\
 \text{CYWW bulk} \\
 \bullet \\
 | \\
 \text{Invertible} \\
 \text{boundary}
 \end{array} . \quad (195)$$

In other words, we take a sandwich of a thin layer of the 3 + 1-dimensional model between the standard and the invertible boundary, and interpret this as a 2 + 1-dimensional model. If we do not want to work on a projective level, i.e., we do not want to ignore phase pre-factors, then the invertible domain wall is not to vacuum, but to the anomaly $e^{2\pi i \frac{\epsilon}{24} P_1}$ all-scalar liquid model. In this case, the compactification yields a 2 + 1-dimensional model at the boundary of the 3 + 1-dimensional all-scalar anomaly model,

$$\begin{array}{c}
 \text{Standard} \\
 \text{boundary} \\
 \bullet \\
 | \\
 \text{CYWW bulk} \\
 \bullet \\
 | \\
 \text{Invertible} \\
 \text{domain wall} \\
 e^{2\pi i \frac{\epsilon}{24} P_1} \\
 \text{anomaly}
 \end{array} \rightarrow \begin{array}{c}
 \text{Compactified model} \\
 \bullet \\
 | \\
 e^{2\pi i \frac{\epsilon}{24} P_1} \\
 \text{anomaly}
 \end{array} . \quad (196)$$

As discussed in Section VII.2, the all-scalar 3 + 1-dimensional

model is nothing but the chiral anomaly of the compactified model.

We now argue why the above 2 + 1-dimensional model obtained from the modular CYWW model indeed represents the chiral phase given by the input UMTC. We will sketch how to show that the anyon content of the 2 + 1-dimensional model above is described by precisely this UMTC. The anyons of the (compactified) 2 + 1-dimensional model are in one-to-one correspondence with the boundaries of the 1 + 1-dimensional model obtained by another compactification with a circle. The two compactifications can be combined into a single compactification of the CYWW with an annulus,

$$\begin{array}{c}
 \text{Red circle} \\
 \text{Blue circle}
 \end{array} \rightarrow \begin{array}{c}
 \text{Red circle} \\
 \text{Blue circle}
 \end{array} . \quad (197)$$

As the red boundary is invertible, this is equivalent to the compactification of the CYWW model with the standard boundary into a disk. As the standard boundary is defined via a cone mapping, this disk is in turn equivalent to a sphere,

$$\begin{array}{c}
 \text{Red circle} \\
 \text{Blue circle}
 \end{array} = \begin{array}{c}
 \text{Blue circle}
 \end{array} = \begin{array}{c}
 \text{Grey circle}
 \end{array} . \quad (198)$$

Thus, the anyons of the 2 + 1-dimensional model are in one-to-one correspondence with the membrane-like (loop-like in space) defects of the CYWW model, which in turn are in one-to-one correspondence to the boundaries of the 1 + 1-dimensional model obtained from the compactification above. The latter is a GHZ-type model, whose boundaries are in one-to-one correspondence with the ground states on S_1 . Those ground states are the same as the ground states of the CYWW model on $S_1 \times S_2$. The ground states of the latter can be thought of as superpositions of networks of lines decorated with simple objects in the 3-dimensional space, weighted by their amplitudes, modulo local relations given by the F - and R -symbols of the UMTC. Since S_2 is simply connected, a set of independent anyon networks spanning the ground state space of the CYWW model on $S_1 \times S_2$ is given by a simple object along $S_1 \times x$ with some fixed $x \in S_2$, for any simple object. So the anyons of the 2 + 1-dimensional model are in one-to-one correspondence with the simple objects of the UMTC. Showing that also the fusion and braiding coincides would require a little more work.

The CYWW model as well as its standard boundary are simplex-liquid models. Thus, the hypothetical fixed-point invertible boundary of the CYWW model can itself not be a boundary-simplex-liquid model. Otherwise, also the compactified 2 + 1-dimensional model would be a 3-simplex-liquid model, which is impossible for a chiral phase. An analogous line of thought can be found in Ref. [7] where it is argued that a QCA disentangling the modular CYWW model cannot be represented by a local unitary circuit. This is because conjugating a commuting-projector Hamiltonian by a local unitary circuit yields another commuting-projector Hamiltonian and a local unitary circuit can be terminated in a light-cone like manner. Thus, a disentangling local unitary circuit could be applied anywhere in the CYWW bulk and terminated just before its standard boundary. This would yield a commuting-projector

Hamiltonian for the boundary alone, which is impossible for a chiral phase. In view of the construction above, we conclude that finding an invertible domain wall for the modular CYWW models seems like the most promising route towards finding vertex-liquid fixed-point models for chiral phases.

VII.6 The three-fermion phase

While we are not in the position to present a fixed-point model for chiral phase of matter, the framework presented here provides a means to tackle this interesting and difficult question. To find an example for a vertex-liquid model of a chiral phase, a good strategy is to concentrate on one simple example of a chiral phase. A promising and reasonable candidate for this is the three-fermion phase [35], labelled by a UMTC with 4 anyons, the trivial one and three fermions. The fusion rules are the same as for the e and m anyons in the toric code, but the braiding is different. The three-fermion phase is a good choice for a number of reasons.

First, it is one of the simplest chiral UMTCs. There are only a few UMTCs with less anyons, including the semion UMTC, or the Fibonacci UMTC. Among them, only the semion UMTC and the \mathbb{Z}_3 UMTC have Abelian fusion rules [36], i.e., unique fusion outcome.

Second, the F - and R -symbols of the three-fermion UMTC can be chosen purely real. Consequently, the three-fermion CYWW model, which is directly built from the F - and R symbols, is a liquid model with real tensors on unoriented triangulations. Physically, reality of the tensors corresponds to imposing a time-reversal symmetry for bosonic models. Accordingly, it has been conjectured that the three-fermion CYWW is a non-trivial SPT phase protected by time-reversal symmetry [35]. In accordance with reality, the chiral central charge of the three-fermion UMTC is $4 \pmod 8$. If we pick the representative with $c = 12$, the chiral anomaly also becomes a purely real all-scalar liquid model,

$$e^{2\pi i \frac{12}{24} P_1} = (-1)^{P_1} = (-1)^{\omega_2^2}, \quad (199)$$

where we used Eq. (271) from Appendix III.4, and the equations are to be understood as equivalences of all-scalar liquid models.

Third, the F - and R -symbols, and hence the tensors of the three-fermion CYWW model, are *stabilizer tensors*, that is, they are tensors which are unique ground states of some stabilizer code. Stabilizer tensors are a subset of array tensors for which tensor networks can be efficiently stored and evaluated even for large networks with many indices. It is thus tempting to think that, in our search for an invertible boundary of the three-fermion CYWW model, we can restrict to models consisting of stabilizer tensors as well.

Fourth, the three-fermion CYWW can be formulated in terms of simplicial cohomology. In general, the CYWW state-sum for an UMTC involves a sum over different anyon labels at every triangle of a 4-dimensional cellulation. At every 4-simplex, we take the 3-dimensional triangulation corresponding to its boundary and thread the corresponding anyon worldlines perpendicular through each triangle. Then, we connect the anyon worldlines coming from the four adjacent triangles at every tetrahedron with fusions. Evaluating the resulting anyon-network in a 3-sphere yields the 15j-symbol associated to the 4-simplex [37]. For the three-fermion UMTC, the anyon labels

on the faces form the group $\mathbb{Z}_2 \times \mathbb{Z}_2$. The fusion rules imply that the two \mathbb{Z}_2 factors of the anyons labelling the faces must be two \mathbb{Z}_2 2-cocycles (cf. Appendix C) A and B . The evaluation of the anyon network corresponding to the 15j-symbol on the 4-simplex is easy since the F -symbols are trivial. It suffices to apply the R -matrix once to the anyon worldlines perpendicular to the triangles 012 and 234 of the branching-structure 4-simplex. This results in a weight

$$(-1)^{A(012)A(234)+B(012)B(234)+A(012)B(234)}, \quad (200)$$

at every 4-simplex [38], which is the same as

$$(-1)^{AUA+BUB+AUB} \quad (201)$$

evaluated on the 4-simplex when we use the cup-product formula from Ref. [39].

Fifth, and most importantly, there is the aforementioned QCA disentangling the three-fermion CYWW model found in Ref. [7]. A QCA is a unitary which maps local operators, acting non-trivially only in some real-space support, to local operators on the same support enlarged by a constant-size margin. When writing the three-fermion CYWW Hamiltonian as a sum of specific commuting projectors, the QCA under consideration maps those projectors to projectors of the form $(1 - Z)/2$ where Z is the Pauli- Z operator on a single qubit. As such, a QCA is *not* a microscopic realization of an invertible domain wall or a continuous gapped path. However, a simple argument [40] shows that any abstract QCA has a concrete representation as conjugation with a *simple PEPO*. The resulting simple PEPO does indeed yield a microscopic model for the invertible boundary of the three-fermion CYWW, which would ultimately result in a microscopic path integral model for the chiral three-fermion phase.

There are two obstacles which prevent the line of thought in the previous paragraph from immediately succeeding in building a vertex-liquid model for the three-fermion phase. First, the QCA found in Ref. [7] is only defined for a regular spatial lattice, whereas we would like to have an invertible boundary that is defined on arbitrary irregular grids and can even be used to change the grid. Second, the simple PEPO resulting from the construction in Ref. [40] is not necessarily uniform, i.e., translation-invariant and determined by the same tensor at every system size. The construction finds a tensor-network super-operator which is a rank-1 projector whose support is the desired QCA unitary. Applying this tensor-network super-operator to any PEPO will yield a PEPO proportional to the QCA unitary, unless the overlap with the latter is 0. One can always find a PEPO with non-zero overlap as PEPOs span the whole operator space (since already product operators do). Now, for a translation-invariant QCA the tensor-network super-operator is uniform as well, but it is not clear whether there exists a uniform PEPO with non-zero overlap with the QCA at any system size.

The disentangling QCA found in Ref. [7] maps Pauli operators to Pauli operators, that is, by definition, it is a Clifford operation. Hence, the QCA unitary as a whole is a stabilizer tensor, just like the tensors of the three-fermion CYWW model itself. Thus, the tensor-network projector super-operator from Ref. [40] consists of stabilizer tensors as well. As stabilizer tensors span the whole vector space, we can obtain a simple PEPO consisting of stabilizer tensors. Moreover, just like the

three-fermion CYWW itself, the QCA as a whole unitary is a real tensor, and thus we can find a real simple PEPO using Ref. [40]. Note that the caveat from the previous paragraph of whether a uniform choice of PEPO exists becomes potentially more severe if we restrict to real and/or stabilizer tensors. E.g., it may well happen that a uniform choice is only possible if we allow tensors with a non-vanishing imaginary part. Note that a real, reflection-invariant invertible domain wall would imply that the conjectured non-trivial three-fermion CYWW time-reversal protected SPT model is actually in a trivial exact phase.

The ultimate goal would be to find an invertible boundary of the three-fermion CYWW model, or more precisely, an invertible domain wall to the all-scalar anomaly liquid model in Eq. (199). Note that in principle, the models $e^{2\pi i \frac{1}{6} P_1}$ and $e^{2\pi i \frac{5}{6} P_1}$ are possible anomalies as well which are evaluate to the same number but are in distinct exact phases. In fact, for the three-fermion CYWW, we can show quite simply that it evaluates to the same number as the suggested anomaly models. Indeed, following Ref. [38], we can use the Wu relation (cf. Eq. (272)) to obtain

$$\begin{aligned}
& \sum_{A,B} (-1)^{\int A \cup A + B \cup B + A \cup B} \\
&= \sum_{A,B} (-1)^{\int (\omega_1^2 + \omega_2 + B) \cup A + B \cup B} \\
&= \sum_B (-1)^{\int B \cup B} \sum_A (-1)^{\int (\omega_1^2 + \omega_2 + B) \cup A} \quad (202) \\
&= \sum_B (-1)^{\int B \cup B} \delta_{0, \omega_1^2 + \omega_2 + B} \\
&= (-1)^{\int (\omega_1^2 + \omega_2)^2} = (-1)^{\int \omega_1^4 + \omega_2^2} = (-1)^{\int \omega_2^2}.
\end{aligned}$$

Note that the first equality is only on the level of evaluations and does not say that the two liquid models are in the same exact phase, since the Wu relation does not correspond to a local equivalence as we stressed in Appendix III.5. All other equality signs do in fact correspond to phase equivalences. The last equation holds for combinatorial oriented 4-manifolds, where ω_1 has a trivializing 4-cycle by definition such that any term containing ω_1 disappears.

Due to the triviality of the 4th Wu class on 4-manifolds, we have

$$\omega_1^4 + \omega_2^2 + \omega_1 \omega_3 + \omega_4 = 0 \quad (203)$$

as equation between cohomology classes. Thus,

$$\omega_2^2 = \omega_4 = \chi \pmod{2} \quad (204)$$

on oriented manifolds, where the first equality is between cohomology classes whereas the second equality is a local equivalence. Thus, judging from the evaluation only, the $(-1)^\chi$ all-scalar model would be another candidate for being in the same phase as the three-fermion CYWW as well. However, this model cannot represent any non-trivial anomaly, since it does have an all-scalar topological boundary as the Euler characteristic is defined on manifolds with boundary. If $(-1)^\chi$ was the anomaly of a 2 + 1-dimensional liquid model, we could compactify with an interval of $(-1)^\chi$ with the 2 + 1-dimensional model on the one and the all-scalar boundary on the other side. This would yield the 2+1-dimensional model without anomaly. Contrary, attempts to construct all-scalar boundaries seem to

consistently fail for the $(-1)^{\omega_2^2}$ model, though we cannot give any proof for this to date.

As we have expressed the 3-fermion CYWW model as a sum over 2-cocycles weighted by a cup product formula, one might hope that the hypothetical invertible boundary can also be expressed in this language. However, this cannot be exactly the case, since the cup product has a formula where its value on an x -simplex only depends on the values of sub-simplices, and consequently can be written as a simplex-liquid model. This would thus yield a simplex-liquid model for the three-fermion phase, which is impossible as argued in the previous section. However, it is possible for the similar toric-code CYWW model. The partition function of the latter can also be written as a sum over two 2-cocycles, this time only weighted by a single cup product,

$$\sum_{A,B} (-1)^{\int A \cup B} \quad (205)$$

(Co-)cycles and the corresponding boundary maps can be extended to manifolds with boundary in two distinct ways. For *closed* cocycles, the boundary map at the boundary is the same as in the bulk and given by summing over values on adjacent simplices. So intuitively, closed cocycles are still given by patterns of closed loops, membranes, etc., inside a manifold with boundary. On the other hand, for *free* cocycles, the boundary map is trivial at the boundary. Thus, free cocycles are patterns of loops, membranes, etc. which are closed in the inside of the manifold, but are allowed to end freely at the boundary.

The cup product of two closed cocycles inside a manifold with boundary can be defined as before. It yields a closed cocycle, and is still compatible with the closed boundary map, i.e., the resulting cohomology class only depends on the cohomology class of the two input cocycles. The same is true for the cup product of a closed and a free cocycle. In contrast, the cup product of two free cocycles is not compatible with the boundary map, as the following example of a green and red free 1-cocycle inside a 2-manifold with blue boundary shows,



The green cocycle is a boundary as a free cocycle and thus in the trivial cohomology class, yet it has an odd intersection number with the red cocycle.

The standard CYWW boundary of both the three-fermion CYWW model in Eq. (201) and the toric-code CYWW model in Eq. (205) corresponds to extending both A and B as closed 2-cocycles. For the toric-code CYWW model, the invertible boundary corresponds to extending A as closed 2-cocycle, but B as free 2-cocycle (or vice versa). In principle, the same type of boundary would also work for the three-fermion CYWW model. However, the term $B \cup B$ in the action is not consistent with cohomology for a free B . The cup product $B \cup B$ can be obtained by shifting one copy of B from a 2-cocycle to a 2-cycle using the branching structure, and then taking the intersection of B with the shifted B . Let B_∂ be the 1-cocycle we get from restricting B to the boundary. For B being a 2-boundary, $B \cup B$ is given by the linking number of B_∂ with its

shifted copy. So we would have to find a path integral defined on B_∂ -coloured 3-triangulations which evaluates to the linking number of B_∂ with its shifted copy if B_∂ is a boundary.

Given a trivialization X of B_∂ , the self-linking number can be obtained by $X \cup B_\partial$, and by summing over all possible X we would obtain a path integral evaluating to the self-linking number. However, summing over trivializations of B_∂ inside the boundary is equivalent to having B closed instead of free. So the resulting boundary would be the standard boundary which is not invertible. The latter would be guaranteed by using an all-scalar path integral evaluating to the self-linking of B_∂ . However, this cannot exist since the self-linking of a single large loop B_∂ can be changed by applying a Dehn twist along another loop linked with the B_∂ -loop which can be arbitrarily far away from B_∂ . Thus, the self-linking cannot be determined only by the triangulation in a constant-size environment of B_∂ . So in order to construct an invertible boundary we would need something in between summing over trivializations of B_∂ and an all-scalar path integral depending on B_∂ . Moreover, the path integral cannot be a state sum of a simplex-liquid type. Attempting to find such a path integral will be left for future work.

VIII. CONCLUSIONS AND OUTLOOK

In this work, we have suggested a new ansatz for fixed point models of topological phases, in terms of tensor-network path integrals with an exact topological invariance. In contrast to other fixed-point ansatzes, it is compatible with the absence of commuting-projector Hamiltonians and gapped boundaries. The inability of fixed-point models to capture chiral topological phases has been the major caveat with this approach to classification. Our ansatz seems like a promising step towards overcoming this restriction. As such, we provide a new instrument for the community to tackle this long-standing question in the study of quantum phases of matter.

The most urgent task remaining is to find a concrete example for a fixed-point model of our ansatz which does not possess a topological boundary. The present work provides a fresh toolbox to tackle such questions. The presumably most promising route for finding such an example seems to be the $3 + 1$ -dimensional modular CYWW model, which is conjectured to be itself in a trivial phase whereas its $2 + 1$ -dimensional standard boundary realizes a possibly chiral topological phase. We have seen that, if the triviality of the modular CYWW actually manifests itself in the existence of an invertible domain wall to vacuum, then this immediately yields a fixed-point model for a chiral phase. Especially promising seem the results of Ref. [7] where the triviality of the three-fermion CYWW is shown via an explicit disentangling QCA. A concrete way forward would be to gain more structural understanding of this QCA, such that one can extend it to a full topological invertible domain wall. This would yield the desired result.

A more direct approach to find new fixed-point models would be to simply solve the equations given by our new fixed-point ansatz and see if we find any new phases. The vertex liquid consists of a finite set of tensor-network equations for a finite set of tensor variables. The latter have a finite number of entries, for which the former define a finite-set of multi-variable polynomial equations. In principle, polynomial equations for a small number of variables can be solved numerically using

a Gauss-Newton or similar method, however, due to the large number of variables even at low bond dimensions, this is practically infeasible. In order to be successful using exhaustive numeric search we have to restrict to a subset of models which can be efficiently optimized or enumerated. Examples for such a restricted subset are models given by stabilizer tensors representing code states of stabilizer codes, or gaussian tensors representing free-fermionic states. An even more restricted subset which might be sufficient to capture the 3-fermion phase is given by a sum over 1-cocycles A in a 3-dimensional triangulation with weights ± 1 associated to the vertices depending on their star and the value of A on its internal edges. We have tried a few different subsets, with no conclusive positive results to date.

The belief that concrete fixed-point models without topological boundary exist is further supported by the situation for classical invariants. As we have seen in Section VII.4 and Appendix C, many classical invariants can be formalized as all-scalar liquid models. In many cases, it seems necessary to use vertex liquid models, and often it appears like they do not feature any topological all-scalar boundaries. It is therefore conceivable that there also exist locally computable quantum invariants which require the vertex liquid.

The suggestion of a new fixed-point ansatz is by no means the only point of this work. In fact, the main technical result is our notion of universality for topological fixed-point ansatzes. Using a tool called a universality mapping, we show that some fixed-point ansatzes can emulate any other fixed-point ansatz for a certain type of topological order. We apply this procedure to topological order in general as well as topological order with topological boundary. In the former case, the vertex liquid is a universal fixed-point ansatz, whereas in the latter case, we arrive at a variant of the simplex liquid, which is indeed equivalent to the most general versions of established fixed-point ansatzes. This way, we are able to provide a very clear explanation why those ansatzes look the way they do. Mathematically, the universality mapping from the vertex liquid could be phrased as providing a normal form of locally computable quantum invariants of piece-wise linear manifolds.

Acknowledgments

We thank the DFG, CRC 183, for which it is a Berlin-Cologne internode publication within project B01, and EI 519/15-1, for support.

References

- [1] Bulmash, D. & Barkeshli, M. Absolute anomalies in (2+1)d symmetry-enriched topological states and exact (3+1)d constructions. *Phys. Rev. Research* **2** 043033 (2020). 2003.11553.
- [2] Levin, M. A. & Wen, X.-G. String-net condensation: A physical mechanism for topological phases. *Phys. Rev. B* **71**, 045110 (2005). cond-mat/0404617.
- [3] Turaev, V. G. & Viro, O. Y. State sum invariants of 3-manifolds and quantum 6j-symbols. *Topology* **31**, 865–902 (1992).

- [4] Barrett, J. W. & Westbury, B. W. Invariants of piecewise-linear 3-manifolds. *Trans. Amer. Math. Soc.* **348**, 3997–4022 (1996). hep-th/9311155.
- [5] Kapustin, A. & Spodyneiko, L. Thermal hall conductance and a relative topological invariant of gapped two-dimensional systems. *Phys. Rev. B* **101**, 045137 (2020). 1905.06488.
- [6] Bultinck, N. *et al.* Anyons and matrix product operator algebras. *Ann. Phys.* **378**, 183–233 (2017). 1511.08090.
- [7] Haah, J., Fidkowski, L. & Hastings, M. B. Nontrivial quantum cellular automata in higher dimensions (2018). 1812.01625.
- [8] Cirac, J. I., Perez-Garcia, D., Schuch, N. & Verstraete, F. Matrix product states and projected entangled pair states: Concepts, symmetries, and theorems (2020). 2011.12127.
- [9] Orús, R. A practical introduction to tensor networks: Matrix product states and projected entangled pair states. *Ann. Phys.* **349**, 117–158 (2014). 1306.2164.
- [10] Eisert, J., Cramer, M. & Plenio, M. B. Area laws for the entanglement entropy. *Rev. Mod. Phys.* **82**, 277 (2010). 0808.3773.
- [11] Bridgeman, J. C. & Chubb, C. T. Hand-waving and interpretive dance: An introductory course on tensor networks. *J. Phys. A* **50**, 223001 (2017). 1603.03039.
- [12] Bauer, A., Eisert, J. & Wille, C. A unified diagrammatic approach to topological fixed point models (2020). 2011.12064.
- [13] Barthel, T., Pineda, C. & Eisert, J. Contraction of fermionic operator circuits and the simulation of strongly correlated fermions. *Phys. Rev. A* **80**, 042333 (2009). 0907.3689.
- [14] Bultinck, N., Williamson, J., Haegeman, J. & Verstraete, F. Fermionic projected entangled-pair states and topological phases. *J. Phys. A* **51**, 025202 (2017). 1707.00470.
- [15] Wille, C., Buerschaper, O. & Eisert, J. Fermionic topological quantum states as tensor networks. *Phys. Rev. B* **95**, 245127 (2017). 1609.02574.
- [16] Bauer, A. & Nietner, A. Tensor types and their usage in physics (2021). In preparation.
- [17] Bravyi, S. & Hastings, M. B. A short proof of stability of topological order under local perturbations. *Commun. Math. Phys.* **307**, 609 (2011). 1001.4363.
- [18] Aasen, D., Bulmash, D., Prem, A., Slagle, K. & Williamson, D. J. Topological defect networks for fractons of all types. *Phys. Rev. Research* **2**, 043165 (2020). 2002.05166.
- [19] Haah, J. Bifurcation in entanglement renormalization group flow of a gapped spin model. *Phys. Rev. B* **89**, 075119 (2014). 1310.4507.
- [20] Pachner, U. P. 1. homeomorphic manifolds are equivalent by elementary shellings. *Europ. J. Comb.* **12**, 129 – 145 (1991).
- [21] Fukuma, M., Hosono, S. & Kawai, H. Lattice topological field theory in two dimensions. *Commun. Math. Phys.* **161**, 157–176 (1994). hep-th/9212154.
- [22] Lauda, A. D. & Pfeiffer, H. State sum construction of two-dimensional open-closed topological quantum field theories. *J. Knot. Theor. Ram.* **16**, 1121–1163 (2007). math/0602047.
- [23] Bauer, A., Eisert, J. & Wille, C. Towards a mathematical formalism for classifying phases of matter (2019). 1903.05413.
- [24] Wen, X.-G. A theory of 2+1d bosonic topological orders. *Natl. Sci. Rev.* **3**, 68–106 (2016). 1506.05768.
- [25] Kapustin, A. & Fidkowski, L. Local commuting projector hamiltonians and the quantum hall effect. *Commun. Math. Phys.* (2019). 1810.07756.
- [26] Dubail, J. & Read, N. Tensor network trial states for chiral topological phases in two dimensions and a no-go theorem in any dimension. *Phys. Rev. B* **92**, 205307 (2015). 1307.7726.
- [27] Reshetikhin, N. & Turaev, V. Invariants of 3-manifolds via link polynomials and quantum groups. *Invent. Math.* **103**, 547–597 (1991).
- [28] Witten, E. Quantum field theory and the jones polynomial. *Comm. Math. Phys.* **121**, 351–399 (1989).
- [29] Gaifullin, A. A. Local formulae for combinatorial pontrjagin classes. *Izv. Math.* **68**, 861–910 (2004). math/0407035.
- [30] Randal-Williams, O., Tsui, L. & Wen, X.-G. Quantization of chern-simons topological invariants for h-type and l-type quantum systems (2020). 2008.02613.
- [31] Chen, X., Gu, Z.-C., Liu, Z.-X. & Wen, X.-G. Symmetry protected topological orders and the group cohomology of their symmetry group. *Phys. Rev. B* **87**, 155114 (2013). 1106.4772.
- [32] DeMarco, M. & Wen, X.-G. A commuting projector model with a non-zero quantized Hall conductance (2021). 2102.13057.
- [33] Crane, L. & Yetter, D. N. A categorical construction of 4d tqfts (1993). hep-th/9301062.
- [34] Walker, K. & Wang, Z. (3+1)-tqfts and topological insulators. *Front. Phys.* **7**, 150 (2012). 1104.2632.
- [35] Burnell, F. J., Chen, X., Fidkowski, L. & Vishwanath, A. Exactly soluble model of a 3d symmetry protected topological phase of bosons with surface topological order. *Phys. Rev. B* **90**, 245122 (2014). 1302.7072.
- [36] Rowell, E., Stong, R. & Wang, Z. On classification of modular tensor categories. *Comm. Math. Phys.* **292**, 343–389 (2009). 0712.1377.

- [37] Williamson, D. J. & Wang, Z. Hamiltonian models for topological phases of matter in three spatial dimensions. *Ann. Phys.* **377**, 311–344 (2017). 1606.07144.
- [38] Chen, Y.-A. & Tata, S. Higher cup products on hypercubic lattices: application to lattice models of topological phases (2021). 2106.052747.
- [39] Steenrod, N. E. Products of cocycles and extensions of mappings. *Ann. Math.* **48**, 290–320 (1947).
- [40] Piroli, L. & Cirac, J. I. Quantum cellular automata, tensor networks, and area laws. *Phys. Rev. Lett.* **125**, 190402 (2020). 2007.15371.
- [41] Levitt, N. & Rourke, C. The existence of combinatorial formulae for characteristic classes. *Transactions of the American Mathematical Society* **239**, 391–397 (1978).
- [42] Goldstein, R. Z. & Turner, E. C. A formula for stiefel-whitney homology classes. *Proc. Amer. Math. Soc.* **58**, 339–342 (1976).
- [43] Gaifullin, A. A. & Gorodkov, D. An explicit local combinatorial formula for the first pontryagin class. *Russ. Math. Surv.* **74**, 6 (2019).
- [44] Gaiotto, D. & Kapustin, A. Spin tqfts and fermionic phases of matter. *Int. J. Mod. Phys. A* **31**, 1645044 (2016). 1505.05856.
- [45] May, J. *A Concise Course in Algebraic Topology*. Chicago Lectures in Mathematics (University of Chicago Press, 1999). URL <https://www.math.uchicago.edu/~may/CONCISE/ConciseRevised.pdf>.
- [46] Brown, E. H. The cohomology of bso_n and bo_n with integer coefficients. *Proc. Amer. Math. Soc.* **85**, 283–288 (1982). URL <http://www.jstor.org/stable/2044298>.
- [47] Milnor, J. W. & Stasheff, J. D. *Characteristic Classes*, vol. 76 of *Annals of Mathematics Studies* (Princeton University Press, 1974).
- [48] Hirzebruch, F., Hirzebruch, R., Schwarzenberger, R. & Borel, A. *Topological Methods in Algebraic Geometry*. Classics in mathematics (Springer-Verlag, 1966). URL https://hirzebruch.mpim-bonn.mpg.de/id/eprint/114/1/M2_Topological%20methods.pdf.

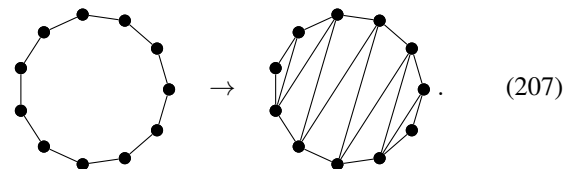
APPENDIX

These appendices provide further material that strengthen points made in the main text. In Appendix A we show that we can restrict to a finite number of vertex links in 2-dimensional triangulations and Pachner moves. In the subsequent Appendix B, we will give a method to simplify the vertex liquid in $1 + 1$ dimensions. Appendix C systematically constructs all-scalar liquid models corresponding to different classical invariants, and elaborates on their equivalence. Appendix D shows the equivalence between two liquids describing domain walls of a $1 + 1$ -dimensional topological liquid.

A RESTRICTING VALENCY OF VERTICES IN 2D TRIANGULATIONS

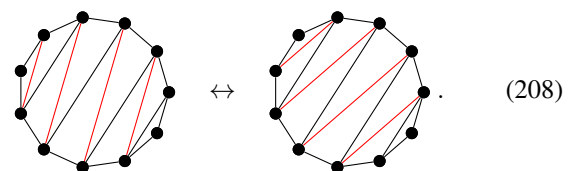
In this appendix, we show that it suffices to restrict ourselves to triangulations with l -valent vertices for $l \leq 10$. More precisely, we show that every manifold admits an $l \leq 9$ triangulation, and that every two such triangulations of the same manifold are connected via Pachner moves such that all intermediate triangulations satisfy $l \leq 10$. Note that we did not make too much effort in optimizing the number 10, and most likely smaller bounds like 8 or 9 are possible. It is clear that we need to allow $3 \leq l \leq 7$ in order to have 1-3 Pachner moves and in order to represent negative curvature.

The first step consists in mapping each triangulation to an equivalent one with $l \leq 9$. To this end, we first go to the dual lattice, which is a 3-valent cellulation consisting of n -gons with arbitrarily high n . We then triangulate each n -gon in a zig-zag manner, e.g., for $n = 11$,



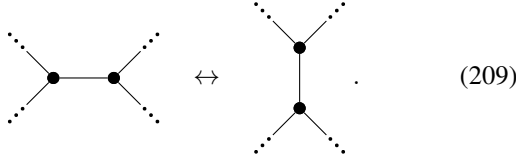
Every vertex on the boundary of this zig-zag triangulation is adjacent to at most 3 triangles. As the dual cellulation is trivalent, vertices in the overall triangulation are adjacent to $l \leq 3 + 3 + 3 = 9$ triangles.

As a second step we realize that pairing up adjacent triangles in the zig-zag triangulation (without leaving any gaps) and then performing a 2-2 Pachner move on all pairs rotates the zig-zag pattern by half a unit, e.g.,

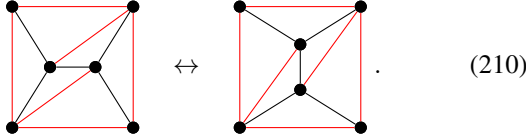


When we perform all the 2-2 Pachner moves in a sequence we obtain intermediate triangulations where a boundary vertex is adjacent to 4 triangles, but not more. There are (at least) two *tip vertices* at the boundary which are only connected to a single triangle, and we can rotate those to an arbitrary position using the moves described above. As argued before, we can do so using 2-2 Pachner moves involving only triangulations with $l \leq 3 + 3 + 4 = 10$.

2-2 Pachner moves of the original triangulation involve two vertices in the dual cellulation,

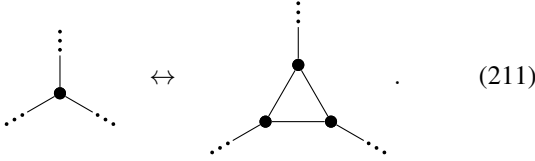


Such a move can be performed using only 2-2 Pachner moves on the dual zig-zag-triangulated triangulation as follows: First, we rotate the zig-zag triangulation of each of the 4 involved plaquettes such that its tip vertex coincides with one of the involved vertices. We are hence left with the following,

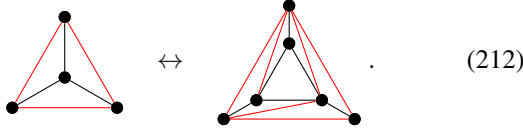


The two pictures are the same combinatorially. We see that after the rotation of the tip vertices, the above move becomes trivial and merely corresponds to a regrouping of which zig-zag triangles belong to which dual cells.

The situation for the 1-3 Pachner moves is similar. In the dual cellulation, the move becomes



After zig-zag triangulating all the plaquettes and rotating the tip vertices towards where the move happens, we are left with



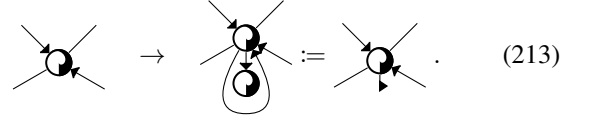
This is nothing but a sequence of two 1-3 Pachner moves. We see that the Pachner moves of the original triangulation can be mimicked by Pachner moves of the dual-zig-zag-triangulated triangulation by rotating the tip vertices and applying 1-3 Pachner moves, all of which involve only $l \leq 10$ triangulations.

B OPERATOR ANSATZ FOR THE VERTEX LIQUID

In this appendix, we take a closer look at the equations of the vertex liquid in $1 + 1$ dimensions. While there does not appear to be much room for simplifying the equations on a purely combinatorial/diagrammatic level, we can do so by using properties specific to array tensors. We will refer to the method of simplification as *operator ansatz*, since instead of specifying all vertex tensors separately, we specify operators which map between those tensors. More precisely, the operators map between tensors whose stars differ only by local moves. We will use a *support truncation argument* to show that the operators do not depend on all of the two stars they map between, but only on the local move.

Let us start by introducing an abbreviated notation. Imagine adding three indices a, b, c between two consecutive indices of

a vertex tensor, connecting a and c by a bond, and connecting b with a new 1-index vertex tensor, e.g.,



We will refer to such an operation as a *loop insertion* between the corresponding indices, and denote it by a little flag between the index lines. The direction of this flag indicates the direction of the bond between a and c .

Consider the following two vertex tensors which we will refer to as A_0 and \tilde{A}_0 ,

$$A_0 : \text{---} \bigcirc \text{---} a \quad \leftarrow \quad \tilde{A}_0 : \text{---} \bigcirc \begin{matrix} c \\ \nearrow \\ b \end{matrix} . \quad (214)$$

Let X be a way to extend A_0 by one further vertex tensor which is connected to the index a . For each such extension we can find an extension \tilde{X} of \tilde{A}_0 by one further vertex tensor which is connected to the both indices b and c as follows. \tilde{X} can be obtained from X by replacing the index connected to a by two indices connected to b and c , with a loop insertion in between. The crucial property of X and \tilde{X} is that A_0 and \tilde{A}_0 together with their respective extension evaluate to the same tensor due to the moves of the vertex liquid. For example, consider the following two extensions,

The equation can be derived from the moves of the vertex liquid as described in Section V.2. We can interpret the tensors A_0 , \tilde{A}_0 , X and \tilde{X} above as linear operators from the left to the right. Then the above equation reads

$$A_0 X = \tilde{A}_0 \tilde{X} . \quad (216)$$

Let \mathcal{X} denote the set of all possible extensions of A_0 . We can combine all the equations of the form Eq. (216) into a single equation,

$$\begin{aligned} A_0 \mathbf{X} &= \tilde{A}_0 \tilde{\mathbf{X}} , \\ \mathbf{X} : \text{dom}(A_0) &\rightarrow \bigoplus_{X \in \mathcal{X}} \text{codom}(X) , \quad \mathbf{X} = \bigoplus_{X \in \mathcal{X}} X , \\ \tilde{\mathbf{X}} : \text{dom}(A_0) &\rightarrow \bigoplus_{X \in \mathcal{X}} \text{codom}(\tilde{X}) , \quad \tilde{\mathbf{X}} = \bigoplus_{X \in \mathcal{X}} \tilde{X} . \end{aligned} \quad (217)$$

Every occurrence of A_0 in a network always comes together with some extension $X \in \mathcal{X}$. Thus, we can without loss of generality assume that the image of the operator A_0 is inside the union of the supports of all possible extensions $X \in \mathcal{X}$. Otherwise, restricting A_0 to this union of supports constitutes an invertible domain wall. We will call this line of reasoning the *support truncation argument*. Thus, the image of A_0 is inside the support of \mathbf{X} . Therefore, we can cancel \mathbf{X} in Eq. (217) with some \mathbf{X}^- ,

$$A_0 = A_0 \mathbf{X} \mathbf{X}^- = \tilde{A}_0 \tilde{\mathbf{X}} \mathbf{X}^- = \tilde{A}_0 Z . \quad (218)$$

The 3-index tensor $Z := \tilde{X}X^-$ will be called *2-1 operator*, and is denoted by

$$\begin{array}{c} \nearrow \\ \bullet \\ \searrow \end{array} \leftarrow \begin{array}{c} \nearrow \\ \bullet \\ \searrow \end{array} \quad (219)$$

Eq. (218) then becomes

$$\begin{array}{c} \bullet \\ \leftarrow \end{array} \begin{array}{c} \bullet \\ \leftarrow \end{array} = \begin{array}{c} \bullet \\ \leftarrow \end{array} \begin{array}{c} \bullet \\ \leftarrow \end{array} \begin{array}{c} \bullet \\ \leftarrow \end{array} \quad (220)$$

Now, consider two stars which differ by inserting/removing an edge,

$$\begin{array}{c} \dots \\ \nearrow \\ \bullet \\ \searrow \\ \dots \end{array} \leftarrow \begin{array}{c} \dots \\ \nearrow \\ \bullet \\ \searrow \\ \dots \end{array} \quad (221)$$

Associated to them is a pair of vertex tensors A and \tilde{A} ,

$$A: \begin{array}{c} \dots \\ \nearrow \\ \bullet \\ \searrow \\ \dots \end{array} \leftarrow a \quad \tilde{A}: \begin{array}{c} \dots \\ \nearrow \\ \bullet \\ \searrow \\ \dots \end{array} \leftarrow \begin{array}{c} c \\ \leftarrow \\ b \end{array} \quad (222)$$

such that \dots stands for an arbitrary sequence of indices which is the same on both sides. Let Y be an extension of \tilde{A} at all indices except b and c . That is, Y consists of the vertex tensors connected to those indices inside some network and the bonds between those vertex tensors. For every such extension, there is an extension Y_0 of \tilde{A}_0 at all indices except for b and c , such that the two extended networks are related by the vertex-liquid moves. E.g., if \dots in Eq. (222) consists of one further index, a possible extension Y of \tilde{A} and the corresponding Y_0 of \tilde{A}_0 are given by

$$\begin{array}{c} \dots \\ \nearrow \\ \bullet \\ \searrow \\ \dots \end{array} \begin{array}{c} \bullet \\ \leftarrow \end{array} \begin{array}{c} \bullet \\ \leftarrow \end{array} = \begin{array}{c} \dots \\ \nearrow \\ \bullet \\ \searrow \\ \dots \end{array} \begin{array}{c} \bullet \\ \leftarrow \end{array} \begin{array}{c} \bullet \\ \leftarrow \end{array} \quad (223)$$

Interpreting Y , \tilde{A} , Y_0 , and \tilde{A}_0 as linear operators, this can be written as

$$Y\tilde{A} = Y_0\tilde{A}_0 \quad (224)$$

Now, Y and Y_0 are at the same time extensions of A and A_0 at all indices except for a , such that the analogous equation in Eq. (223) holds with one instead of two open indices on the right. So we also get the equation

$$YA = Y_0A_0 \quad (225)$$

Similar to Eq. (217), we can stack all possible extensions $Y \in \mathcal{Y}$ into a single operator

$$\mathbf{Y}: \bigoplus_{Y \in \mathcal{Y}} \text{codom}(Y) \rightarrow \text{dom}(\tilde{A}), \quad (226)$$

and the same for Y_0 . We get two combined equations,

$$\mathbf{Y}A = \mathbf{Y}_0A_0, \quad (227)$$

and

$$\mathbf{Y}\tilde{A} = \mathbf{Y}_0\tilde{A}_0. \quad (228)$$

Applying the support truncation argument, the co-image of both A and \tilde{A} has to be inside the co-support of \mathbf{Y} . Thus, there is an operator \mathbf{Y}^- cancelling \mathbf{Y} , and we find

$$\begin{aligned} \tilde{A}Z &= \mathbf{Y}^- \mathbf{Y} \tilde{A} Z = \mathbf{Y}^- \mathbf{Y}_0 \tilde{A}_0 Z \\ &= \mathbf{Y}^- \mathbf{Y}_0 A_0 = \mathbf{Y}^- \mathbf{Y} A = A. \end{aligned} \quad (229)$$

So, we have in general,

$$\begin{array}{c} \dots \\ \nearrow \\ \bullet \\ \searrow \\ \dots \end{array} \begin{array}{c} \bullet \\ \leftarrow \end{array} = \begin{array}{c} \dots \\ \nearrow \\ \bullet \\ \searrow \\ \dots \end{array} \begin{array}{c} \bullet \\ \leftarrow \end{array} \begin{array}{c} \bullet \\ \leftarrow \end{array}, \quad (230)$$

representing the tensor Z by a triangle shape. Note that Z cannot be used to fuse any two indices of a vertex tensor to one, but can only be applied to index pairs such that the edge directions of the 4 neighbouring triangles are as in Eq. (221). For other choices of edge directions we need a different operator Z .

To summarize, we considered pairs of vertex tensors whose stars differed by the local move in Eq. (221). We found that every such pair of tensors are related by applying the same operator to the indices around where the move happens. The analogous arguments can also be applied to all other local moves of stars.

For example, consider the opposite direction of the move in Eq. (221). To this end, we exchange what we call A_0 and \tilde{A}_0 in Eq. (214), and the extensions X consist of two tensors whereas \tilde{X} consists of one tensor with a loop insertion on the opposite side of where it is connected to A_0 . E.g., a pair of extensions is given by

$$\begin{array}{c} \dots \\ \nearrow \\ \bullet \\ \searrow \\ \dots \end{array} \begin{array}{c} \bullet \\ \leftarrow \end{array} \begin{array}{c} \bullet \\ \leftarrow \end{array} = \begin{array}{c} \dots \\ \nearrow \\ \bullet \\ \searrow \\ \dots \end{array} \begin{array}{c} \bullet \\ \leftarrow \end{array} \begin{array}{c} \bullet \\ \leftarrow \end{array} \quad (231)$$

Again we can combine all the X and \tilde{X} into a single operator each, and apply the support truncation argument to show that A_0 is obtained from \tilde{A}_0 via some operator Z . We can then look at arbitrary A and \tilde{A} like in Eq. (222) with A and \tilde{A} exchanged. The equations Eq. (223) and its version without tilde are the same. From them, it follows that Z is the same for all pairs of A and \tilde{A} , and we get an equation

$$\begin{array}{c} \dots \\ \nearrow \\ \bullet \\ \searrow \\ \dots \end{array} \begin{array}{c} \bullet \\ \leftarrow \end{array} = \begin{array}{c} \dots \\ \nearrow \\ \bullet \\ \searrow \\ \dots \end{array} \begin{array}{c} \bullet \\ \leftarrow \end{array} \begin{array}{c} \blacktriangle \\ \leftarrow \end{array}, \quad (232)$$

where the black triangle will be called the *1-2 operator*.

As another example, consider two stars differing by reversing the direction of an outer edge,

$$\begin{array}{c} \dots \\ \nearrow \\ \bullet \\ \searrow \\ \dots \end{array} \leftarrow \begin{array}{c} \dots \\ \nearrow \\ \bullet \\ \searrow \\ \dots \end{array} \quad (233)$$

In this case we need to not only include the two neighbouring

tensors in X and \tilde{X} , but also the other tensor connected to both,

$$\text{Diagram (234)} \quad (234)$$

In the end, we get an equation,

$$\text{Diagram (235)} \quad (235)$$

We will call the tensor Z represented by a square the *outer edge flip operator*.

As a last example, consider changing the direction of an internal edge of the star,

$$\text{Diagram (236)} \quad (236)$$

Examples for extensions are

$$\text{Diagram (237)} \quad (237)$$

We get another equation

$$\text{Diagram (238)} \quad (238)$$

We will call the tensor Z represented by a square the *inner edge flip operator*.

Given the 1-2 operator together with some variants of edge flip operators, we can generate all vertex tensors from one very simple vertex tensor, say, a 1-index tensor. Even though the set of all those operators is more complicated than the set of tensors specifying common algebraic structures, such as Hopf algebras, it is still considerably easier than the set of all vertex tensors for a sufficient set of stars.

The operator ansatz does not only simplify the set of tensors, but also the set of axioms. Applying different sequences of operators can have the same effect on the stars, yielding coherence axioms for the operators. For example, we have

$$\text{Diagram (239)} \quad (239)$$

This holds for any sequence of indices \dots , that is, for any way to extend the index between the vertex tensor and the 1-2 operator by some network to the left. Thus, via the support truncation argument, we can deduce the coherence axiom

$$\text{Diagram (240)} \quad (240)$$

Another example for such a coherence axiom is

$$\text{Diagram (241)} \quad (241)$$

Furthermore there is a bunch of coherence axioms involving the edge flip operators. We cannot write down any of them here since we so far only defined two specific edge flip operators which are not compatible. In addition to the coherence axioms, we still need to impose the Pachner moves. Instead of having one 2-2 Pachner move for every set of 4 stars, we can reduce to a much smaller set. If we ignore all the edge directions for a moment, then the Pachner moves can be implemented by only one single equation,

$$\text{Diagram (242)} \quad (242)$$

The axiom in Eq. (240) is familiar. If we interpret the 1-2 operator as a bi-linear operator from the right to the left, it defines an associative algebra. Furthermore, the cyclic symmetry of the 3-index tensor yields

$$\text{Diagram (243)} \quad (243)$$

If we interpret the 2-index vertex tensor as a bilinear form, the equation above is just the equation fulfilled by a Frobenius form (apart from being non-degenerate). We further have

$$\text{Diagram (244)} \quad (244)$$

so the 1-index vertex tensor can be interpreted as a linear form generating the bilinear form through the product. If the bilinear form is non-degenerate, the corresponding matrix has an inverse,

$$\text{Diagram (245)} \quad (245)$$

which allows us to also construct a unit,

$$\text{Diagram (246)} \quad (246)$$

We note that the Frobenius form (the 2-index vertex tensor) as well as its inverse are symmetric. We indeed find that the above defined vector is a left unit,

$$\text{Diagram (247)} \quad (247)$$

and analogously a right unit. Thus, the 1-2 operator forms a symmetric Frobenius algebra.

C ALL-SCALAR VERTEX LIQUID MODELS FROM CHARACTERISTIC CLASSES

In Section VII.4, we have described two simple all-scalar liquid models, one of which required to be written as a vertex-liquid model. In this appendix, we explain how to systematically obtain all-scalar vertex liquid models via *cohomology*, in particular so-called *characteristic classes*. We start by introducing the basic vocabulary of simplicial cohomology, and then introduce local combinatorial formulas for generating characteristic classes and show how to combine them into all-scalar liquid models. Finally, we will discuss which of the obtained liquid models are in the same phases, and which only yield the same invariants when evaluated on a manifold.

III.1 Simplicial homology

The central entities of cohomology are *i-cycles* (or, cycles of degree i), which intuitively can be thought of as a pattern of points, closed loops, closed membranes, or generally networks of closed $n - i$ -dimensional embedded submanifolds. Moreover, the closed embedded submanifolds are coloured by elements of an abelian group A and they can be moved locally, such that when two submanifolds overlap the corresponding A -elements are added. In order to define cycles, we first need to define *chains*. On a n -dimensional triangulation T an A -valued *i-chain* for $0 \leq i \leq n$ is a function

$$c : S^i(T) \rightarrow A, \quad (248)$$

where S^i is the set of i -simplices of T . We will here assume $A = \mathbb{Z}_2$, and then thus sometimes talk about c in terms of the subset of i -simplices s with $c(s) = 1$ (with \mathbb{Z}_2 written additively). For abelian groups A with elements of order larger than 2, the analogous expressions will be a little bit more complicated and involve the non-trivial group inverse. The *boundary* of a i -chain is the $i - 1$ -chain

$$(\delta c)(s) = \sum_{t \in S^{i+1}(s)} c(t), \quad (249)$$

for all $s \in S^{i-1}(T)$, where $S^{i+1}(s)$ is the set of i -simplices containing s . If A is not \mathbb{Z}_2 , then some of the $c(t)$ will be inverted depending on some additional decorations. In the \mathbb{Z}_2 case, if we think of the set of i -simplices in c as an open i -dimensional submanifold with boundary, then the boundary of c is literally this submanifold's boundary.

We can shift the above notions to the Poincaré dual cellulations such that what used to be the i -simplices are now $n - i$ -simplices. An *i-cochain* is then a function

$$c : S^{n-i}(T) \rightarrow A, \quad (250)$$

and the boundary of a i -cochain is the $i + 1$ -cochain

$$(dc)(s) = \sum_{t \in S^{(n-i)-}(s)} c(t), \quad (251)$$

for all $s \in S^{n-i+1}(T)$, where $S^{x-}(s)$ is the set of x -simplices contained in s . The boundary maps on both chains and cochains define *chain complexes*, meaning for any (co-)chain c , $d^2c = 0$ ($\delta^2c = 0$). c is called *(co-)cycle* if $\delta c = 0$ ($dc = 0$) and *(co-)boundary* if $c = \delta x$ ($c = dx$) for some chain x . x is

then called a *trivialization* of c . The sets of (co-)chains, (co-)cycles, and (co-)boundaries form groups under simplex-wise A -addition. The group of i -(co-)cycles modulo the group of i -(co-)boundaries is known as the i th *(co-)homology group*, and the corresponding equivalence class of a (co-)cycle is known as its *(co-)homology class*. Intuitively, (co-)cycles can be thought of as collections/networks of i -dimensional embedded submanifolds.

III.2 Generating characteristic classes and their combinatorial formulas

Roughly speaking, characteristic classes are prescriptions to compute a non-trivial (co-)cycle locally from any presentation of a (vector) bundle with a fixed structure group over a manifold. For our purposes, the vector bundle will be the tangent bundle of the n -dimensional space-time manifold, with structure group $O(n)$, or $SO(n)$ in the oriented case. There are three families of characteristic classes which generate all of them through operations given in the next section. The *Euler class* e is represented by a \mathbb{Z} -valued n -cocycle on unoriented n -manifolds with even n . The i th *Stiefel-Whitney class* ω_i is a \mathbb{Z}_2 -valued i -cocycle on unoriented n -manifolds with $0 < i \leq n$. The i th *Pontryagin class* P_i is a \mathbb{Z} -valued $4i$ -cocycle on oriented n -manifolds with $0 < 4i \leq n$, and reversing the orientation corresponds to a \mathbb{Z} -inversion of the Pontryagin class.

On a triangulation, characteristic classes are more naturally represented as cycles than co-cycles. It has been shown in Ref. [41] that for all characteristic classes there exist local formulas which determine the value of a representing cycle on a simplex only from the star of that simplex. Let us describe those local formulas for the three families of generating characteristic classes mentioned in the previous paragraph.

Let us start by giving the local formula which computes a 0-cycle e representing the Euler class on a vertex v . We have

$$e(v) = \sum_{0 \leq x \leq n} (-1)^x \sum_{s \in S^{x+}(v)} \delta_{v, S_0^{0-}(s)}, \quad (252)$$

where $S_E^{x-}(s)$ is the sub x -simplex E of s when s is identified with the standard branching structure simplex. E is specified by the ordered sequence of numbers corresponding to its vertices, when the vertices of s are numbered according to the branching structure ordering. So, $S_0^{0-}(s)$ is the 0-vertex of s . $e(v)$ is thus the number of x -simplices which contain v as their 0-vertex (including v itself), weighted by $(-1)^x$.

Next, we give a local formula which computes a $(n - i)$ -cycle ω_i representing the i th Stiefel-Whitney class. Following Ref. [42], its value on an $n - i$ -simplex s is given by

$$\omega_i(s) = \sum_{n-i \leq x \leq n} \sum_{t \in S^{x+}(s)} \sum_{E \in \mathbf{E}(n-i, x)} \delta_{s, S_E^{(n-i)-}(t)}. \quad (253)$$

$\mathbf{E}(y, x)$ is the set of ordered sequences E , $0 \leq \{E_l\}_{0 \leq l \leq y} \leq x$, for which $E_{2l} = E_{2l-1} + 1$ for all $1 \leq l < y/2$, $E_0 = 0$, and $E_y = x$ if y is even. E.g., for $i = n$, $\mathbf{E}(0, x)$ consists of only the sequence 0, so the formula coincides with the \mathbb{Z}_2 -valued version of the Euler class in Eq. (252). For $i = 1$, $\mathbf{E}(n - 1, n - 1)$ consists of only the full subsimplex, and $\mathbf{E}(n - 1, n)$ consists of the $n - 1$ -sub-simplices complementary to a vertex of the n -simplex, for every odd vertex of the n -simplex. All of those $n - 1$ -sub-simplices have the same handedness relative to the

n -simplex. Thus, ω_1 precisely consists of the $n - 1$ -simplices where the handedness of the n -simplices changes if we locally choose an orientation.

The Pontryagin classes appear to be more difficult, and local formulas comparable to the ones above in simplicity do not exist to date. Nonetheless, it has been shown in Ref. [29] that there exist formulas for computing a \mathbb{Q} -valued $n - 4i$ -cycle P_i representing the i th Pontryagin class locally from a triangulation. The value of P_i on an $n - 4i$ -simplex depends only on its link and the orientation on the latter. The formula depends neither on a branching structure nor any other decoration of the triangulation. Ref. [43] presents a more or less explicit formula computing the \mathbb{Q} -value of P_1 from the link of a $n - 4$ -simplex. It is conceivable that a formula for a \mathbb{Z} -valued instead of \mathbb{Q} -valued $n - 4i$ -cycle is possible when it is allowed to depend on a branching structure or other decorations.

III.3 Combining characteristic classes

While characteristic classes are interesting for many reasons, the ones which give rise to all-scalar liquid models are the top-degree ones, represented by a n -cocycle or a 0-cycle c . Such a model is then given by assigning to a vertex v the scalar $(-1)^{c(v)}$ for \mathbb{Z}_2 -valued classes, or $\alpha^{c(v)}$ for \mathbb{Z} -valued classes. In order to obtain such top-dimensional classes, we can combine or modify some of the generating classes from the previous section in a way compatible with homology. That is, we use operations whose output is a cycle if all inputs are cycles, and whose output is a boundary if at least one input is a boundary. Note that the latter operations do not depend on the (tangent) vector bundle but only on the homology classes which makes them distinct from the generating characteristic classes themselves.

The most notable way to combine cycles is via the *cup product*. Intuitively, the cup product of two cycles is the cycle formed by the intersections of the corresponding networks of submanifolds. If we want to define the intersection of two (co-)cycles X and Y on a triangulation, we run into an ambiguity if X and Y coincide on some simplex. This ambiguity can be removed by infinitesimally shifting X or Y in a direction which is determined by some additional decoration, like a branching structure. Indeed, Ref. [39] gives a very simple formula for the cup product of an x -cocycles X and a y -cocycle Y which can be interpreted as shifting X towards the 0-vertex of every simplex,

$$(X \cup Y)(s) = x(S_{(0, \dots, x)}^{x-}(s)) \cdot y(S_{(x, \dots, x+y)}^{y-}(s)), \quad (254)$$

where s is a $x + y$ -simplex. Note that in order to define the cup product we need to extend \mathbb{Z}_2 (or more generally A) to a ring, and the above product is the multiplication in that ring. Unfortunately, we cannot directly use this formula since the characteristic classes from the previous section are given as cycles and not cocycles. To define the cup product on cycles we need an analogue of a branching structure on the cellulation dual to the triangulation, which is precisely given by the notion of a dual branching introduced in Section VI.3.

We start by giving a recipe to turn an i -cycle into an $n - i$ -cocycle inside a 0-dual-branched triangulation (cf. Section VI.3). The construction depends on a couple of choices which yield different, but equivalent formulas. For every representative of a star L of a y -simplex with $y \leq i$ and every

$n - i + y + 1$ -coboundary B on the interior simplices of L , we need to choose a trivialization, i.e., a $n - i + y$ -cochain $I(L, B)$ on the interior simplices of L , such that

$$dI(L, B) = B. \quad (255)$$

For $y = i$, B would be an $n + 1$ -cocycle and is thus not defined. In this case, we choose $I(L, \{\})$ to be a n -cocycle consisting of a single n -simplex (it would also suffice for it to be in the homology class of 1, e.g., consisting of an odd number of n -simplices for \mathbb{Z}_2 -valued cycles). Note that such a choice of trivialization is a choice on the level of star representatives and not a choice for the stars of concrete simplices in a triangulation, and does therefore not correspond to adding a new decoration to the triangulations.

With the choice of I , given a i -cycle c , we can obtain a shifted $n - i$ -cocycle c^* as follows. For every y -simplex Y with $y \leq i$, we construct a $n - i + y$ -cochain $\Phi(Y)$ on the interior simplices of the star $\text{Star}(Y)$ in the following way. For $y = i$, we set

$$\Phi(Y) = c(Y) \cdot I(\text{Star}(Y), \{\}). \quad (256)$$

Then, we iteratively set

$$\Phi(Y) = I(\text{Star}(Y), \sum_{X \in S^{(n-i+y+1)+}(Y)} \Phi(X)), \quad (257)$$

where we think of $\Phi(X)$ as embedded in $\text{Star}(Y)$. Then, we use

$$c^* = \sum_{v \in S_0(T)} \Phi(v). \quad (258)$$

Using the formula for the Poincaré dual above, we can define the *linking number* $a \otimes b$ between an i -boundary a and a $n - i - 1$ -boundary b inside a 0-dual-branched triangulation of an n -sphere. It is obtained by constructing the $i + 1$ -coboundary b^* , choosing a trivialization x of b^* , i.e., an i -coboundary x such that $dx = b^*$, and then simply calculating the overlap of a and x on the i -simplices,

$$a \otimes b = \sum_{s \in S_i} a(s) \cdot x(s). \quad (259)$$

Using the linking number, we can construct the cup product of an a -cycle A and a b -cycle B as the following $a + b - n$ -cycle $A \cup B$. The link of an $a + b - n$ -simplex s in a 1-dual-branched triangulation is a $a + b - 1$ -dimensional triangulation which is 0-dual-branched. Within the link, A becomes a $n - b - 1$ -boundary \tilde{A} , and B a $n - a - 1$ -boundary \tilde{B} by identifying each $n - b - 1$ -simplex of the link with the corresponding internal a -simplex of the star. We then set

$$(A \cup B)(s) = \tilde{A} \otimes \tilde{B}. \quad (260)$$

Let us give a small example to illustrate the construction of the cup product for cycles. The simplest example is the cup product of two 1-cycles A and B in two dimensions. The star of an edge consists of the two adjacent triangles. If the branching structure of the two triangles is reflection-symmetric around the edge, there are two different possible identifications with the standard representative if there is no orientation of the 2-manifold. An identification can be indicated by specifying a

favourite adjacent triangle of the edge, i.e., giving it a dual direction. So a 1-dual-branched triangulation is one where all edges have dual directions. The link of a vertex v is an l -gon, and A and B turn into 0-boundaries \tilde{A} and \tilde{B} on that l -gon. The vertices of the link have favourite edges, due to the dual directions of the corresponding internal edges of the star. We can turn \tilde{B} into a 1-boundary \tilde{B}^* by shifting it from each vertex to its favourite edge. Now imagine moving \tilde{A} -coloured vertices and annihilating pairs of them till there are none left, and collecting a \mathbb{Z}_2 -valued summand 1 for every time moving an \tilde{A} -vertex past a \tilde{B}^* -edge. The resulting value is the linking number of \tilde{A} and \tilde{B} which is the value of $A \cup B$ on v . Using this procedure for both A and B equal to the characteristic class cycle ω_1 yields exactly the $(-1)^{\omega_1^2} = (-1)^{\omega_1 \cup \omega_1}$ vertex-liquid model from Section VII.4.

Another valid operation is the so-called *Bockstein homomorphism*, which can be defined for any short exact sequence

$$B \xrightarrow{f} C \xrightarrow{g} A. \quad (261)$$

A , B and C are abelian groups, f is an injective and g a surjective group homomorphism, and $g \circ f$ is the trivial homomorphism sending everything to the identity of A . The Bockstein homomorphism β has a simple combinatorial formula in terms of triangulations, and maps a i -cocycle c to a $i+1$ -cocycle

$$\beta(c) = f^{-1}(d(g^{-1}(c))), \quad (262)$$

where both g^{-1} and f^{-1} are applied simplex-wise. Different choices for the right inverse g^{-1} of g yield different operations, whose outputs only differ by a locally trivializable boundary though. The formula for cycles instead of cocycles is completely analogous. Of particular importance is the Bockstein homomorphism for the short exact sequence

$$\mathbb{Z} \xrightarrow{\cdot 2} \mathbb{Z} \xrightarrow{\text{mod } 2} \mathbb{Z}_2. \quad (263)$$

It can be used to map a \mathbb{Z}_2 -valued i -cocycle to a \mathbb{Z} -valued $i+1$ -cocycle.

Furthermore, there is the so-called k th *Steenrod square* $\text{Sq}^k(x)$, which turns an i -cocycle x into an $i+k$ -cocycle for $1 \leq k \leq i$. An explicit combinatorial formula for cocycles can be found in terms of a *higher-order cup product* in Ref. [39] and Ref. [44],

$$\text{Sq}^k(x) = x \cup_{i-k} x. \quad (264)$$

By shifting cycles to cocycles and back using the dual branching and branching, we can obtain a formula transforming a k -cycle into a $k-i$ -cycle.

Last but not least, we can of course take the simplex-wise \mathbb{Z}_2 -valued (or more generally, A -valued) sum of two i -(co-)cycles with the same i . Note that for 0-cycles corresponding to all-scalar liquid models, taking the sum is the same as stacking the models on top of each other.

Now, we can start with some characteristic class cycles, and then use cup products and Steenrod squares and sums to obtain a 0-cycle. E.g., on a 4-manifold, we could build a \mathbb{Z}_2 -valued 0-cycle $\omega_1 \cup \text{Sq}^1(\omega_2 + \omega_1 \cup \omega_1)$. For all the used local formulas, the result on an i -simplex only depends on the star of that i -simplex. Thus, the value of the final 0-cycle on a vertex can be computed by a formula $F(\text{Star}(v))$ which only depends on the star of that vertex v . The homology class of the resulting 0-cycle depends only on the topology of the manifold, so the sum

of the 0-cycle over all vertices is a topological invariant. Thus, assigning $\alpha^{F(\text{Star}(v))}$ in the \mathbb{Z} -valued case and $(-1)^{F(\text{Star}(v))}$ in the \mathbb{Z}_2 -valued case to every vertex v defines an all-scalar topological vertex-liquid model. If the resulting 0-cycle is \mathbb{Z}_2 -valued we must have $\alpha = -1$.

The Euler class is already a 0-cycle, so all we need to do is to sum over it, which yields a classical manifold invariant. Every x -simplex of a triangulation contributes $(-1)^x$ to the Euler class of exactly one vertex, namely its 0-vertex. Thus, the classical invariant is a sum of $(-1)^x$ over all x -simplices, which is nothing but the Euler characteristic. Thus, this yields a α^x vertex-liquid model as described above.

Summations of \mathbb{Z}_2 -valued 0-cycles which are cup products of Stiefel-Whitney classes are known as *Stiefel-Whitney numbers*. In n dimensions, there is one Stiefel-Whitney number for each partitioning $n = n_0 + \dots + n_x$ of n as a sum over x non-negative integers. On an n -manifold M , it can be computed by

$$\text{St}_{\vec{n}}(M) = \int_M \omega_{n_0} \cup \dots \cup \omega_{n_x}, \quad (265)$$

and can be written as a $(-1)^{\text{St}_{\vec{n}}}$ vertex-liquid model as described above. Similar are the *Pontryagin numbers* defined on oriented manifolds of dimensions divisible by 4. In $4n$ dimensions, there is one such number for each partitioning $n = n_0 + \dots + n_x$ of n as a sum over x non-negative integers. On a $4n$ -manifold M , it can be computed by

$$\text{Pn}_{\vec{n}}(M) = \int_M P_{n_0} \cup \dots \cup P_{n_x}, \quad (266)$$

and yields an $\alpha^{\text{Pn}_{\vec{n}}}$ vertex-liquid model as described above. Surely, the only directly physically relevant Pontryagin number is P_1 alone in 4 dimensions. Note that the Pontryagin classes change their sign when we invert the orientation. So if α is a phase, then the vertex-liquid model is Hermitian. This is to be contrasted with the also \mathbb{Z} -valued Euler characteristic, which does not depend on the orientation, and is therefore Hermitian for real α .

III.4 Local equivalence between combinatorial formulas

Not all all-scalar liquid models obtained via the prescription from the previous two sections are different, but some of them are in the same exact phase. Note that two invertible all-scalar models are in the same phase, if stacking one with the inverse of the second yields a trivial model. Furthermore, a characteristic-class all-scalar liquid model has an invertible boundary, if the corresponding 0-cycle is trivializable by a local combinatorial formula, such as a 1-chain whose values on edges only depend on the star of that edge. This can be generalized to arbitrary i -cycles computed by a local formula. We will call those *locally trivial*, if there is a local formula for a trivializing $i+1$ -cycle, and two locally computable i -cycles *locally equivalent*, if they differ by a locally trivial cycle. Note that cup products, Bockstein homomorphisms, or Steenrod squares applied to a (or at least one) locally trivial characteristic cycle will again result in a locally trivial cycle.

Let us give some examples of locally trivial cycles. First of all, according to its interpretation as intersections, the cup product should be associative,

$$(A \cup B) \cup C = A \cup (B \cup C). \quad (267)$$

This is in fact true exactly on the level of cocycles if we use the formula in Eq. (254), so the difference between the left and right is empty and locally trivializable by the empty chain. Another relation which holds exactly on the level of (co-)cycles is bilinearity of the cup product,

$$A \cup (B + C) = A \cup B + A \cup C. \quad (268)$$

Note that equations like this holding exactly is a property of a specific combinatorial implementation of the cup product, whereas any implementation should share the feature that the difference between the two sides is trivializable. An example where this can be seen is the commutativity of the cup product,

$$A \cup B = B \cup A, \quad (269)$$

which does not hold on the level of concrete (co-)cycles if we use the formula in Eq. (254), since it is not symmetric in A and B . However, a trivialization of $A \cup B - B \cup A$ can still be computed locally, and is in fact given in terms of the higher-order cup product as $d(A \cup_1 B)$ [44]. All in all, different orderings, placing brackets, or expanding sums yield locally equivalent cycles, or vertex-liquid models which are all in the same exact phase. We will consequently drop the brackets and write AB instead of $A \cup B$.

In order to obtain more interesting local equivalences between characteristic cycles, it is useful to make contact to the conventional mathematical literature on the subject which is not focused on a combinatorial treatment. There, characteristic classes like ω_i or P_i are defined for arbitrary bundles with structure group $O(n)$ or $SO(n)$, and the characteristic classes as defined above are those of the tangent bundle of a (oriented) manifold. Vector bundles over a manifold with fixed structure group are in one-to-one equivalence to homotopy classes of maps from the manifold to the so-called *classifying space* of the structure group. The bundle is obtained by pulling back the so-called *universal bundle* over the classifying space via the map. In the same way we can also pull back cohomology classes from the classifying space to the manifold. Those pullbacks of cohomology classes are precisely the characteristic classes. If we have concrete realizations of the manifold, bundle, classifying space, its universal bundle, and explicit cocycles representing the cohomology classes of the classifying space, this yields concrete local expressions for the characteristic classes. Moreover, coboundaries on the classifying space yield locally trivial formulas, since a choice of trivialization in the classifying space yields a trivializing locally computable chain.

It is known that the different products of Stiefel-Whitney classes are the pullbacks of a set of \mathbb{Z}_2 cohomology classes of the classifying space $O(n)$ spanning its whole cohomology. Thus, polynomials (with cup product and sum) of Stiefel-Whitney classes exhaust all locally computable cycles, and Stiefel-Whitney numbers span all non-trivial all-scalar liquid models. As a consequence, also the Steenrod square of a Stiefel-Whitney class must be locally equivalent to such a polynomial. Concretely, we have

$$Sq^i(\omega_j) = \sum_{t=0}^i \binom{j-i-1+t}{t} \omega_{i-t} \omega_{j+t}, \quad (270)$$

for all i and j which is known under the name *Wu formula* (cf. page 197 in Ref. [45]).

The \mathbb{Z} -valued cohomology of the classifying space of $SO(n)$, which is the structure group of the tangent bundle for oriented manifolds, is more complicated to describe [46]. Most notably, it contains the Euler class and different products of Pontryagin classes, but also of the Bockstein homomorphisms under Eq. (263) of products of different even-degree Stiefel-Whitney classes ω_{2i} , subject to several relations. The $\text{mod } 2$ quotient of \mathbb{Z} -valued characteristic classes are \mathbb{Z}_2 -valued characteristic classes, and thus locally equivalent to products of Stiefel-Whitney classes. The $\text{mod } 2$ quotient of a Bockstein homomorphism is known to be the same as the Steenrod square Sq^1 , which applied to a product of Stiefel-Whitney classes can be obtained from Eq. (270). For the Pontryagin classes, the relation is

$$P_i \text{ mod } 2 = \omega_{2i}^2, \quad (271)$$

cf. page 181 in Ref. [47]. Again, the equation holds for the corresponding cohomology classes on classifying space, and hence also as local equivalence between local formulas.

III.5 Local versus global equivalence

If two liquid models are in the same exact phase, then they yield the same numbers when evaluated on different manifolds. However, the converse is not necessarily true – there can be different exact phases which still produce the same global invariants. The analogue of this for locally computable cycles is the following. Locally trivial cycles always yield boundaries on different manifolds, but the converse is not true. There can be local cycles which always yield boundaries but are not locally trivial, i.e., the trivialization cannot be locally computed. In this section we will give some examples for this.

The so-called *Wu relation* states that the i th Steenrod square of a $n - i$ -cocycle A in n dimensions is equivalent to its cup product with a degree- i characteristic class ν_i ,

$$Sq^i(A) = \nu_i \cup A, \quad (272)$$

where ν_i is known as the i th *Wu class* ν_i , and is a polynomial in Stiefel-Whitney classes of the tangent bundle. For $i = 1, 2, 3$, the ν_i are given by $\nu_1 = \omega_1$, $\nu_2 = \omega_1^2 + \omega_2$, and $\nu_3 = \omega_1 \omega_2$. The equation only holds as an equation between homology classes on different manifolds, but it does not hold for the cohomology classes in classifying space. In accordance with that, it does not hold for arbitrary vector bundles but only for the tangent bundle, since the left-hand side does not even depend on the bundle whereas the right-hand side does. Thus, we do not expect the two sides of the equation to be locally equivalent. So two vertex-liquid models related by the application of Wu relation above need to evaluate to the same numbers on manifolds, but can be in distinct exact phases.

Part of the definition of the Steenrod square is $Sq^i(A) = 0$ if A is a j -cocycle with $j < i$, where 0 denotes the trivial chain. Thus, we must have $\nu_j = 0$ on n -manifolds for $j > n/2$. This yields equations for polynomials of Stiefel-Whitney classes alone, such as $\nu_2 = \omega_1^2 + \omega_2 = 0$ on 2-manifolds and 3-manifolds, or $\omega_1 \omega_2 = 0$ on 3-, 4- and 5-manifolds. This implies, e.g., that the liquid models $(-1)^{\omega_1^2}$ and $(-1)^{\omega_2}$ evaluate to the same numbers on any 2-manifold. However, we have argued in Section VII.4 that the latter two models are in different exact phases. This is in accordance with the fact that ω_1^2 and ω_2 are independent cohomology classes of the classifying space,

and we thus do not expect them to be locally equivalent or the two liquid models being in the same exact phase.

Let us provide a more detailed combinatorial explanation of why there is no invertible domain wall between $(-1)^{\omega_1^2}$ and $(-1)^{\omega_2}$ in two dimensions. Imagine a regular triangulation of a cylinder, by dividing it into a $n \times m$ grid and then dividing every plaquette into two triangles. ω_2 is empty inside such a regular triangulation, and also ω_1 is trivial in the sense that it has a local trivialization consisting of taking the same out of two triangles for every plaquette. Thus, also ω_1^2 has a local trivialization, or can even be made empty with the appropriate choice of dual orientations. Now, consider closing one end of the cylinder with a disk. Since the disk is orientable, the local trivialization of ω_1 in the cylinder can be extended to a trivialization of ω_1 in the disk. Thus, the sum over ω_1^2 inside the disk is 0. On the other hand, the Euler characteristic of the disk is 1, and so is the sum over ω_2 . Note that both sums are unambiguously defined since ω_1^2 and ω_2 are trivial on the regular cylinder. Now, if there was an invertible domain wall between the two models, then we could place this domain wall around the non-contractible loop of the cylinder. Since the models themselves are trivial on the regular triangulations, the domain wall itself is a 1-dimensional liquid model given by a vector space, whose evaluation on a circle yields the dimension of that vector space, which is a positive integer x . Pulling the invertible domain wall through the disk yields

$$x = x \cdot (-1)^{\omega_1^2}[\text{disk}] = (-1)^{\omega_2}[\text{disk}] = -1, \quad (273)$$

which contradicts x being a positive integer.

Another relation between characteristic classes which is not a local equivalence follows from the *Hirzebruch signature theorem* (cf. page 86 in Ref. [48]),

$$\sigma(X) = \int_X P_1/3, \quad (274)$$

for all 4-manifolds X , where σ is the *signature* of X . That is, it is the signature of the matrix whose rows and columns correspond to the generators of the 2nd \mathbb{Z} -valued cohomology classes and whose entries are the integrals over cup products between the latter. Since the signature is an integer, we conclude that

$$\int_X P_1 \pmod 3 = 0. \quad (275)$$

However, this relation holds only for tangent bundles of 4-manifolds, and $P_1 \pmod 3$ is not trivial on the classifying space. Hence, we do not expect that there is a locally computable trivialization of $P_1 \pmod 3$ on triangulations.

We would like to remind the reader that all-scalar liquid models are physically trivial since they do not have any degrees of freedom. Furthermore, they are in trivial exact phases, i.e., have invertible boundaries, if we restrict to regular lattices. Moreover, note that for all-scalar liquid models, being in the same exact phase via an invertible domain wall is not the same as being connected by a continuous gapped path. For all-scalar models, ‘gapped’ simply means that the model is non-zero on any disk-like patch. Obviously, all α^x models including the trivial model at $\alpha = 1$ are connected by gapped paths. Also the $(-1)^{\text{St}\pi}$ models can be connected to the trivial model, even though then the models on the path are not themselves topological liquid models. Those paths are not possible anymore if

we restrict to real instead of complex numbers, as then paths would have to go through 0. E.g., all α^x models for negative α are then still continuously connected to each other but not to the trivial model. Interestingly, when we restrict to real numbers, then also the invertible boundary of the odd-dimensional α^x model with negative α fails, since, e.g., there is no real number $\alpha^{1/2}$.

In summary, we have seen that there are three different notions of equivalence between expressions involving characteristic classes, cup products and Steenrod squares. Either, the local formulas are directly equal, or they are unequal but there is a local formula computing a trivialization of the difference of the resulting cycles, or are they in the same homology class but there is no locally computable trivialization.

D DOMAIN WALL TRIANGLE LIQUID

In this section, we show that the moves of the domain wall liquid mentioned in Section IV.6 are equivalent to those of the triangle boundary liquid for the stack of two models. The mapping from the former to the latter is given by

$$\text{Red square with arrow} := \text{Blue square with arrow and loop}, \quad (276)$$

and analogously with red and blue exchanged. The boundary Pachner move in Eq. (61) is derived by

$$\text{Red square with arrow} \stackrel{276}{=} \text{Black square with arrow} \stackrel{61}{=} \text{Black square with arrow and loop} \stackrel{276}{=} \text{Blue square with arrow and loop} \stackrel{26}{=} \text{Blue square with arrow and loop} \stackrel{276}{=} \text{Red square with arrow and loop}, \quad (277)$$

where in the second equation we used the moves of the blue triangle liquid, and in the third equation, we used the moves for the triangle boundary liquid of the stacked model. The commutativity in Eq. (102) can be derived by

$$\text{Red square with arrow and blue square with arrow} \stackrel{276}{=} \text{Black square with arrow and loop} \stackrel{61}{=} \text{Black square with arrow and loop} \stackrel{276}{=} \text{Black square with arrow and loop} \stackrel{26}{=} \text{Black square with arrow and loop} \stackrel{26}{=} \text{Blue square with arrow and loop} \stackrel{26}{=} \text{Blue square with arrow and loop}, \quad (278)$$

where the last equation holds for symmetry reasons.

The reverse mapping from the boundary triangle liquid for the stack to the domain wall triangle liquid is even more straight forward,

$$\text{Black square with arrow} := \text{Red square with arrow and blue square with arrow}. \quad (279)$$

The mapped boundary Pachner move for the stacked model can be derived from the boundary Pachner moves of the individual liquids plus the commutativity move in Eq. (102).